学位論文

上脇　隼一

目次

1. 主論文

Studies on the structure and function relationships of the unstructured regions in protein

(タンパク質に内在する非構造領域の構造機能相関に関する研究)

上脇　隼一

2. 公表論文

Preferential domain orientation of HMGB2 determined by the weak intramolecular interactions mediated by the interdomain linker

J. Uewaki, H. Kamikubo, J. Kurita, N. Hiroguchi, H. Moriuchi, M. Yoshida, M. Kataoka, N. Utsunomiya-Tate, S. Tate,

Chemical Physics. **419**, 212-223. (2013)

主論文

Contents

Page

Chapter I

General introduction 1

Chapter II

Preferential domain orientation of HMGB2 determined by the weak intramolecular interactions mediated by the interdomain linker

Abstract 5

1. Introduction 6

2. Materials and methods 9

3. Results and discussion 16

Chapter III

The effect of DNA binding and bending activity by mutation on the interdomain linker of HMGB2

Abstract 53

1. Introduction 54

2. Materials and methods 55

3. Results and discussion 57

Chapter IV

Conclusions 60

Acknowledgments 62

References 63

Chapter I

General Introduction

Proteins have their own structures, and there are close relationships between their structures and functions. Therefore, it is necessary for revealing the function of a protein to determine its structure. Before now, many protein structures have determined by NMR and X-ray crystallography, and everyone can use this structure information by internet. However, there are many proteins that have intrinsically unstructured regions. In fact, genomes sequence prediction suggests that anywhere between 25 % and 41 % of the proteins in eukaryotic genomes contain unstructured regions [1]. The functions of the unstructured regions predicted by its sequences could show such as protein-protein interaction, protein-DNA interaction, catalytic site and so on. Thus unstructured regions may have important roles, therefore, detailed analysis of the unstructured regions are necessary to reveal functional mechanisms of proteins.

One of proteins that has unstructured region is high mobility group B2 (HMGB2). HMGB2 protein is homolog of HMGB1 and a member of a highly abundant class of nonhistone chromosomal protein in nuclei of higher eukaryotic cells [2-4]. HMGB2 contains two domains, called HMG box A and B, linked by unstructured linker. In addition, intact HMGB2 has carboxyl terminal region (C-tail) consisting of a continuous run of 23 acidic amino acids connected to box B through a joiner region [6]. For HMGB1, a closed

conformation in which the dynamically bound acidic tail makes extensive contact with the DNA-binding surfaces on the HMG boxes [7, 8]. In the presence of H1 or H5, the acidic tail of HMGB1 is displaced from the boxes by interaction with the basic C-terminal domain of the linker histone. In the resulting open conformation of HMGB1 the DNA-binding surface of the two boxes are free to bind DNA [9]. In previous study, for HMGB1, the DNA complex structure was determined by using chimera protein that was replaced A-domain with sex-determining region on the Y chromosome (SRY) that had sequence specificity for DNA binding [10].

The unstructured region of HMGB2 contains ten amino acid residues Y^{78}VPPKGDKKG^{87}. This linker region has high flexibility, therefore, HMGB1 AB di-domain structure determined in solution by NMR cannot determine the domain orientation. This result suggests that the interdomain linker just links the domains. In contrast, DNA bending functions of HMGB1 and 2 tandem domain are more efficiently than a single HMG box does [6, 11]. This result suggests that the linker has important role for the function of HMGB1 and 2. These two results are inconsistent. Therefore, there is something important function in the unstructured linker. In this study, I focused on the interdomain linker of HMGB2, and analyzed the effect of the linker to HMGB2 structure by NMR and small angle X-ray scattering (SAXS) and HMGB2 functions by DNA interaction assay.

In Chapter II, I present the result of the contribution of interdomain linker for HMGB2 structure. The interdomain linker of HMGB2 links N-terminal HMG box A and C-terminal HMG box B. The spectral comparison

with the fragment that box A and B linked by linker (HMGB2-AlB) and single box A and B showed that only the signal for single box A was significantly different from that of box A in HMGB2-AlB. It suggested that the interdomain linker interacted with only box A. Therefore, I tried to reveal the residue involved in the interaction by making site direct mutants of interdomain linker for HMGB2. As a result, Y78 was the critical residue for the box A and interdomain linker interaction. The ^{15}N edited NOESY spectra showed Y78 contacted with K8 and the contact was transient. Then, I analyzed relative domain orientation and whole structure for HMGB2-AlB wild-type and Y78G mutant by NMR and SAXS. As a result, for wild-type, the DNA binding surfaces of HMG box A and B were in the opposite direction and elongate shape than Y78G mutant. These results suggested that the interdomain linker had a role to define the HMGB2 whole structure transiently.

In Chapter III, it is known that HMGB2 has DNA binding and bending activity and the interdomain linker contributes to this function [6, 11]. Therefore, I analyzed the contribution of the interdomain linker for DNA binding and bending activity of HMGB2 wild-type and linker mutants (Y78G, P80G/P81G). As a result, the DNA binding ability was almost same for wild-type and mutants, on the other hand, the DNA bending activity showed differences. The bending activity of HMGB2 interdomain linker mutants were inefficient compared to that of wild-type. This result showed that the residues caused NMR spectral changes effected on the DNA bending activity of HMGB2.

In Chapter IV, I present the conclusions of Chapter II and Chapter III, and discuss the contribution of the interdomain linker for structure and function of HMGB2.

Chapter II

Preferential domain orientation of HMGB2 determined by the weak intramolecular interactions mediated by the interdomain linker

Abstract

High mobility group box protein 2 (HMGB2) contains homologous tandem HMG box DNA-binding domains, boxes A and B. These two boxes are linked by a short basic linker having a sequence characteristic of an intrinsically disordered element. The combined use of NMR and small angle X-ray scattering (SAXS) showed that the two boxes assume a preferred orientation to make their DNA binding surface in opposite directions, although the linker does not keep any specific conformation. A series of site directed mutations to the residues in the linker showed that a network of CH-π interactions changed the interdomain dynamics and their dynamic averaged orientation relative to the wild-type. This work demonstrates that the apparently unstructured linker plays a role in defining the preferential domain orientation through the intramolecular CH-π interactions, even though the interactions are weak and transient.

1. Introduction

Accurate view on the conformational state of the modular protein having the folding units joined by apparently unstructured short linkers should be essential for understanding its function. The type of proteins including intrinsically unstructured parts plays pivotal roles in biological processes through its structural flexibility that allows adopting various forms in binding to partner molecules [12]. In elucidating how the proteins work by using its structural plasticity, we have to see how the proteins work by using its structural plasticity, we have to see how the modular protein whose domain arraignment is artificially defined by crystal packing, in addition to the lack of the electron density for the flexible linker parts. NMR can give solution structures of such protein, but NOE-based distance restrains are often scarce in the dynamic interdomain linker, thus the obtained domain arrangements do not represent the realistic conformational state.

Alternative approaches are available for the structural elucidation of the modular proteins. Another type of NMR experiment using residual dipolar couplings (RDCs) provides long-range structural information that defines the relative domain orientation and interdomain dynamics [13-19]. Small angle X-ray scattering (SAXS) is also used for the same purpose by its ability to give molecular shape information [20]. Independent use of each approach, however, cannot accurately determine the structure of modular protein. The RDCs define the domain orientation but cannot give the inter-domain distance. SAXS gives rather limited structural details due to

its intrinsically low resolution, in particular for the cases of medium sized protein, although it can accurately determine the molecular radii [20]. NMR with the RDCs and SAXS are, therefore, the complementary methods in determining the modular protein structure determination [13, 14, 21].

High mobility group box 2 (HMGB2) protein consists of two DNA-binding domains, HMG boxes A and B and a short inter-domain linker ('l-region'), which connects the HMG boxes (Figure II-1a). HMGB2 and its homologous protein HMGB1 are non-histone chromosomal proteins abundant in eukaryotic cells [1-3]. HMGB1 and 2 share high sequence homology with their orthologues (Figure II-1a). The preceding works have solved the structures for the two HMG boxes in HMGB1, both of which showed characteristic 'L-shaped' structures [22, 23]. HMGB2 was also determined two HMG boxes A and B by Kurita and co-workers (PDB accession code: 1J3X and 1J3D, respectively). The roles for each HMG boxes were characterized; box A has preferential affinity to the deformed DNA structure, while the box B shows strong DNA binding and bending ability [12, 24]. The tandem aligned HMG boxes with different DNA binding ability have cooperative functions in DNA binding and inducing DNA bending [4, 5, 25]. The accumulated insights into the functional cooperation of the boxes in HMGB1 and 2 suggest that the spatial arrangement of the boxes has some functional meanings, which prompted us to see how the boxes in HMGB2 stay in solution with the combined use of NMR and SAXS.

In this work, we found the interdomain linker defines the relative domain orientation of the HMG boxes. A series of site-directed mutagenesis

to the linker showed that a part of the linker has specific contact with box A; which is mediated by a network of CH-π interactions [26] as elucidated by the box A structure in HMGB1 in comparison with the counterpart in HMGB2 determined in this work [23]. HMG boxes in the wild-type HMGB2 showed preferential orientation to locate their DNA binding surfaces in the opposite side of the molecule. The interdomain linker mutants having impaired CH-π interactions changed the relative domain orientation with increased interdomain dynamics. This finding adds another functional role associated with the interdomain linker of HMGB2.

2. Materials and methods

Plasmids

The cDNA encoding porcine HMGB2 was provided by Prof. Yoshida. The fragments of HMGB2 used in this work are schematically described in Figure II-1b; HMGB2-A (residues 1-77), HMGB2-B (88-165), HMGB2-Al (1-87), and HMGB2-AlB (1-165). The box A used in this work has C23S mutation to improve the sample stability according to the previous work [23]. The gene encoding each fragment was cloned into pET28a (Merck Chemicals, Germany) using *Nde*I and *Eco*RI sites Site-directed mutagenesis of HMGB2 was performed using QuikChange (Stratagene) and KOD-plus mutagenesis (Toyobo), to make the following mutants (P80G/P81G, K82G, D84G, K85G, K86G and Y78G).

Expression and purification of HMGB2 fragments

Each HMGB2 fragment was purified from *E. coli* grown in M9 minimal medium. For backbone assignment, medium also contained $^{15}NH_4Cl$ and ^{13}C glucose. The purification procedure is briefly described below. Cells were grown at 37 °C to OD_{600} = 0.6 and IPTG (isopropyl β-D-thiogalactopyranoside) was then added to the medium to induce protein expression (final conc. 0.5 mM). After induction, cell growth was continued for 5 h. Cells were collected by centrifugation and resuspended in buffer solution (50 mM Tris-HCl, pH 8.0; solution A), and then subjected to sonication. Cell debris was removed by centrifugation (15,000 rpm for 30 min) and supernatant was applied to a His-Trap affinity column (GE

Healthcare). The column was washed with solution A containing 20 mM imidazole followed by the elution of the His-tagged HMGB2 fragment by solution A containing 500 mM imidazole. The His-tag was cleaved by thrombin for 12 h at 4 °C in a dialysis bag in solution A. The resultant protein was applied to Hi-Trap SP cation-exchanger equilibrated by solution A. The desired protein was purified using a linker NaCl concentration gradient from 0 mM to 800 mM in solution A. The purified protein was dialyzed against buffer solution (50 mM sodium phosphate, pH 6.4) prior to use in NMR experiments. All HMGB2 fragments used in this work were obtained using the above protocol. A three-residue attachment from the construct, having the sequence, GSH, is attached to the N-terminal part of the proteins used.

NMR experiments

NMR experiments were performed using solutions typically containing 1 mM protein; the buffer solution used was 50 mM sodium phosphate, pH 6.4, containing 1 mM PefaBloc (Sinus Biochemistry and Electrophoresis GmbH). All experiments were performed at 293 K or 298 K on a Bruker DMX600 or DRX700 spectrometer. The backbone resonance assignments were determined for the fragments HMGB2-A, HMGB2-B, HMGB2-Al, and HMGB2-AlB using a standard set of triple resonance spectra [27] collected in non-uniform sampling manner [28] on a DMX600 spectrometer. 3D ^{15}N-edited NOESY (mixing time 100 ms) and ^{15}N-edited TOCSY (mixing time 40 ms) were also used for confirming the backbone

resonance assignments [27]. The triple-resonance data were processed with the Roland NMR toolkit [29]. The ^{15}N-edited NOESY and TOCSY data were processed using the program, NMRPipe [30]. The backbone resonance assignments were determined on the NMRview software platform [31] using the KUJIRA suites [32].

SAXS experiments

SAXS measurements were carried out at BL-10C, Photon Factory, Tsukuba, Japan [33]. The wavelength of the X-ray was adjusted to 1.488 Å using a Si monochromater. All samples were prepared in 50 mM sodium phosphate, pH 6.4, containing 5 mM DTT. The scattering profiles were collected at 20 °C using an online imaging plate detector (R-Axis VII, Rigaku). The exposure time was 10 min. The obtained two-dimensional data were circularly averaged, and then the final one-dimensional data was obtained by subtraction the profile of the sample buffer solution. To eliminate inter-particle interference from the observed profiles, a series of the profiles at five different concentrations, ranging from 17.5 to 3.5 mg/ml, were extrapolated to obtain that a concentration of zero.

Determining the alignment tensors for the HMG domains in HMGB2

The relative orientation of the HMG domains in the HMGB2-AlB fragment was estimated based on the alignment tensors obtained for each domain. The alignment induced TROSY shift changes were used to determine the alignment tensor for each HMG domain, which is referred to

as DIORITE [16, 33]. Because of the 'L-shape' of each HMG domain and the entirely extended structure of the HMGB2-AlB fragment, which has two HMG domains, the signals showed severe broadening under weak-alignment conditions; most of the anti-TROSY components on the IPAP-HSQC [35] spectra for the HMGB2-AlB fragment showed poor signals or disappeared. The alignment tensor determination was done according to the procedure described in our previous paper using optimized ^{15}N CSA tensor parameters [33]. The ^{15}N CSA tensor used for the residues in α-helix was $\Delta\sigma$ = -173.0 ppm, η = 0.23, and β = 19.8°. In the present analysis, the ^{15}N CSA tensor value that is specific for α-helix was used.

The weak-alignment of proteins was achieved using stretched acrylamide gels [36]. Acrylamide and *N,N'*-methylenebisacrylamide (bis-acrylamide) copolymer was prepared at a monomer concentration of 5% with a 75 : 1 molar ratio of acrylamide to bis-acrylamide. Polymerization was achieved using 0.05% (w/v) ammonium persulfate (APS) and 0.2% (v/v) *N,N,N',N'*-tetramethlyethane-1,2-diamine (TEMED). One gel was cast in a Teflon block to make a rod of 4 mm diameter, which was used as the ' reference gel'. The other gel was a rod with an ellipsoidal cross-section having 7 mm and 5 mm diameters, which was used as the 'aligning gel'. The gels were extensively dialyzed against buffer (50 mM sodium phosphate, pH 6.4), for over three days to completely remove residual reagents from polymerization. Gels were then soaked in 250 µl protein solution containing 1 mM protein. The solutions were incubated at 4 °C for three days to allow complete uptake of protein into the gel rod. Each gel was inserted into an

NMR tube with open ends (New Era) using a Teflon device having a tapered head [37]. The NMR tube was sealed at one end with an Ultem plug (New Era). At the other end, 50 µl sample solution was poured onto the gel and sealed with an inner rod position to exclude the solution squeezed from the gel, the sample was subjected to NMR measurement.

Before TROSY measurements, the ^{2}H split was measured to correct the chemical shift drift caused by residual quadrupole splitting of the ^{2}H signal used for the frequency lock. In the HMGB2-AlB fragment experiments, the residual quadrupole ^{2}H split was kept around 2 Hz for the weakly aligned samples. The reference chemical shifts were measured for the sample in the reference gel, where protein is not aligned but is dissolved in the same acrylamide non-stretched gel. It was confirmed that no ^{2}H split was observed for the sample solution in the reference gel.

The NMR refined structure coordinate HMGB2-A and B domains were used for the alignment tensor calculation; PDB codes for boxes A and B are 1J3X and 1J3D, respectively.

The error estimation for the obtained tensor parameters was done by the jack-knife method [38]; 128 times with 10% of the experiment data reduction at random in each calculation. In random number generation, 'Mersenne twister' algorism [39] was used to improve the sampling.

Rigid-body minimization

The overall structure of the wild-type and Y78G mutant HMGB2-AlB were determined using the ΔδTROSY and SAXS data using XPLOR-NIH

2.31 software platform [40]: ΔδTROSY values were incorporated into the calculation as pseudo CSA (PCSA) restraints for amide nitrogen atoms [41], which assumes the ^{15}N CSA to the above values for the α-helix part. The used python routine was generated with modifications from the one for CSA restraints in XPLOR-NIH. In the calculation, the structures for boxes A and B were treated as 'rigid bodies' by keeping the coordinates fixed, while the residues in the N-terminal and interdomain linkers were allowed to have free dihedral angle rotations during the calculation [17, 18]. In the calculation, a low-temperature torsion angle dynamics simulated annealing, followed by a standard conjugate gradient minimization [17, 18]. The calculation procedure used for determining the overall structure of HMGB2-AlB with the residual PCSA (RPCSA) and SAXS scattering data as structural constraints followed the preceding work [42].

The initial structures for the wild-type and Y78G mutant, which were subjected to the rigid-body refinement, were generated in the following way. The box A in the wild-type HMGB2-AlB was generated from the box A in HMGB1 (PDB: 1AAB) [23] by the homology modeling with the program MODELLER 9v8 [43]; the generated box A structure has altered orientation in the third helix and attached C-terminal segment comprising residues 78-84. In the case of the Y78G mutant, the box A NMR structure (residues 1-77) was used without any modifications. The box B structure (residues 88-165) was the NMR structure determined in this work. The HMGB2-AlB structure coordinate was generated by combining the boxes A and B with the computer generated interdomain linker (residues 85-87 for the wild-type,

and residues 78-87 for the Y78G mutant) followed by energy minimization by XPLOR-NIH.

Liner peptide titration experiments

Synthetic peptide having the same sequence as the linker, Ac-YVPPKGDKKG-NH_2, was purchased in an HPLC purified grade (GL Biochem, Shanghai, China). The peptide was dissolved in NMR buffer (50 mM sodium phosphate, pH 6.4), and its pH was adjusted to pH 6.4 using 0.1 M NaOH solution. The peptide was titrated against ^{15}N-labeled HMGB-A or HMGB2-AlB fragment solutions at 0.7 mM protein. A series of HSQC spectra were collected for the samples with different molar ratios of the peptide (0.2, 0.5, 1.0, 1.5, 2.0 and 4.0) against the HMGB2 fragments.

3. Results and discussion

Specific interaction of the interdomain linker with box A revealed by chemical shift changes

The primary sequence of box A and B in HMGB2 are shown with those of the homologous HMGB1 proteins and the orthologous (Figure II-1a): the boxes A and B domain consist of the residues 1-77 and 88-165, respectively (Figure II-1b) [24]. It is noted that the residue number adopted here is for the immature HMGB proteins having initial methionine.

The sequence position of the box A in this work is different from that defined in the homologous HMGB1 box A (residues 1-84) [23]; the present box A position was defined according to the original report on HMGB2 by Yoshida and co-workers [12, 24]. The box A in HMGB2 (residues 1-77) was determined based on the HMGB1 box A structure [22, 44]: the HMGB1 box A has the structured part ended at T77 and the following segment, residues from Y78 to E84, is rich in amino acids of Pro, Gly, and Lys, which segment can be recognized as an unstructured linker due to its characteristic amino acid compositions (Figure II-1a) [45]. In also considering the box B structure [22], the part of the residues 78-87 in HMGB2 was defined as the interdomain linker in this work (Figure II-1, shown in green). The box B position in HMGB2 was defined as for the case of HMGB1 [22]. The fragments used in this work are schematically summarized with domain structures of the entire protein (Figure II-1b); the interdomain linker is denoted as 'l', and the 'Al' stands for the fragment having the domain A with the interdomain linker, for example.

The ^{1}H-^{15}N heteronuclear single quantum coherence (HSQC) spectra for the fragments HMGB2-A, B and AlB are overlaid for comparison (Figure II-2a): each spectrum with resonance assignments is in Figures II-3, 4 and 5. The spectral comparison showed the significant differences between the signals for HMGB2-A and the box A in HMGB2-AlB, while the signals for HMGB2-B mostly overlapped to those of the box B in HMGB2-AlB (Figure II-2a and b). The observed chemical sift differences are plotted against the residue number of HMGB2-AlB (Figure II- 2c). The chemical shift changes were observed in the limited parts of box A, which may demonstrate that the inter-domain linker, $Y^{78}VPPKGDKKG^{87}$, specifically interacts with the N- and C- termini of the box A. The residues showing the changes over the average plus one standard deviation (σ), and those in the rage from an average +0.5σ to +1.0σ are marked in red and orange on the HMGB2-A structure, respectively (Figure II-6a).

Estimation of the affinity of the interdomain linker to the box A using a synthetic peptide

We elucidate the affinity of the inter-domain linker to the box A by the NMR titration experiments using a synthetic peptide of the sequence, Ac-YVPPKGDKKG-NH_2. The four equimolar amount of the peptide input to ^{15}N-labeled HMGB2-A caused no apparent spectral change (data Figure II-7). The linker has, thus, only limited affinity to the box A; the K_D should be greater than 2×10^{-4} M, in assuming that a 1% population of the bound from gives observable spectral changes.

The same peptide was titrated to the ^{15}N labeled HMGB2-AlB fragment, which also caused no apparent spectral changes (data not shown).

The results showed that the interdomain linker has limited affinity to the box A in HMGB2; its tethering to the parts in the box A, which showed the significant spectral changes.

The interdomain linker contact to box A is primarily mediated by Y78

The spectral comparison between the HMGB2-AlB and Al fragments has shown that the signals for HMGB2-AlB (data Figure II-8a and b). Plot for the chemical shift changes along the residue number demonstrated no apparent spectral differences for the box A part between HMGB2-Al and HMGB2-AlB fragments (data Figure II-8c). In focusing on the residues in the interdomain linker, two amide-containing residues ($Y^{78}V^{79}$) in the N-terminal four-reisdue segment, $Y^{78}VPP^{81}$, showed the signals resonating very close to those of the corresponding part in the AlB fragment (data Figure II-8c). The two residues are in remarkable contrast to the following interdomain linker residues, 82-87, showing apparent spectral changes; the changes should be ascribed to the end-effect by the truncation of the following part originally existing in the AlB (Figure II-8). Although the four-residue segment, residues 78-81, is apparently unstructured in the HMGB1 box-A structure (Figure II-6) [23], the spectral comparison between the Al and AlB fragments shows the N-terminal two residues, at least, in the interdomain linker should specifically contact to the box A, irrespective of the existence of the following part (Figure II-8c).

A series of the site-directed mutation to the residues in the interdomain linker was done to identify the residues primarily engaged in the contact to box A (Figure II-9). The results demonstrated that the Y78G mutation mostly reproduced the spectral changes observed for the spectral comparison between the HMGB2-AlB and HMGB2-A fragments (Figure II-10b and 2c); P80G/P81G mutation, also caused spectral changes, but the change were rather limited to the C-terminal part of the box A (Figure II-10). Y78 was, thus, identified as the primarily responsible for the interdomain linker contact to the box A.

Structural insight into the interdomain linker contact to box A

The structural details were explored in respect to the interaction between the interdomain linker and the box A (Figure II-6b). HMGB2-A lacks the segment ($Y^{78}VPPK^{82}$) that follows the structural part, while the box A in HMGB1 has the C-terminal extension as a part of the interdomain linker ($Y^{78}IPPKGE^{84}$) (PDB accession code: 1AAB) (Figure II-6c) [23]. HMGB1 and 2 have high sequence identity (Figure II-1a); the HMGB1 box A, residues 1-84, has only 11 different residues against the box A in HMGB2 (87% sequence identity) (Figure II-1a). The high sequence identity allows for exploring the binding mode of the interdomain segment, $Y^{78}VPPK^{82}$, to the box A through the structural comparison of the boxes A in HMGB1 and 2 (Figures II-6a and b).

The five-residue segment, $Y^{78}VPPK^{82}$, in the HMGB1 box A contacts the N-terminal part through Y78 (Figure II-6b). The side chain contacts in

the NMR structure suggest that they are mediated through CH-π interactions; Y78 ting moiety may play as an acceptor π-system for CH donors in P80, K8 and P9 (Figure II-6d). Similarly, Y71 may also be in the CH-π interactions with P9 and K12 (Figure II-6d); the Y71 mediating interactions were noted as hydrophobic contacts in the original report on the structure of box A in HMGB1 (Figure II-6b) [23]. Because Y78 is in the floppy part in the overlaid structure presentation, the intramolecular interactions mediated by Y78 were not focused in that original report [23].

The CH-π interaction is a type of non-bonded interaction giving a stabilization energy of about 0.5-1.0 kcal/mol per interaction, being comparable to single hydrogen bond; CH-π interaction is formed between aliphatic CH donors and aromatic π-acceptors as in tyrosine-rings [26]. The structural details in the atomic interactions associated with Y71 and Y78 are summarized in Table 1, which demonstrate that they are recognized as CH-π interactions according to the criteria defined in previous report [26].

The role of Y78 found in the HMGB1 box A structure, which mediates the interactions between the interdomain linker and box A, consistently explains the chemical shift changes by Y78G in HMGB2-Al fragment (Figure II-10b): the spectral changes caused by the lack of the C-terminal part, after Y78, to the residues in the box A in HMGB2 were mostly reproduced by the Y78G mutation to the HMGB2-Al (Figures II-2c and 10b). The residues showing the significant spectral changes by Y78G are consistent with the residues in the CH-π interaction network (Figure II-6a and b).

Y78 in the unstructured interdomain linker, therefore, may direct the

linker and the C-terminal half of the third helix of the box A in HMGB2, as expected by the structure comparison (Figure II-6c). It should be noted that the interdomain segment of the residues 78-84 in HMGB1 box A is not fixed in that conformation, but it may be in a dynamic equilibrium between the bound and unbound states (Figure II-6c): the distance restraints from NOEs bias the contact form of the segment. The structure fluctuation is evident for the interdomain segment by the low $^{15}N\{^{1}H\}$ NOE values, less than 0.5 (Figure II-8). The Y78 mediated interactions to direct the interdomain segment, therefore, should be weak and transient.

The role of Y78 in connecting the interdomain segment to box A was confirmed by the ^{15}N edited NOESY spectra (Figure II-11): the NOE signal between K8 amide proton and Y78 ring proton (Hε) was observed in the HMGB2-Al and the wild-type HMGB2-AlB (Figure II-11a and b), whilst the corresponding NOE signal was absent in the HMGB2-AlB (Y78G) mutant (Figure II-11c). It is noted that the NOE intensity observed between the residues K8 and Y78 in the wild-type HMGB2-AlB was extremely small relative to the sequential NOE between amide protons of K7 and K8, which may also suggest that the Y78 mediated interdomain segment contact to box A is transient (Figure II-11b).

The change in the dynamics of the interdomain linker by the mutation to Y78

The engagement of Y78 in the transient interactions of the interdomain linker to box A was found as described above. The changes in

the dynamics, in psec-nsec time range, of the interdomain linker by Y78G and P80G/P81G mutation were elucidated by $^{15}N\{^{1}H\}$ NOEs (Figure II-12).

The P80G/P81G mutation slightly increased the order of the interdomain linker and also that of the C-terminal segment down-stream of the third helix (residues 72-77) but significantly reduced the order of G4 (Figure II-12a). The unexpected increase in the order of the interdomain linker may be related to the intrinsically elongated shape of the polyglycine sequence as revealed SAXS analysis [46]. The Y78G mutant reduced the order of the linker and the part of the residues 69-77 following the third helix (Figure II-12b).

The change in the $^{15}N\{^{1}H\}$ NOE profile for the Y78G mutant demonstrated that the impaired CH-π network mediated by Y78 increased the flexibility of the linker segment (Figure II-12b). The loss of the Y78 mediated interactions should have made the closed contact forms between the linker and the box A less populated. Although the Y78 mediated CH-π interactions have limited stabilization energies, the lack of them significantly increased the flexibility of the linker.

The altered reorientation dynamics of the tandem HMG boxes caused by linker mutation

The changes in the fluctuation of the interdomain linker by mutations, P80G/P81G and Y78G, should alter the interdomain dynamics in HMGB2-AlB. The interdomain dynamics was elucidated through the alignment tensors determined by the residual pseudo-^{15}N CSA (RPCSA),

which are measured as the TROSY chemical shift differences between the isotropic and aligned states [15, 16, 33, 41].

The observed ΔδTROSY shift changes, TROSY, induced by weak-alignment are shown on the overlaid spectra for the wild-type, P80G/P81G and Y78G mutants (Figure II-13a-c, left). The correlations between the observed and back calculated ΔδTROSY values using the alignment tensors for the boxes A and B are also shown (Figure II-13a-c, right). In considering the possible structure difference between the isolated box A lacking the C-terminal segment $Y^{78}VPPK^{82}$ and the box A in the HMGB2-AlB (Figure II-6c), we limited the residues used in the alignment tensor calculation for the box A; the residues having shown the chemical shift changes by mutations were omitted (see Section 2 and the legend to Table 2). The determined alignment tensors and the root mean square deviation (rmsd) values, with corresponding Q-factors, between the observed and back calculated ΔδTROSY are listed Table 2. The good correlations between the observed and back calculated values, as evidenced by the small values for the rmsds and Q-factors, credit the tensors are well determined.

The alignment tensor magnitude, *D*a, shows the extent of the domain reorientation dynamics. The larger difference in *D*a values between boxes A and B demonstrates the increased independency for their reorientation motions [14]. Significant difference in *D*a values was observed between boxes A and B in both P80G/P81G and Y78G mutants, while the *D*a values were coincident within the errors for wild-type (Table 2). The greater alignment magnitude, as indicated by large *D*a value, for box B than for box A show

that box B has preferential contact with the alignmedium [14]. The changes in the aligning magnitudes for the protein (Table 2) show the two boxes in the wild-type HMGB2-AlB reorient within the restricted space, whilst the boxes in the Y78G mutant reorient rather independently. The boxes in P80G/P81G mutant, showing the moderate differences in *D*a values imply the less significant interdomain dynamics relative to Y78G mutant.

The $^{15}N\{^{1}H\}$ NOE profiles for the P80G/P81G and Y78G mutants shared the cooperative reduction in the values for G4 and G83 relative to the wild-type (Figure II-12). The increased flexibility to the parts including G4 and G83 residues, thus, may be responsible for enhancing the interdomain dynamics, irrespective of the flexure of the following segment to the residues; G83, in contact to G4, might play as a joint to link the reorienting domains (Figure II-12).

The wild-type HMGB2-AlB showed close alignment tensor magnitudes, *D*a and *D*r, between boxes A and B, which allows for determining the relative domain orientation by the alignment tensors of the individual domains. P80G/P81G and Y78Gmutants, instead, showed significantly different alignment tensor magnitudes, therefore their domain orientations are not readily determined [13, 14, 47]. In the mutants, two domains simply described as in a pronounced motion in a cone with approximate half angles of the bounding cone for P80G/P81G and Y78G, 47° and 53°, respectively [47].

Relative domain orientation of the boxes A and B in HMGB2-AlB

The pair-distance distribution functions $P(r)$ from SAXS measurements for the wild-type and Y78G mutant HMGB2-AlB fragments were compared (Figure II-14). The profiles were significantly different; the wild-type has greater values over the mutant in the longer pair-distance (r) region over 30 Å (Figure II-14). This observation may imply that the boxes in the wild-type HMGB2-AlB are populated to form more extended forms relative to the Y78G mutant (Figure II-14). The Kratky plots for the wild-type and Y78G mutant showed the increased unfolded structural parts in the mutant, as demonstrated by the greater values for the mutant in the q-range greater than 0.3 $Å^{-1}$ (Figure II-15).

The RPCSA values for boxes A and B and the scattering data from SAXS measurements for the wild-type HMGB2-AlB were directly used as structural restraints to determine the entire structure: it is noted that the RPCSA-based structure calculation was possible due to the close aligning magnitudes for the boxes A and B in the wild-type HMGB2-AlB (Table 2). The structures fulfilling the experimental restraints from RPCSA and SAXS were obtained by the rigid-body minimization using XPLOR-NIH (Figure II-16). The SAXS scattering profile was reproduced within experimental errors by the resultant structure (Figure II-16a), while the correlation between the observed and back calculated $\Delta\delta$TROSY values became worse relative to those for the isolated domains (Figures II-16b and 13a): the reduced correlation would come from the neglecting interdomain dynamics assumed in the present calculation, which is significant in reality. In spite of the reduced fitting quality, the correlation for the RPCSA was still good,

which implies the interdomain dynamics in the wild-type HMGB2-AlB should be rather limited. The lowest energy structure, the best consistent structure with the experimental data, is depicted in the ribbon representation (Figure II-17a), which demonstrates the dynamically averaged structure for the HMGB2-AlB in solution. It is noted that the sole SAXS data without RPCSA merely ambiguously defines the domain orientation, although the ensemble structures reproducing the SAXS scattering profile share the extended arrangement of the boxes (Figure II-18).

Because of the larger domain dynamics for the Y78G mutant, as evident by the mismatch in the alignment tensor magnitudes for the boxes, the RPCSA based orientation restraints cannot be used to determine the structure. The entire structure of the Y78G mutant was calculated by only SAXS data; the structure giving the closest scattering profile to the observed data is depicted (Figure II-17b). The structure comparison demonstrates that the wild-type has more elongated structure than that of the Y78G mutant (Figure II-17), which is consistent with the $P(r)$ profiles (Figure II-14). The relative domain angle differences between the wild-type and Y78G seems close to the estimated half angle of the bounding cone, 52°, which was calculated from the difference in the alignment magnitudes between the boxes A and B in Y78G mutant (Table 2) [47].

(a)

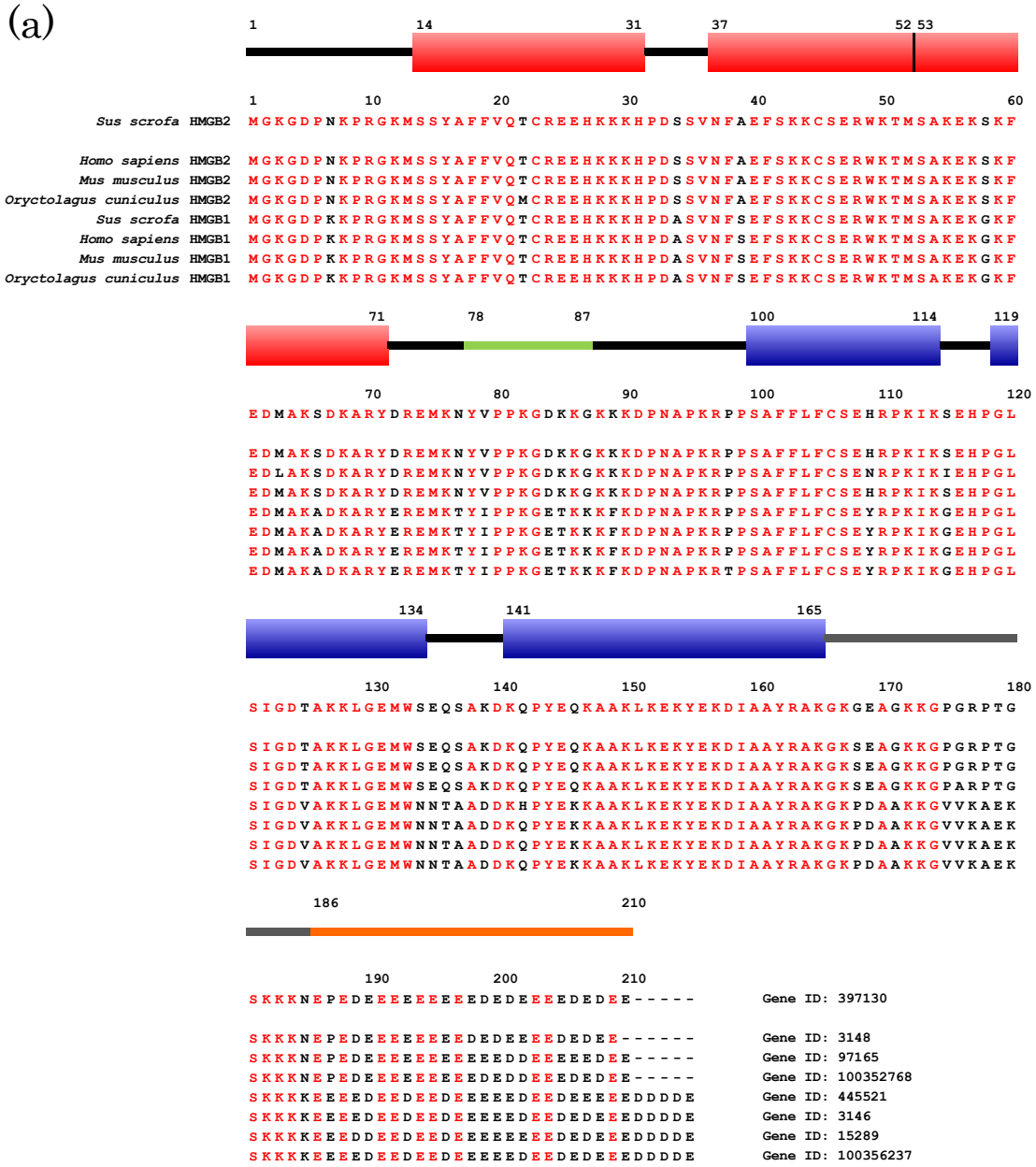
1 14 31 37 52 53
1 10 20 30 40 50 60
Sus scrofa HMGB2 MGKGDPNKPRGKMSSYAFFVQTCREEHKKKHPDSSVNFAEFSKKCSERWKTMSAKEKSKF
Homo sapiens HMGB2 MGKGDPNKPRGKMSSYAFFVQTCREEHKKKHPDSSVNFAEFSKKCSERWKTMSAKEKSKF
Mus musculus HMGB2 MGKGDPNKPRGKMSSYAFFVQTCREEHKKKHPDSSVNFAEFSKKCSERWKTMSAKEKSKF
Oryctolagus cuniculus HMGB2 MGKGDPNKPRGKMSSYAFFVQMCREEHKKKHPDSSVNFAEFSKKCSERWKTMSAKEKSKF
Sus scrofa HMGB1 MGKGDPKKPRGKMSSYAFFVQTCREEHKKKHPDASVNFSEFSKKCSERWKTMSAKEKGKF
Homo sapiens HMGB1 MGKGDPKKPRGKMSSYAFFVQTCREEHKKKHPDASVNFSEFSKKCSERWKTMSAKEKGKF
Mus musculus HMGB1 MGKGDPKKPRGKMSSYAFFVQTCREEHKKKHPDASVNFSEFSKKCSERWKTMSAKEKGKF
Oryctolagus cuniculus HMGB1 MGKGDPKKPRGKMSSYAFFVQTCREEHKKKHPDASVNFSEFSKKCSERWKTMSAKEKGKF
71 78 87 100 114 119
70 80 90 100 110 120
EDMAKSDKARYDREMKNYVPPKGDKKGKKKDPNAPKRPPSAFFLFCSEHRPKIKSEHPGL
EDMAKSDKARYDREMKNYVPPKGDKKGKKKDPNAPKRPPSAFFLFCSEHRPKIKSEHPGL
EDLAKSDKARYDREMKNYVPPKGDKKGKKKDPNAPKRPPSAFFLFCSENRPKIKIEHPGL
EDMAKSDKARYDREMKNYVPPKGDKKGKKKDPNAPKRPPSAFFLFCSEHRPKIKSEHPGL
EDMAKADKARYEREMKTYIPPKGETKKKFKDPNAPKRPPSAFFLFCSEYRPKIKGEHPGL
EDMAKADKARYEREMKTYIPPKGETKKKFKDPNAPKRPPSAFFLFCSEYRPKIKGEHPGL
EDMAKADKARYEREMKTYIPPKGETKKKFKDPNAPKRPPSAFFLFCSEYRPKIKGEHPGL
134 141 165
130 140 150 160 170 180
SIGDTAKKLGEMWSEQSAKDKQPYEQKAAKLKEKYEKDIAAYRAKGKGEAGKKGPGRPTG
SIGDTAKKLGEMWSEQSAKDKQPYEQKAAKLKEKYEKDIAAYRAKGKSEAGKKGPGRPTG
SIGDTAKKLGEMWSEQSAKDKQPYEQKAAKLKEKYEKDIAAYRAKGKSEAGKKGPGRPTG
SIGDTAKKLGEMWSEQSAKDKQPYEQKAAKLKEKYEKDIAAYRAKGKSEAGKKGPARPTG
SIGDVAKKLGEMWNNTAADDKHPYEKKAAKLKEKYEKDIAAYRAKGKPDAAKKGVVKAEK
SIGDVAKKLGEMWNNTAADDKQPYEKKAAKLKEKYEKDIAAYRAKGKPDAAKKGVVKAEK
SIGDVAKKLGEMWNNTAADDKQPYEKKAAKLKEKYEKDIAAYRAKGKPDAAKKGVVKAEK
SIGDVAKKLGEMWNNTAADDKQPYEKKAAKLKEKYEKDIAAYRAKGKPDAAKKGVVKAEK
186 210
190 200 210
SKKKNEPEDEEEEEEEEEDEDEEEEDEDEE-----
Gene ID: 397130
SKKKNEPEDEEEEEEEEEDEDEEEEDEDEE------
Gene ID: 3148
SKKKNEPEDEEEEEEEEEDEEEEEDEDEE-----
Gene ID: 97165
SKKKNEPEDEEEEEEEEEDEDDEEEDEDEE-----
Gene ID: 100352768
SKKKKEEEEDEEDEEDEEEEEDEEDEEEEEDDDDE
Gene ID: 445521
SKKKKEEEEDEEDEEDEEEEEDEEDEDEEEDDDDE
Gene ID: 3146
SKKKKEEEDDEEDEEDEEEEEEEEDEDEEEDDDDE
Gene ID: 15289
SKKKKEEEEDEEDEEDEEEEEDEEDEDEEEDDDDE
Gene ID: 100356237

(b)

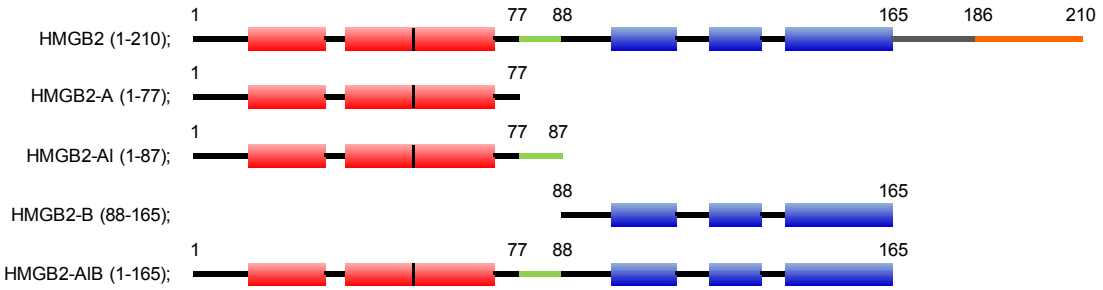
HMGB2 (1-210);
1 77 88 165 186 210
HMGB2-A (1-77);
1 77
HMGB2-AI (1-87);
1 77 87
HMGB2-B (88-165);
88 165
HMGB2-AIB (1-165);
1 77 88 165

Figure II-1

Multiple alignment of HMGB2 and HMGB1 ortholog sequences from four representative species, which was prepared by ClustalW [48] (a). Gene ID and the species are indicated for each sequence. The HMGB2 sequence from Sus scrofa is shown on the top line, with the secondary structures defined in the NMR structures of boxes A and B (PDB: 1J3X and 1J3D). The domains in HMGB2 are defined as: box A (residues 1–77), linker (residues 78–87), box B (residues 88–165), joiner (residues 166–185) and the acidic tail (186–210). Identical amino acids are shown in red. The residue C23 in the present HMGB2 was changed to serine to increase the sample stability [16]; the residue is marked with asterisk. Schematic drawings of the HMGB2 fragments used in this work with full-length HMGB2 indicated at the top (b). The 'l' denotes the linker region (residues 78–87); Al and AlB stand for the fragments of box A with the linker and boxes A and B linked by the linker, respectively.

(a)

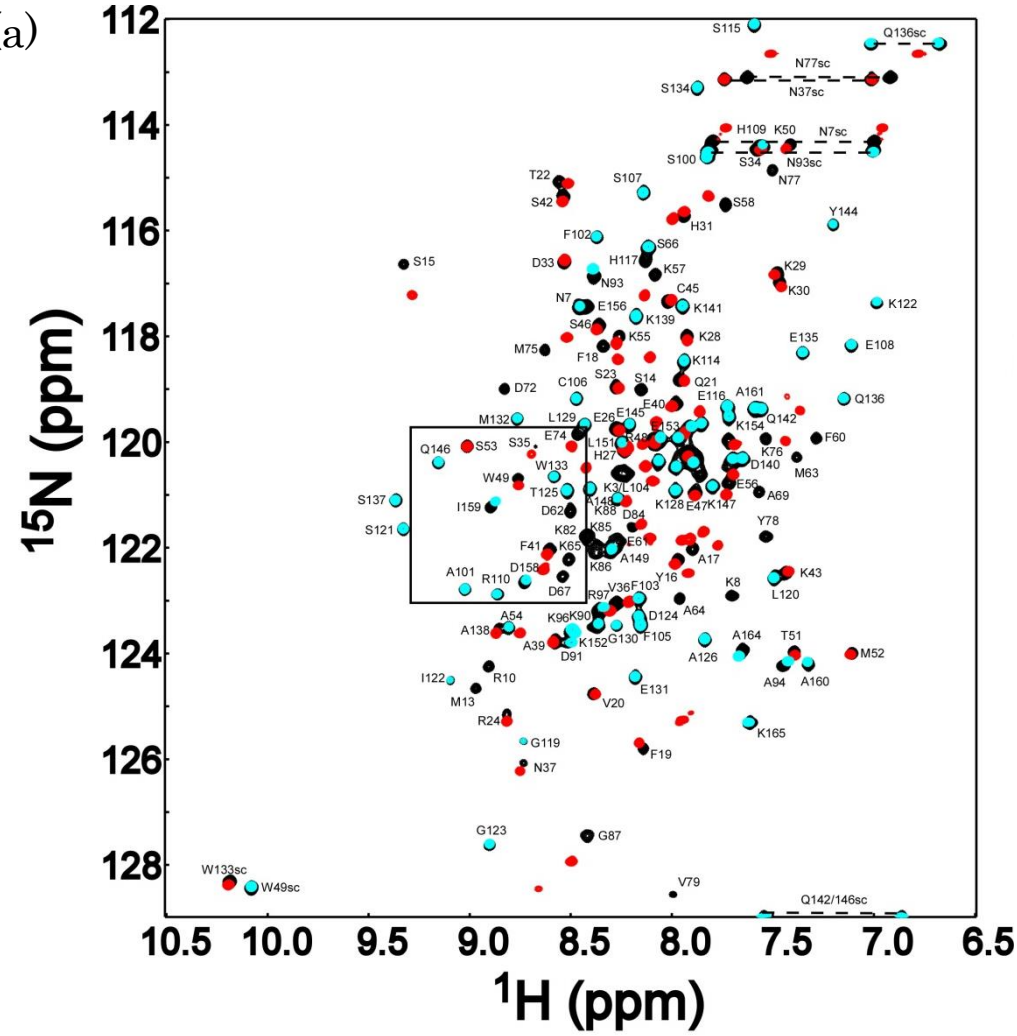

112
114
116
118
120
122
124
126
128
15N (ppm)
10.5
10.0
9.5
9.0
8.5
8.0
7.5
7.0
6.5
1H (ppm)

(b)

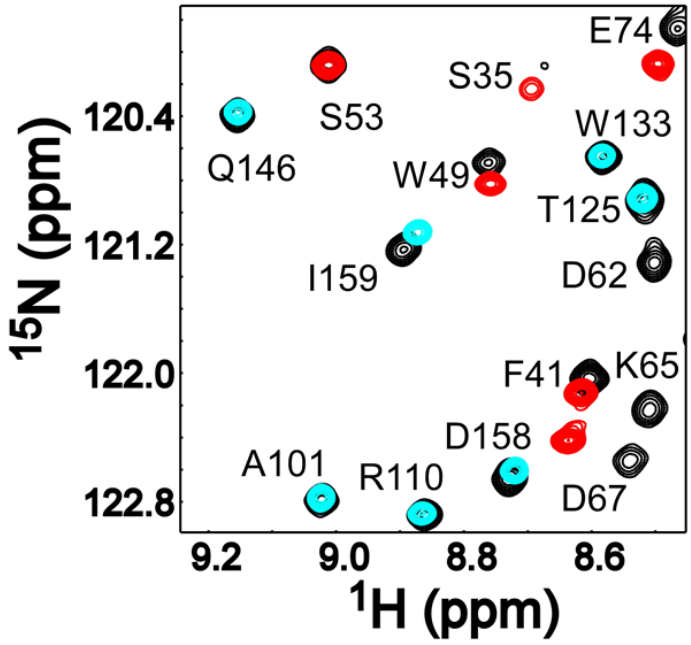

E74
S35
S53
W133
Q146
W49
T125
I159
D62
F41
K65
D158
A101
R110
D67
120.4
121.2
122.0
122.8
15N (ppm)
9.2
9.0
8.8
8.6
1H (ppm)

(c)

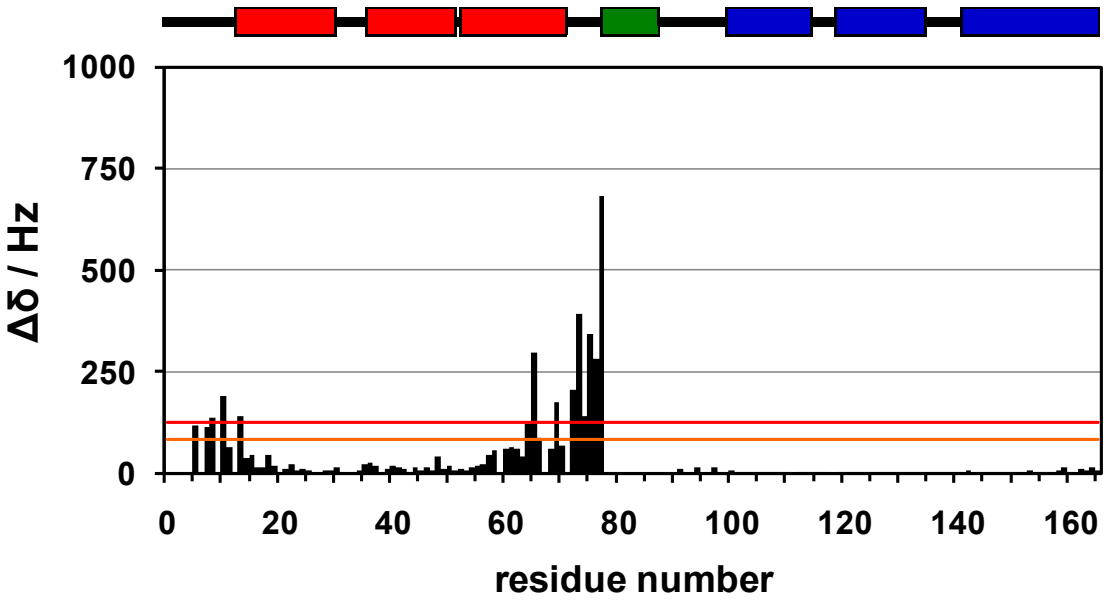

Figure II-2

^{1}H-^{15}N HSQC spectra for HMGB2-A (red) and HMGB2-B (cyan) overlaid onto that for HMGB2-AlB with the resonance assignments (black) (a). Expanded part (boxed in a) of the overlaid ^{1}H-^{15}N HSQC spectra (b). The chemical shift differences observed between the spectra for HMGB2-AlB and those for HMGB2-A and HMGB2-B are plot against the residue number (c). Changes in backbone ^{1}H-^{15}N shifts ($\Delta\delta$) are shown in Hz units. The lines represent the values of the average change plus one (red) and half (orange) standard deviations, respectively. The colored boxes on the top of the graph represent the positions for the helices in the HMGB2-AlB, which were determined by the NMR analyses in this work.

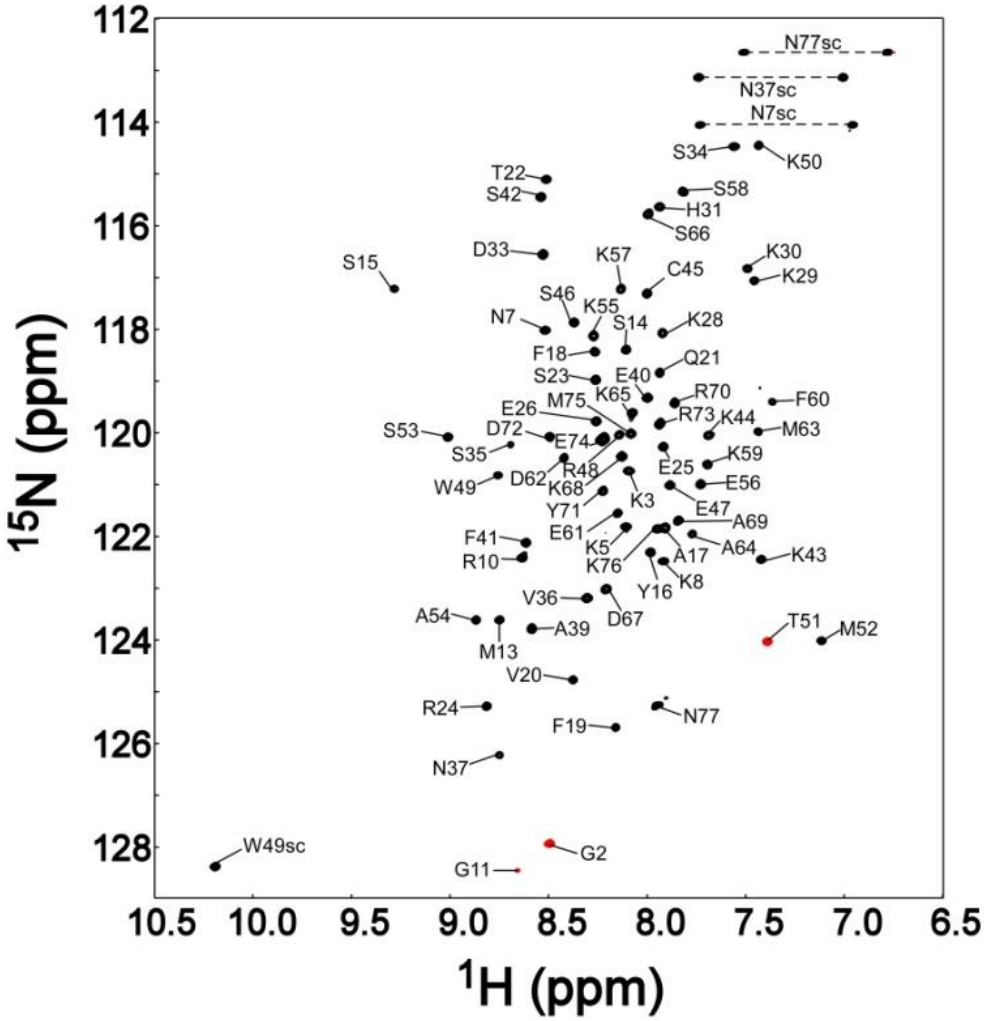

Figure II-3

Backbone resonance assignment for boxes A fragment drawn on the ^{1}H-^{15}N HSQC spectrum.

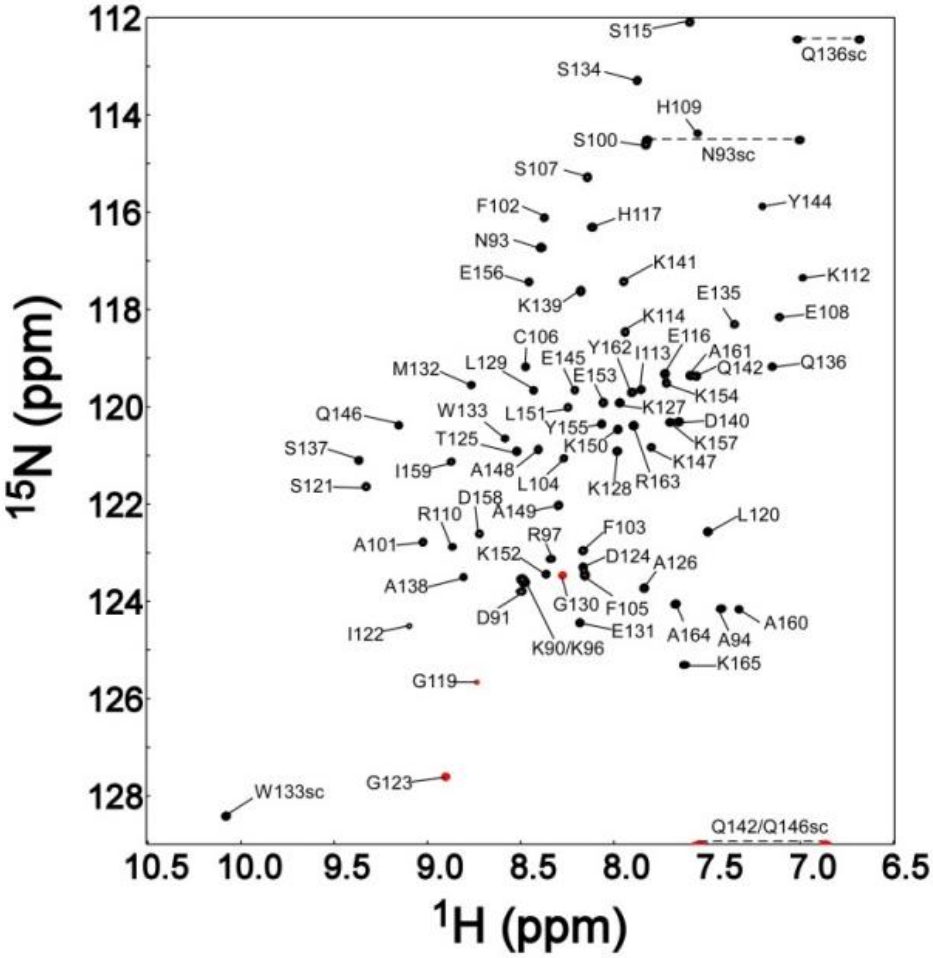

Figure II-4

Backbone resonance assignment for box B fragment drawn on the ^{1}H-^{15}N HSQC spectra.

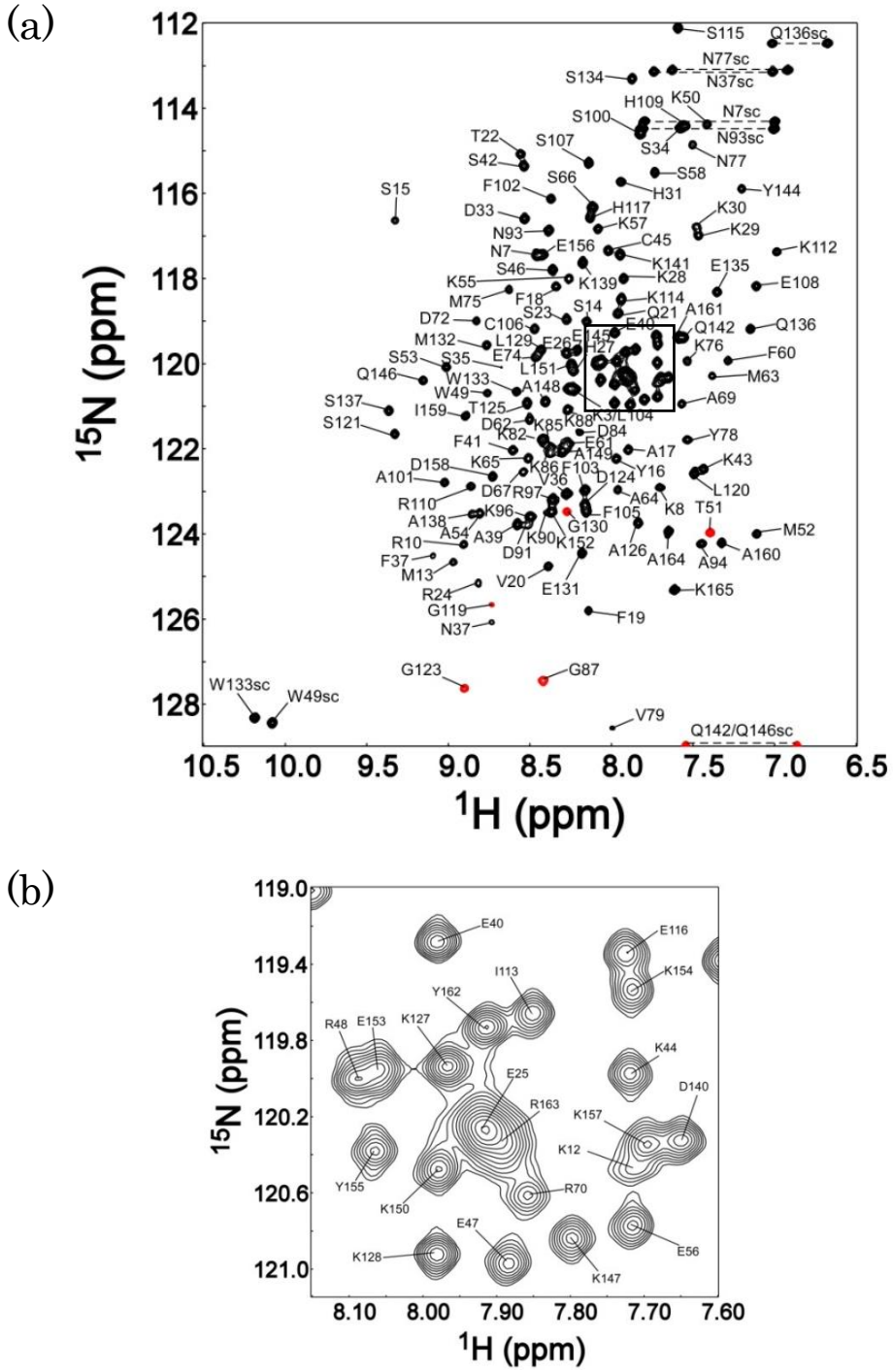

Figure II-5

Backbone resonance assignment for AlB fragment drawn on the ^{1}H-^{15}N HSQC spectrum (a). The expanded spectrum (b) corresponds to the boxed part in the spectrum for the AlB fragment (a).

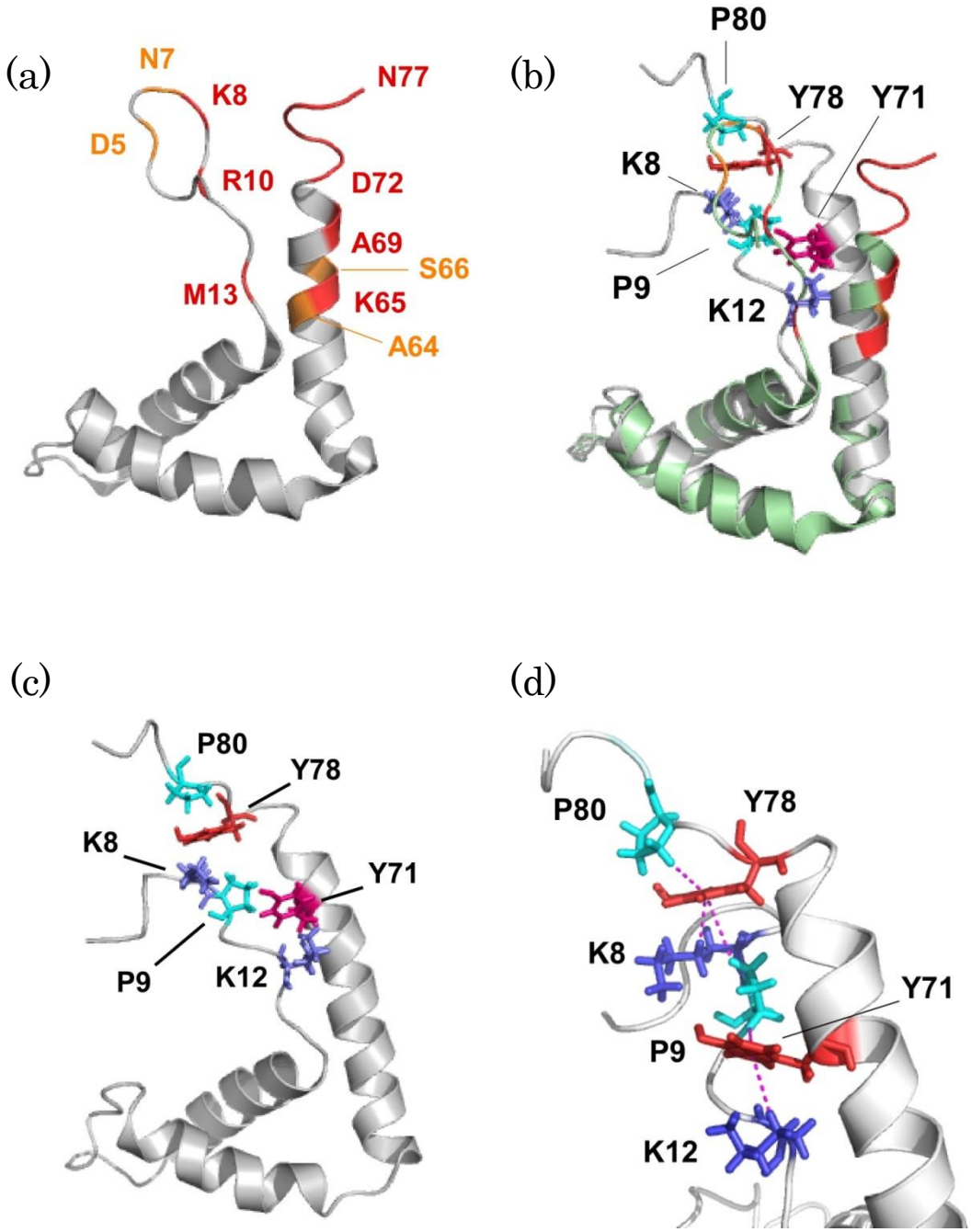
(a)
N7
K8
N77
D5
R10
D72
A69
S66
M13
K65
A64
(b)
P80
Y78
Y71
K8
P9
K12
(c)
P80
Y78
K8
Y71
P9
K12
(d)
P80
Y78
K8
Y71
P9
K12

Figure II-6

HMGB2-A residues that showed significant chemical shift differences in the spectral comparison with HMGB2-AlB (Figure II-2a) are colored on the NMR structure (PDB: 1J3X) (a); the residues in red and orange showed chemical shift changes over the lines in red and orange in Figure II-2a, respectively. The residues in possible CH-π interactions are drawn in ball-and-stick format on the NMR structure of HMGB1 box A (PDB: 1AAB) (b): two tyrosine residues Y71 and Y78 are colored in red and orange, respectively, while prolines and lysines are colored in cyan and dark blue, respectively. Overlay of the structures of box A in HMGB1 (gray) and of box A in HMGB2 (green) (c). The potentially interacting residues in box A of HMGB1 are shown in the ball-and-stick representation and the residues showing significant chemical shift differences in box A in HMGB2 are colored as in Figure II-6a. The structure overlay was calculated to maximally fit the backbone atoms (N, Cα, C') in the helical parts; H1 (residues 15–29), H2 (39–51) and H3 (54– 71). The calculation was performed using the program PyMol (Schrödinger, LLC) and the rmsd for the atomic displacement was 1.1 Å. A close-up view of the potentially interacting residues in box A in the HMGB1 structure (d). The pseudo atom position was assumed to be the center of the aromatic ring in the distance calculations for the parts defined by the dotted lines.

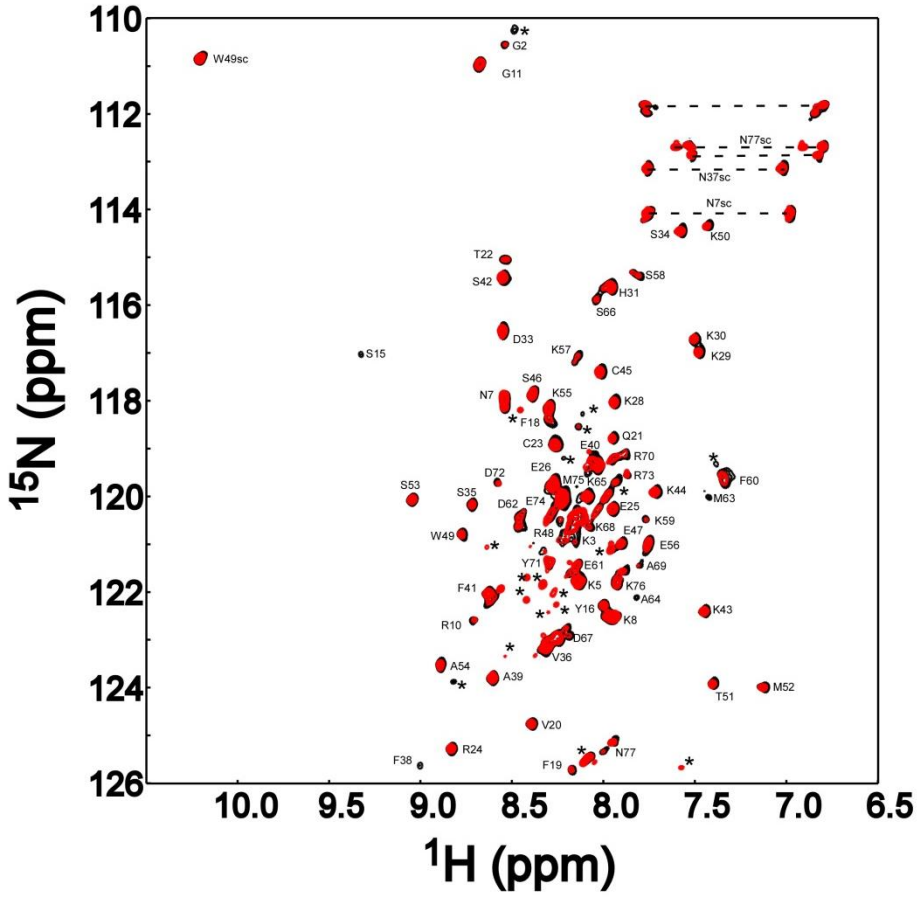

Figure II-7

Interaction of the inter-domain linker peptide and the ^{15}N-labeled wild-type HMG2B-A. The ^{1}H-^{15}N HSQC spectrum for the wild-type HMGB2-A in the absence of the peptide (black) is overlaid by the spectrum for the sample containing twice the equimolar amount of linker peptide, Ac-YVPPKGDKKG-NH_2, to HMGB2-A (red). Apparently no significant spectral change was observed between the two spectra. On the spectra, a small number of signals from the degraded protein components were observed due to the long storage after sample purification, which are marked with asterisks. The partial degradation of the sample does not affect the result, because no spectral changes were observed for both the intact and the marked signals upon titration of the peptide.

(a)

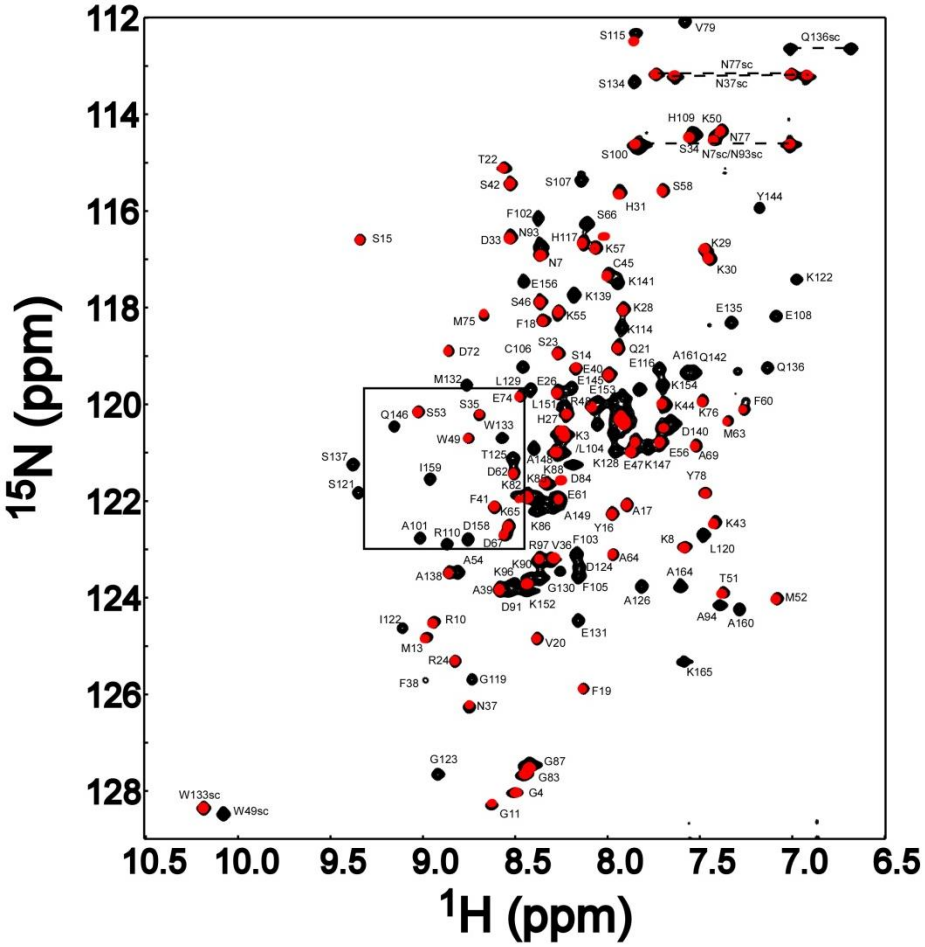
112
114
116
118
120
122
124
126
128
15N (ppm)
10.5
10.0
9.5
9.0
8.5
8.0
7.5
7.0
6.5
1H (ppm)

(b)

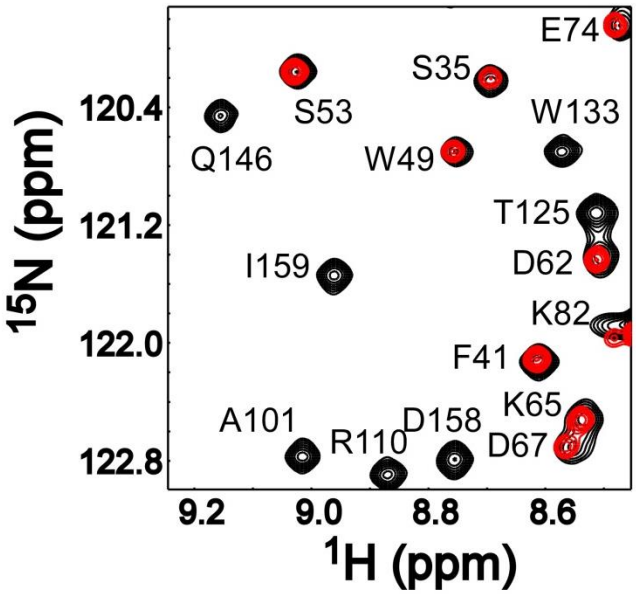
E74
S35
S53
W133
Q146
W49
T125
D62
I159
K82
F41
K65
A101
D158
R110
D67
120.4
121.2
122.0
122.8
15N (ppm)
9.2
9.0
8.8
8.6
1H (ppm)

(c)

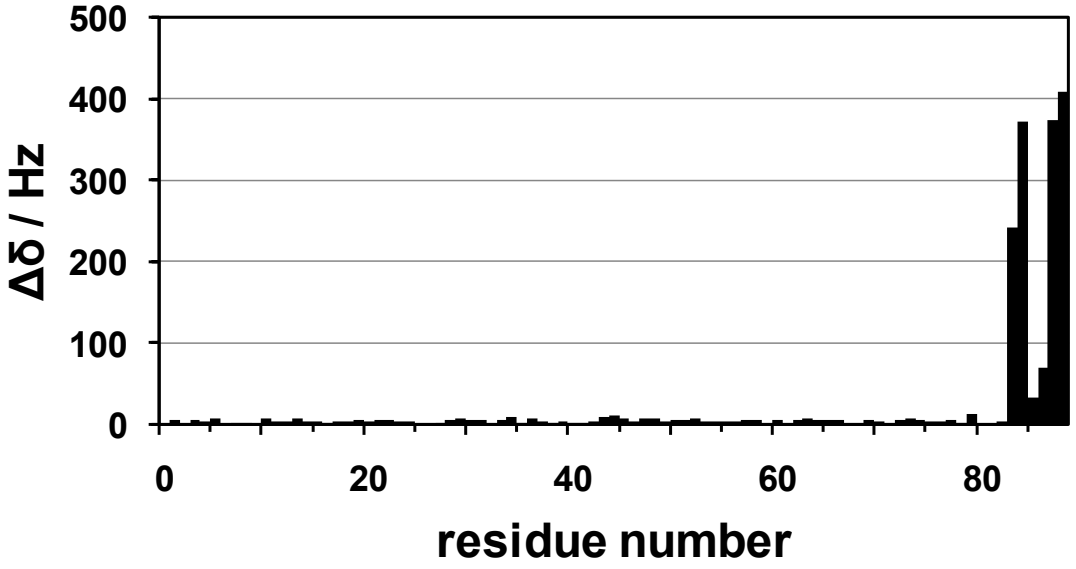

Figure II-8

^{1}H-^{15}N HSQC spectral comparison between the HMGB2-AlB (black) and HMGB2-Al (red) fragments (a). Expanded part (boxed in a) of the overlaid spectra (b). The chemical shift differences observed in the spectral comparison between the HMGB2-AlB and HMGB2-Al fragments (c). The chemical shifts for the residues in box A are almost the same as those in the HMGB2-AlB and HMGB2-Al fragments. The significant chemical shift differences were found for the C-terminal residues in the HMGB2-Al fragment, which can be ascribed to the end-effect by the truncation of box B. The data were collected at 293 K due to the instability of the HMGB2-Al fragment at 298 K, at which temperature the data in Figure II-2 were collected.

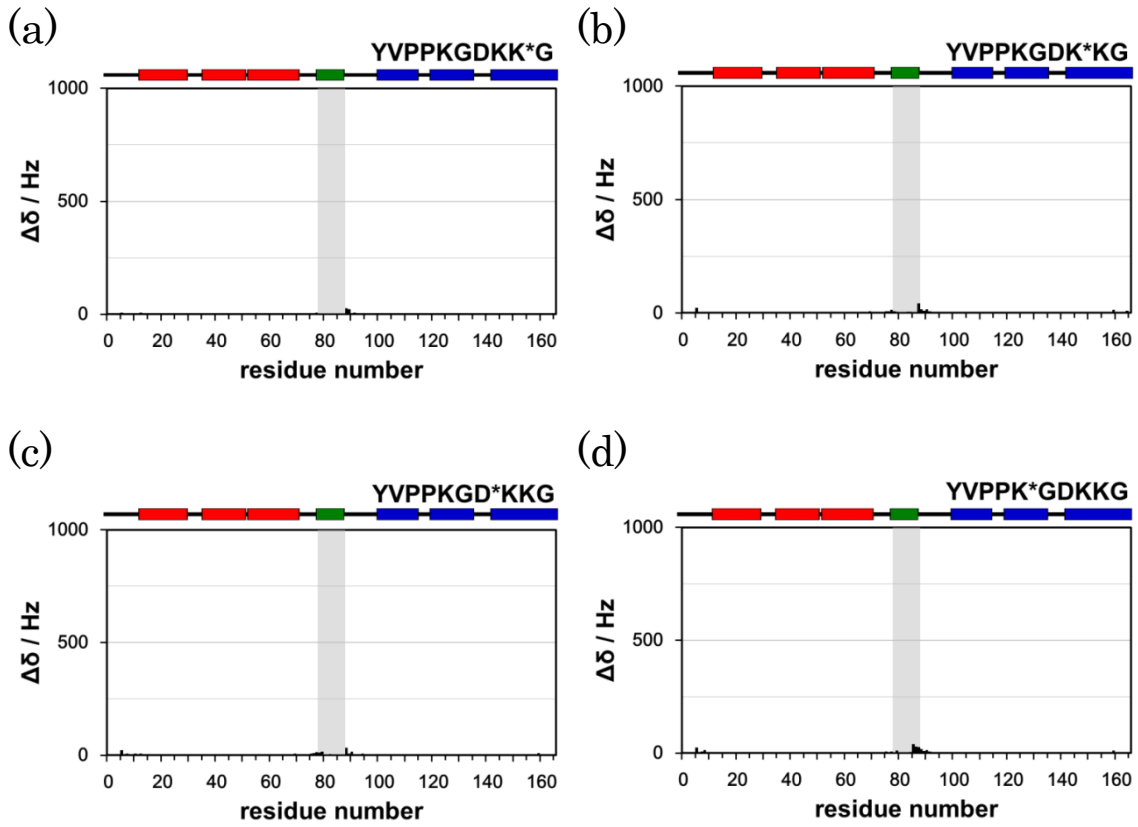

Figure II-9

Chemical shift changes induced by site-directed mutation in the linker. The chemical shift changes in the backbone ^{1}H-^{15}N signals induced by each site-directed mutation are plotted in Hz units against the residue number. Each mutation site is marked with an asterisk(s) on the linker sequence shown on the top right of each panel (a) – (d).

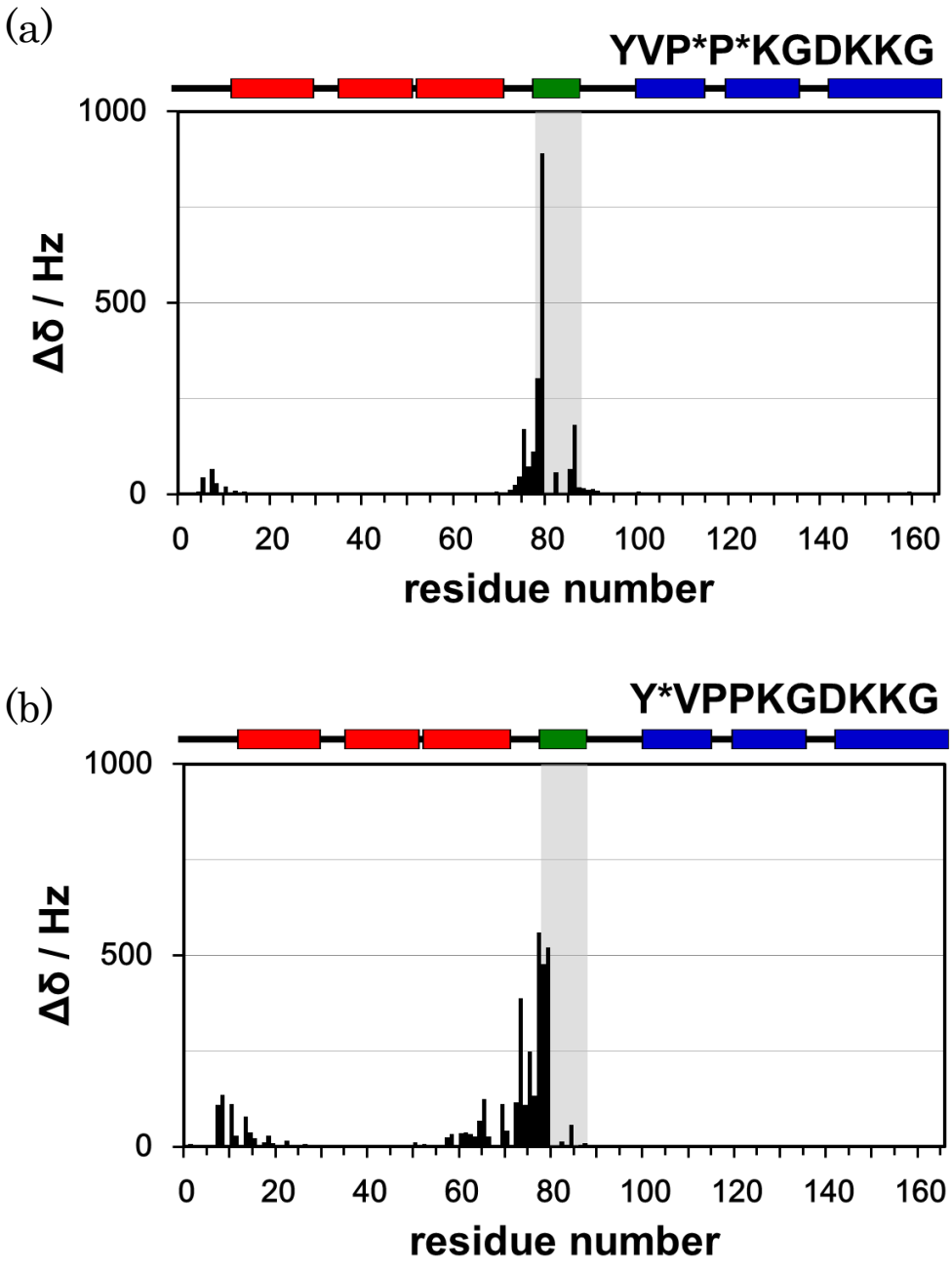

Figure II-10

Chemical shift changes caused by the mutations to the interdomain linker. Chemical shift differences observed on the ^{1}H-^{15}N HSQC spectra between the wild-type HMGB2-AlB and P80G/P81G mutant (a), and Y78G mutant (b). The colored boxes on each graph show the positions of the helices.

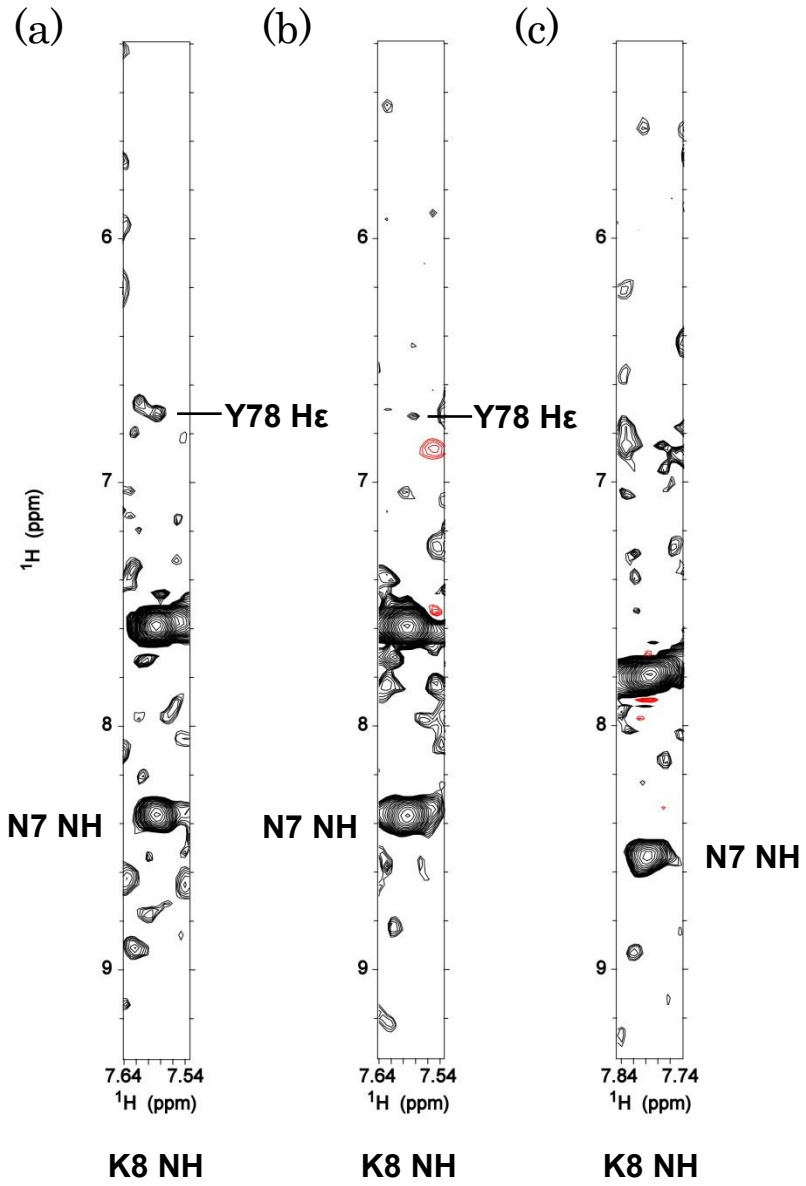

Figure II-11

Comparison of the ^{15}N-edited NOESY strips derived from K8 amide proton. K8 amide proton strip at 7.59 ppm (^{1}H) and 123.0 ppm (^{15}N) for HMGB2-Al (a) and HMGB2-AlB (wild-type) (b). The corresponding NOESY strip from K8 amide proton in HMGB2-AlB (Y78G) mutant at 7.79 ppm (^{1}H) and 122.1 ppm (^{15}N) (c). No NOE signal to G78 was observed from K8 amide proton in HMGB2-AlB (Y78G) mutant.

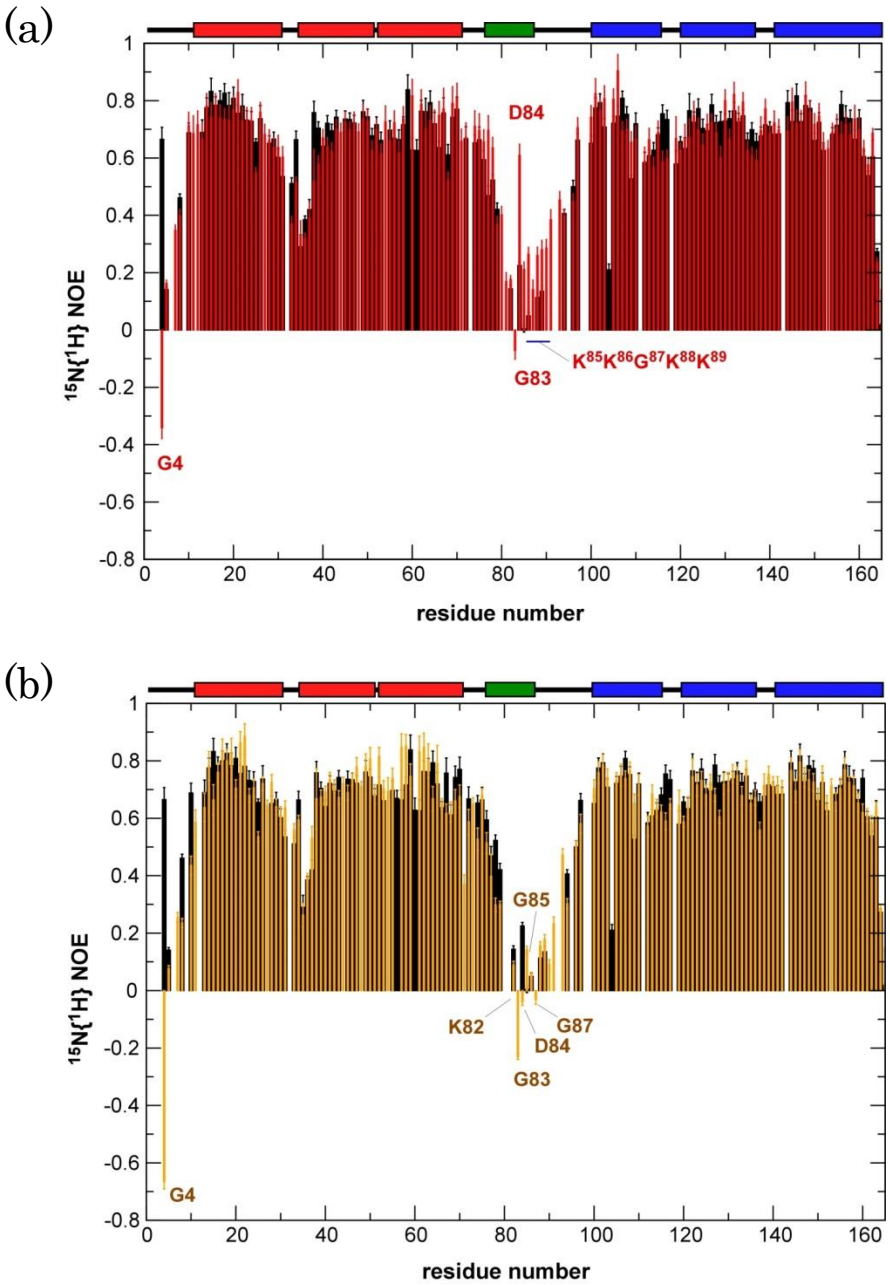

Figure II-12

Comparison of the $^{15}N\{^{1}H\}$ heteronuclear NOE profiles between the wild type and each mutant. The wild type (black bars) versus the P80G/P81G mutant (red bars) (a). The wild type (black bars) and the Y78G mutant (yellow bars) (b). The rectangular boxes above the graphs represent the positions of a-helices (red and blue boxes for boxes A and B, respectively) and the linker part (residues 78–87; green box).

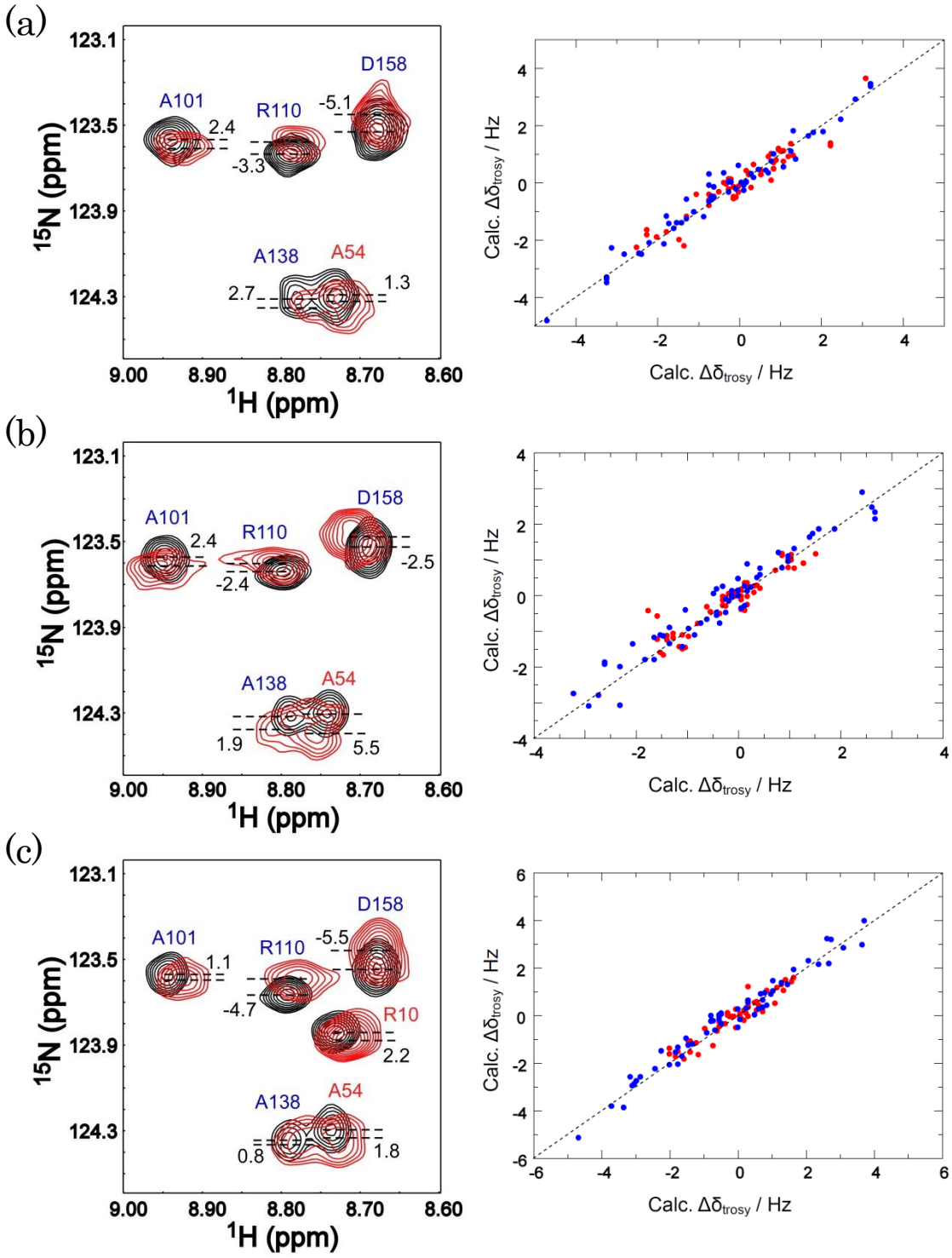
(a)
A101
R110
D158
A138
A54
2.4
-5.1
-3.3
2.7
1.3
(b)
A101
R110
D158
A138
A54
2.4
-2.4
-2.5
1.9
5.5
(c)
A101
R110
D158
R10
A138
A54
1.1
-5.5
-4.7
2.2
0.8
1.8
^{15}N (ppm)
^{1}H (ppm)
Calc. $\Delta\delta_{trosy}$ / Hz

Figure II-13

Alignment tensor determination based on the ^{15}N TROSY shift changes induced by weak alignment. The expanded part of the overlaid ^{1}H-^{15}N TROSY spectra collected for the protein in isotropic (black) and aligned (red) states; wild type (a), P80G/P81G mutant (b) and Y78G mutant (c). The chemical shift differences observed for the signals collected in the isotropic and aligned states are drawn on the spectra in Hz; the chemical shift correction for the aligned spectrum is not applied to those spectra displayed, which is required due to the residual quadrupole splitting of the deuterium lock signal. In the alignment tensor calculation, the correction to each shift difference was applied based on the directly observed deuterium signal in the aligned state. The correlation between the observed $\Delta\delta$TROSY and the back calculated $\Delta\delta$TROSY from the determined alignment tensor is plotted on the right side of each observed spectrum. In each correlation plot, blue and red dots represent data from the residues in box A and box B, respectively. In the calculations, only residues in the secondary structure parts were considered in calculation.

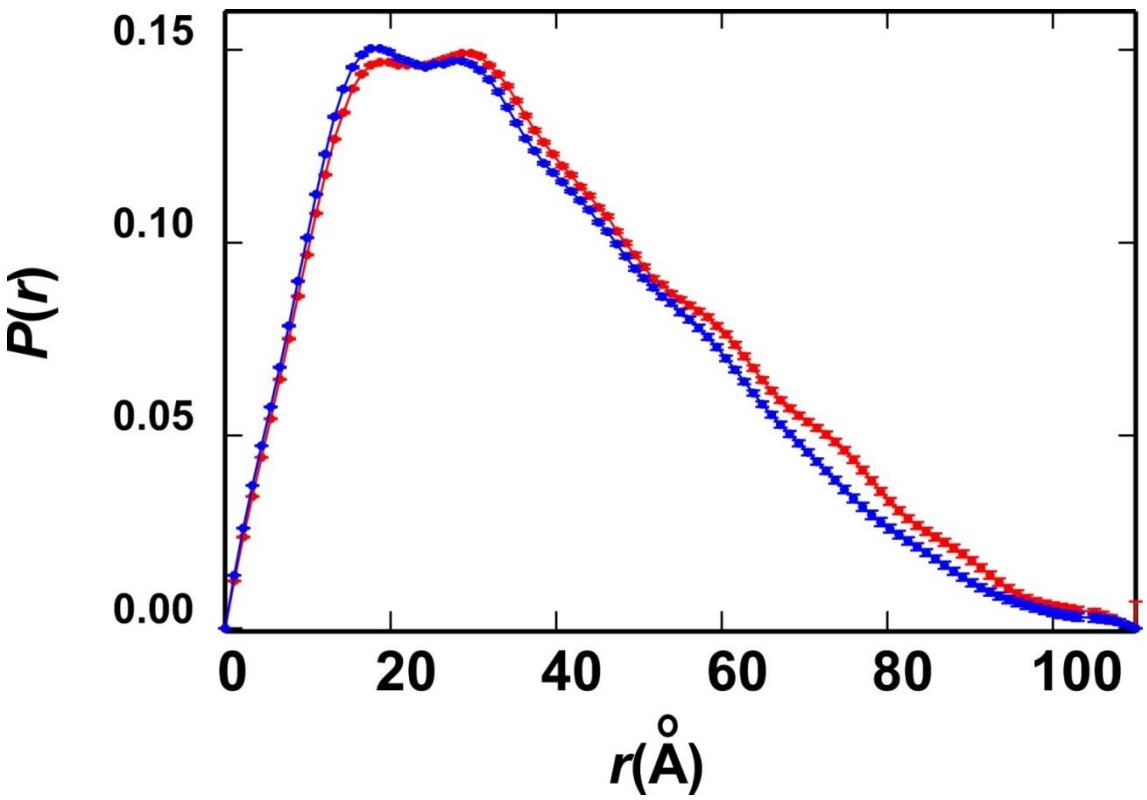

Figure II-14

Atom-pair distributions for HMGB2-AlB fragments. The *P*(r)-vs-r profiles for the wild-type and Y78G mutant are plot in red and blue, respectively

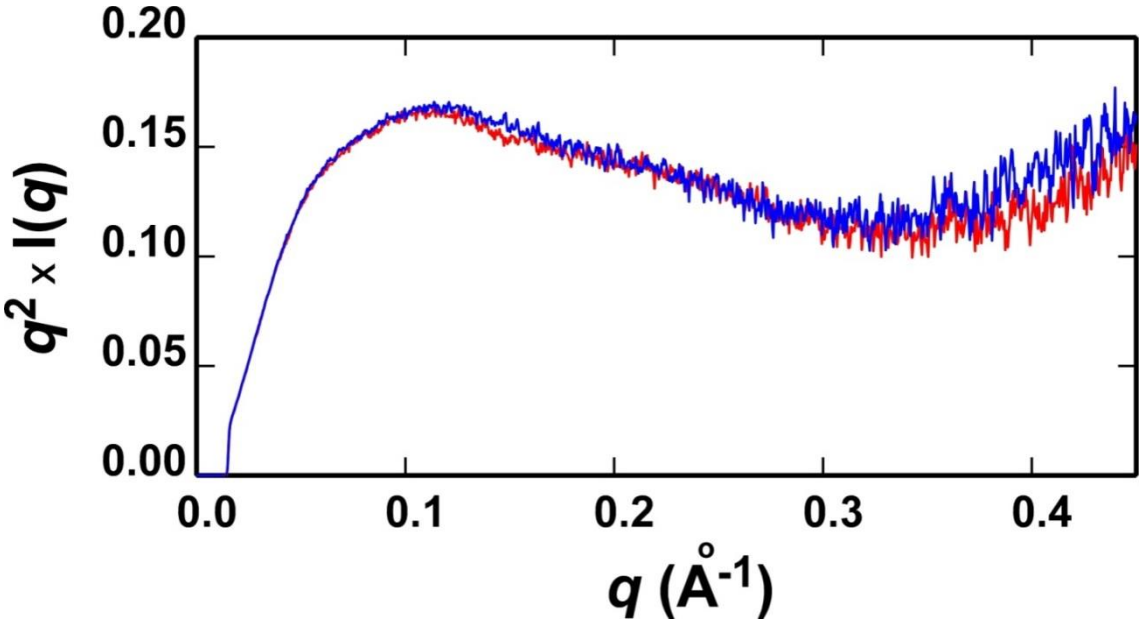

Figure II-15

Kratky plots for HMGB2-AlB wild-type and Y78G mutant. The plots for the wild-type and Y78G mutant are drawn in red and blue, respectively. The non-parabolic nature of the high q regions indicates the presence of the unstructured regions. The higher intensity in the high q region for Y78G relative to the wild-type shows the increased content of the unstructured regions by the Y78G mutation.

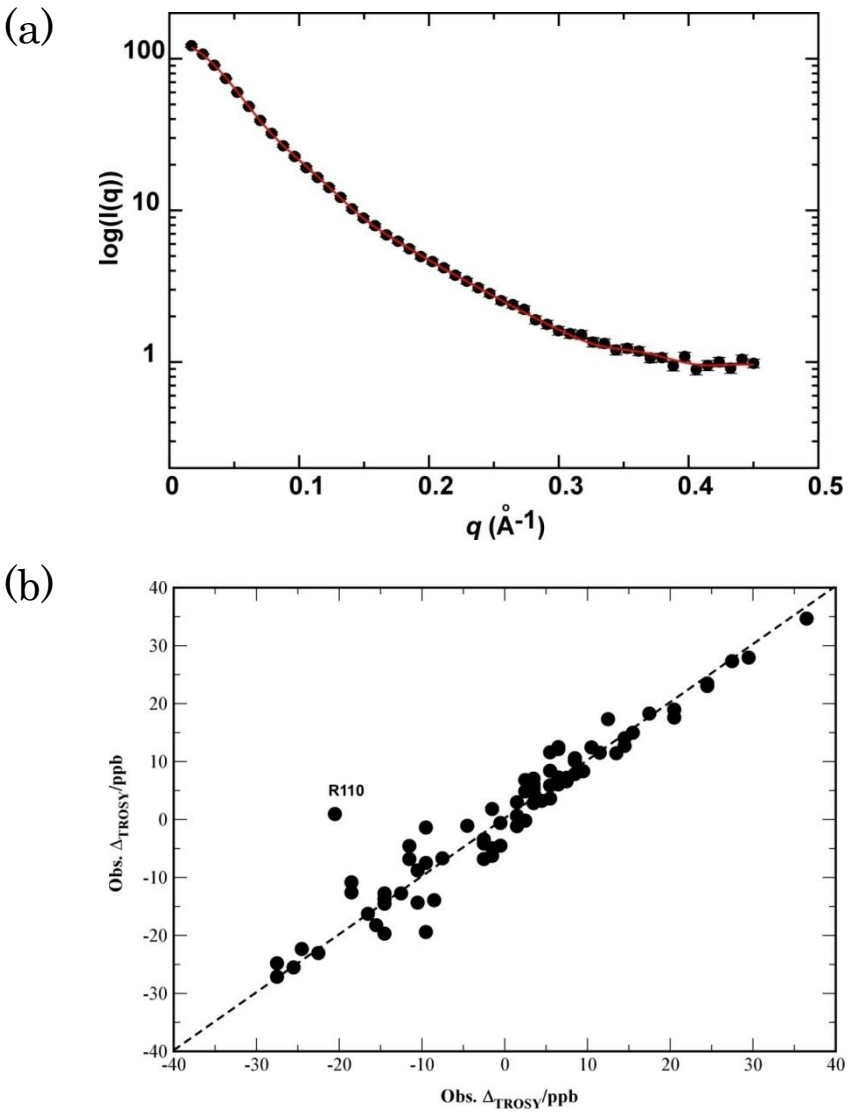

Figure II-16

Quality of the wild-type HMGB2-AlB domain arrangement determined using the RPCSA (ΔδTROSY) and SAXS derived restraints. Experimental scattering profile for the wild-type HMGB2-AlB (●) and the calculated scattering curve in red (a). The correlation between the experimental RPCSA (ΔδTROSY) values for the wild-type HMGB2-AlB and those calculated from the refined structure by XPLOR-NIH calculation (Figure II-17a) (b). Q-factor, and rmsd for the fitting quality against the experimental RPCSAs were 0.30, and 4.1 ppb (0.29 Hz), respectively.

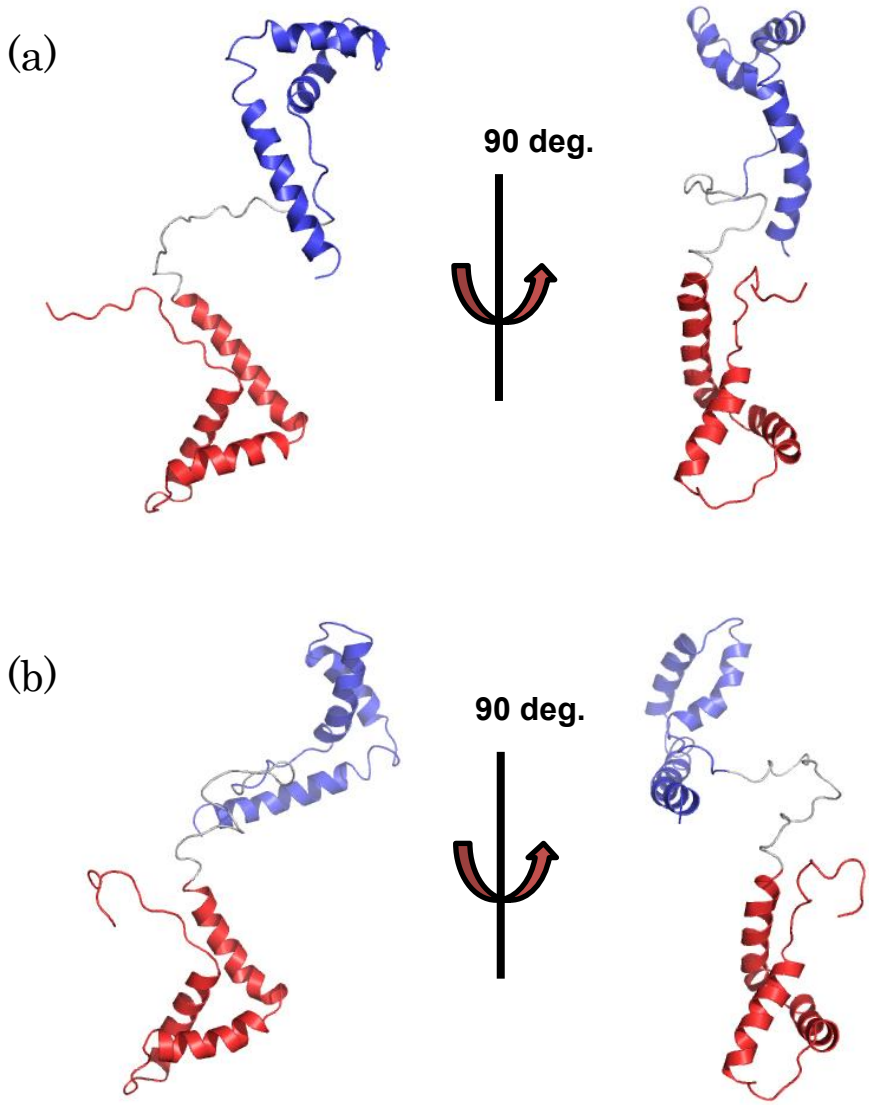

Figure II-17

Structures for the wild-type and Y78G mutant HMGB2-AlB. The lowest energy structure of the wild-type HMGB2-AlB refined by the constraints from RPCSA and SAXS (a). The lowest energy structure of the Y78G mutant HMGB2-AlB determined by only the constraints from the SAXS scattering data (b).

(a)

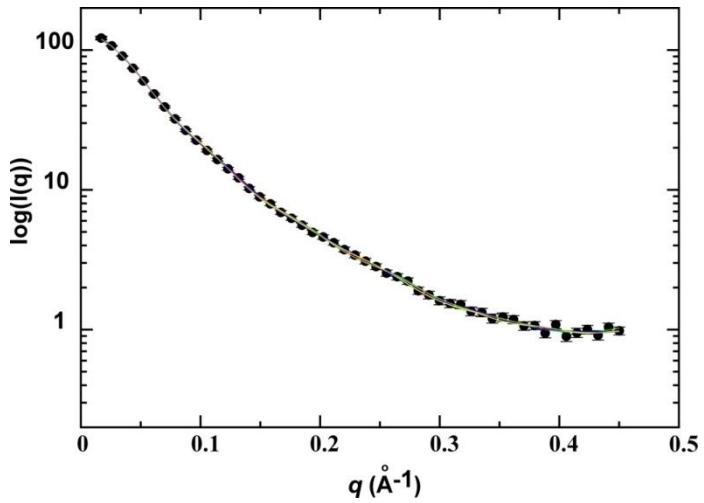

(b)

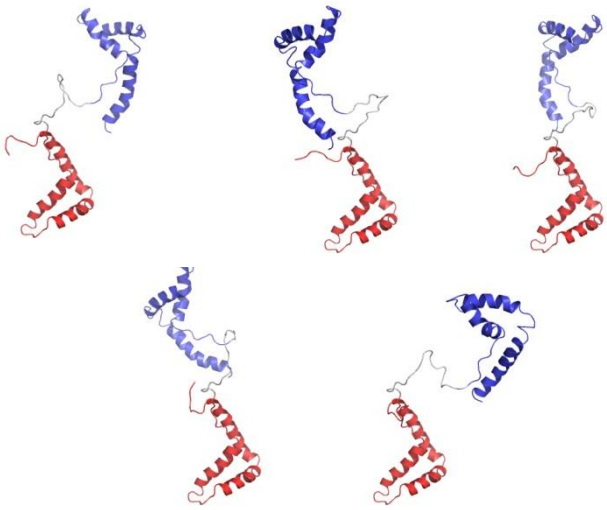

Figure II-18

Five lowest energy domain arrangements for the wild-type HMGB2-AlB obtained to reproduce the SAXS scattering profile. The rigid-body minimization using the SAXS scattering profile as the sole structural restraints reproduced the scattering profile within the errors (a). The five lowest energy structures are displayed in a ribbon representation with boxes A and B in red and blue, respectively (b). Without NMR restraints, the only using SAXS data cannot determine the relative domain orientation, although the obtained structures shared the extended shapes.

Table I-1

Distance and angles between the potential donor and acceptor groups in CH-π interactions found in the box A structure of HMGB1

PDB code[a]	Aromatic π-system as acceptor[b]	CH donor		$d_{C\text{-}X}$ (Å)[c]	Angle (C-H-X) (deg.)[c]
1AAB	Y71	P9	HB2	4.5 ± 0.4	125 ± 15
		K12	HG3	4.3 ± 0.5	125 ± 25
	Y78	K8	HG3	4.9 ± 0.8	126 ± 25
		P9	HD2	4.8 ± 0.7	110 ± 16
		P80	HD3	4.0 ± 0.3	144 ± 11
2YRQ	Y71	P9	HB2	5.8 ± 0.7	138 ± 20
		K12	HG3	3.6 ± 0.6	141 ± 17
	Y78	K8	HG3	5.1 ± 0.7	129 ± 11
		P9	HD2	4.3 ± 0.6	107 ± 12
		P80	HD3	4.3 ± 0.5	130 ± 14

[a] Two independently determined NMR ensemble structures were used; 1AAB (rat box A) [23] and 2YRQ (human di-domain). 2YRQ (Tomizawa *et al.,* 2007) results from the Riken structural genomics/proteomics initiative (RSGI).

[b] The center-of-mass of the tyrosine ring was used for calculation.

[c] All ensemble NMR structures were used to give the average and standard deviation of the distance and angle values; 1AAB (33 structures) and 2YRQ (20 structures). The used criteria for identifying CH-π interaction were $d_{C\text{-}X} \leq 4.5$ Å and $\angle_{C\text{-}H\text{-}X} \geq 120°$ [26]

Table I-2

Summary of the alignment tensors[a] determined from ΔδTROSY.

Sample	Box[b]	*D*a /Hz	*D*r /Hz	Euler angles /deg.			Q-factor[c] [rmsd Hz]
				α	β	γ	
HMGB2-AlB wild-type[d]	A	-3.3 (0.4)	-1.4 (0.7)	100 (7)	100 (4)	113 (9)	0.17 [0.17]
	B	-3.9 (0.5)	-1.6 (0.5)	111 (7)	66 (2)	104 (4)	0.20 [0.19]
HMGB2-AlB P80G/P81G[d]	A	-3.8 (0.5)	-1.5 (0.4)	120 (16)	104 (5)	124 (5)	0.24 [0.23]
	B	-5.3 (0.8)	-3.2 (1.2)	100 (7)	68 (4)	110 (7)	0.35 [0.24]
HMGB2-AlB Y78G[d]	A	-3.5 (0.6)	-3.5 (0.6)	139 (8)	105 (8)	122 (5)	0.21 [0.21]
	B	-7.2 (0.8)	-7.2 (0.8)	95 (5)	63 (2)	109 (4)	0.17 [0.31]

[a] Values in parentheses are the standard errors estimated by the jack-knife method [40]; 128 times with 10% of the experimental ΔδTROSY data reduction at random in each calculation. The calculation was done by home-written program using 'Mersenne twister' algorithm for random number generation [41].

[b] The lowest energy structure among the NMR refined coordinates was used for each analysis. In each structural refinement, the RDC derived constraints were also used (Kurita et al. in preparation). The PDB codes for boxes A and B were 1J3X and 1J3D, respectively.

[c] The quality factor Q is defined as

$$Q = \sqrt{\sum_{i=1,N} \frac{\left(\Delta\delta_{\mathrm{TROSY}}^{\mathrm{obs.}} - \Delta\delta_{\mathrm{TROSY}}^{\mathrm{calc.}}\right)^2}{\sum_{i=1,N}\left(\Delta\delta_{\mathrm{TROSY}}^{\mathrm{obs.}}\right)^2}}$$

which is in accordance with the Q-factor defined for the RDC analysis [49].

[d] In the tensor determination, the residues were selected according to the following criteria; the residues (1) being in the secondary structure, (2) showing $^{15}N\{^{1}H\}$ NOE value greater than 0.6, 3) giving small chemical shift changes (less than 10 Hz) on the ^{1}H-^{15}N HSQC spectra between the mutant, P80G/P81G or Y78G, and the wild-type HMGB2-AlB. As exceptions, the residues S15 and F18, which showed 23 Hz and 29 Hz shift changes caused by Y78G mutation, respectively, were incorporated in the tensor calculation for the wild-type, with intention to increase the number of input data: the addition of these two data did not significantly change the resultant tensor value. The residues used in the calculation were the followings: the wild-type (box A), residues 15–30 and 38–55, the P80/P81G mutant (box A), residues 15–30 and 38–64, and the Y78G mutant (box A), residues 15–30 and 38–71. For the box B, the residues 102–116 and 120–161 were used in all the fragments, the wild-type, P80G/P81G and Y78G mutants. Some residues showing severe signal overlaps and low signal intensities were omitted in the calculation.

Chapter III

The effect of DNA binding and bending activity by mutation on the interdomain linker of HMGB2

Abstract

HMGB2 has two DNA-binding domains, box A and B, linked by ten amino acid linker, and a DNA binding of HMGB2 causes DNA bending. DNA binding assay showed the DNA binding affinity of linker mutants (P80G/P81G and Y78G) were almost same that of wild-type. In contrast, DNA bending activity that is estimated by DNA circularization assay showed the activity of the linker mutants (P80G/P81G and Y78G) were less efficient than that of wild-type. This work demonstrates that the residues interact with box A effect on the DNA bending function of HMGB2.

1. Introduction

HMGB1 and B2 bind DNA in a sequence-nonspecific manner [50, 51]. They preferentially bind to super-coiled [52] and non-B form DNA, such as for-way junctions [53], cruciform DNA [52, 54], and B-Z junctions [55]. In addition to their preferential binding to deformed DNA structures, they themselves bend and unwind DNA through binding of the HMG boxes to the minor groove [56]. The ability to deform DNA structure is the basis of HMGB1 and B2 biological functions.

The two HMG boxes in HMGB1 and 2 show structural similarities; however, they have different roles in their interaction with DNA. Box B has a major role in DNA binding and bending [5, 57]. Box A has less ability to deform DNA [11] but it preferentially binds to distorted DNA compared to box B, as exemplified in its interaction with four-way junction DNA [26]. The interdomain linker is effect on HMGB1 and 2 function. Tandem HMG boxes, as in HMGB1 and 2, more efficiently bend DNA than a single HMG box does, as evidenced in DNA circularization assays [6, 11]. Tandem HMG boxes may cooperatively bind to DNA and subsequently induce abrupt bending; box B initially binds DNA and changes its structure, which will be followed by the box A binding through its preferential affinity to the deformed DNA structure [6, 11].

In this work, we found the interdomain linker effect on DNA bending activity of HMGB2. The DNA bending activity of linker mutants (P80G/P81G and Y78G) reduced that of wild-type. This finding suggests that the interdomain linker has a role to support the function of HMGB2.

2. Materials and methods

DNA binding assay for HMGB2 wild-type and mutants

The 202 bp DNA fragment was obtained by PCR from the plasmid, pET32a, using S-tag primer (Merck Chemicals) and T7 terminator primer (TAKARA) as forward and reverse primers, respectively. The amplified DNA fragment was purified from an agarose gel following electrophoresis. The purified 202 bp DNA fragment (100 nM) was incubated with increasing amounts of protein in 8 µl of 20 mM Tris-HCl (pH 8.0), 0.1 mM EDTA, 150 mM NaCl, and 5 mM ß–mercaptoethanol on ice for 10 min. The applied HMGB2-AlB fragment concentrations were 0.05, 0.25, 0.5, 1.0, 1.5, 2.0, and 2.5 µM. Samples were analyzed by electrophoresis in 2 % agarose gels containing 1 × TAE buffer solution. DNA was detected by ethidium bromide staining.

DNA circularization assay for HMGB2 wild-type and mutants

A 91 bp DNA fragment was obtained by PCR from the expression plasmid pET32a, which encodes the cDNA of HMGB1, using the forward primer (5'-ATCGCATATGGGCAAAGGAGATCCTAA-3') and the reverse primer (5'-CTTATGCTCCTCCCGAGAAGTTTGCAC-3'). The amplified DNA fragment was purified from an agarose gel following electrophoresis. Both primer oligonucleotides were phosphorylated by T4 polynucleotide kinase (TAKARA) prior to PCR application. DNA circularization was carried out on the linear 91 bp DNA fragment (5 nM) in the presence of various amounts of protein (1 nM, 5 nM and 20 nM for each protein). The reaction buffer solution

consisted of 50 mM Tris-HCl (pH 7.5), 10 mM $MgCl_2$, 1 mM ATP, and 10 mM DTT. The total amount of the sample solution was set to 400 µl, which was pre-incubated on ice for 30 min before the ligation. The ligation was performed with 400 units of T4 DNA ligase (New England Biolabs) for 3 hours at 22 °C. The resultant DNA was purified using a Wizard SV Gel and PCR clean-up system (Promega) to remove proteins from the DNA. The purified DNA solution was analyzed by electrophoresis in a 4.5 % polyacrylamide gel (29:1 acrylamide and bis-acrylamide) containing 0.5 × TBE buffer solution. The DNA was stained by GelRed (BIOTIUM).

3. Results and discussion

The linker mutants showed almost same DNA binding activity to that of the wild-type, as shown by the gel-shift assays using linear DNA (Figure III-1). However, they showed reduce DNA bending activities relative to the wild-type in DNA-circularization assays (Figure III-2).

In DNA circularization assay, the amount of circularized DNA increased and then decreased according to the increasing amount of wild-type HMGB2-AlB input (Figure III-2b). This dependency in DNA circularization is consistent with the previous observation [58]. The overloaded HMGB2-AlB onto DNA may induce over-bended architecture, which should make the end of DNA apart to obstruct ligase reaction to join them. This could explain the reduced circularization at high HMGB2-AlB input. In contrast to the wild-type, the P80G/P81G and Y78G mutants showed maximum circularization at higher amount, showing their reduced bending activities (Figure III-2b). Because their DNA binding activities were not apparently changed (Figure III-1a-c), their less efficient circularization could be ascribed to the reduced DNA bending angles by their binding. This effect should come from interaction with interdomain linker and DNA binding domain. The linker is flexible, but seems to take efficient domain orientation for DNA bending transiently.

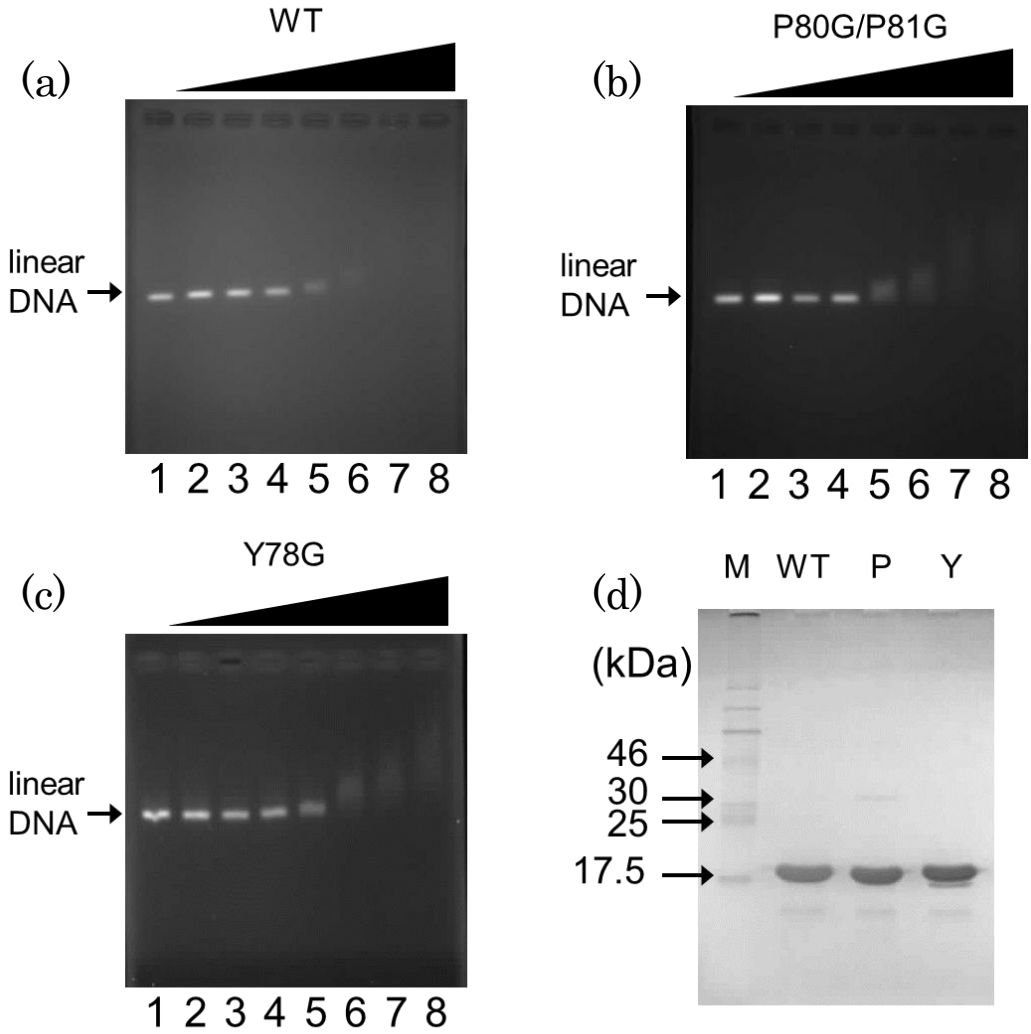

Figure III-1

DNA binding abilities of the HMGB2-AlB frangments. The wild-type (a), P80G/P81G (b), and Y78G (c) mutants are shown. The SDS-PAGE for the purified proteins used in this work (d); M: molecular size marker, WT: wild-type, P: P80G/P81G mutant, and Y: Y78G mutant. The amount of the dsDNA fragment (202 bp) was 100 nM. The applied HMGB2-AlB fragments were 0.05, 0.25, 0.5, 1.0, 1.5, 2.0, and 2.5 μM (from 2 to 8, lane 1 is for the free DNA).

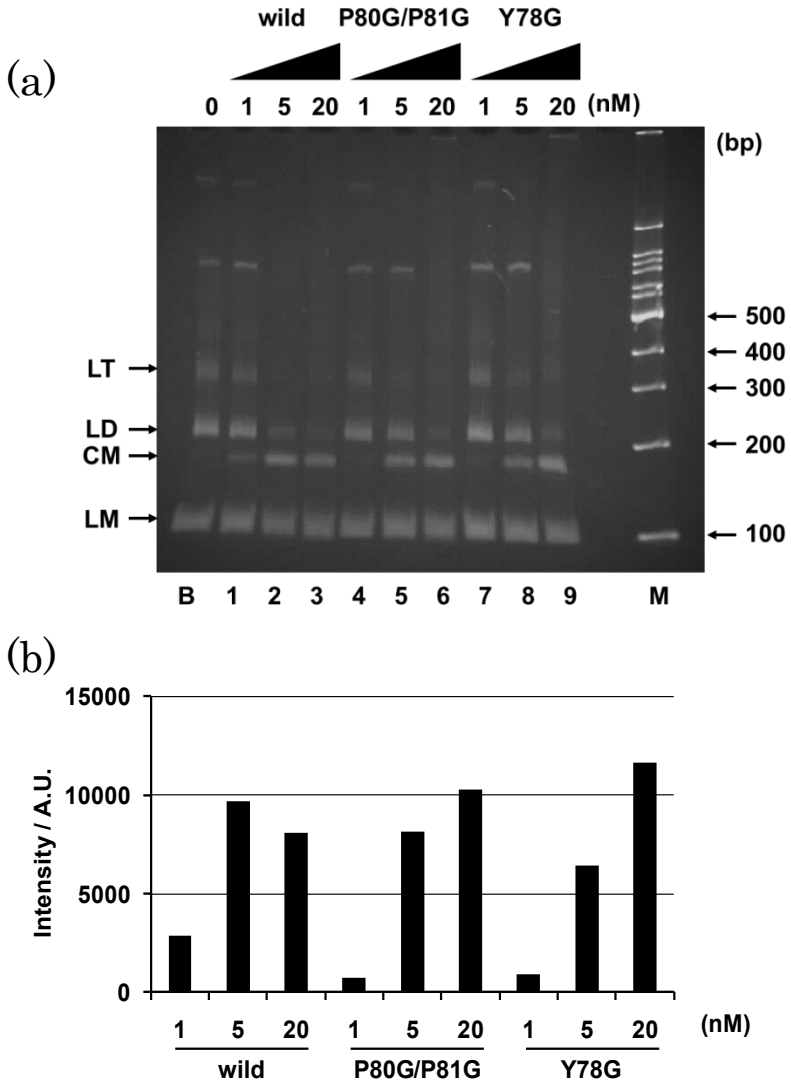

Figure III-2

DNA circularization assays of the 91 bp DNA fragment. (a) Input amounts of the protein were 1.0 nM, 5.0 nM and 20 nM with DNA at 5 nM; wild type (lanes 1-3), P80G/P81G (lanes 4-6), and Y78G HMGB2-AlB (lanes 7-9). CM indicates the band position for circularized DNA. LM, LD and LT denote monomer linear, dimer linear, and trimer linear DNA. In lane B, the 91 bp DNA fragment was subjected to the DNA ligase reaction in the absence of HMGB2-AlB, as control. Lane M, molecular size marker. (b) The relative band intensities of the circularized DNA run in the gel, recorded by densitometry.

Chapter IV

Conclusions

In Chapter II, the present work has shown that the interdomain linker (residues 78-87) has a role to define the overall structure having preferential domain orientation. The N-terminal part of the interdomain linker, $Y^{78}VPP^{81}$, is particularly connected to the N-terminus of box A through a CH-π interaction network primarily mediated by the conserved Y78 (Figure II-6d). The weak and transient intramolecular interactions make the DNA binding surfaces of the box A and B preferentially stay in the opposite direction (Figure II-17a). The Y78G mutant having impaired intramolecular interactions altered preferential domain orientation and the interdomain dynamics, as revealed by the alignment tensors determined by RPCSA (Table 1), which suggest Y78 mediating weak and transient interactions are structurally significant.

In Chapter III, the present work has shown that linker mutation affected HMGB2 function. The DNA binding activity of HMGB2-AlB linker mutants (P80G/P81G and Y78G) and that of wild-type is almost same, however, DNA bending activity of mutants is less than that of wild-type. This result should relate to the difference of HMGB2 domain orientaion between wild-type and mutants mediated by interdomain linker.

For HMGB2 wild-type, each domain transiently stays in the opposite direction by the CH-π interaction between the box A and the interdomain linker. Owing to the weak limited domain orientation, HMGB2 wild-type can

bend DNA effectively. In contrast, there is no interaction between the box A and the linker for the linker mutants. Because of this, the linker mutants have no limitation of relative domain orientation, and are inefficient for DNA bending. That is to say that the interdomain linker has roles both defining overall structure and function of HMGB2. This is a new insight into the unstructured linker of HMGB2.

Acknowledgments

I would like to express my sincere gratitude to Professor Shin-ichi Tate (Hiroshima University) for his variable discussion and great encouragement. I thank to Professor Katsuo Katayanagi and Professor Eiji Ohmae (Hiroshima University) for advices and technical supports. I thank to Professor Daisuke Kohda and Professor Takashi Saitoh (Kyushu University) for the access to 700 MHz NMR instrument. I thank to Professor Hironari Kamikubo (Nara Institute of Science and Technology) to provide SAXS data for this work. I thank to Professor Naoko Utsunomiya-Tate and Professor Hiroshi Moriuchi (Musashino University) for making construct of HMGB2. I thank to Professor Naoaki Sakamoto (Hiroshima University) for his advice to DNA experiments. I thank to Dr. Shogo Nakano (Hiroshima University) for his help in generating a homology modeled structure used in this work. I thank to members of my lab for experimental supports. Finally, I would like to thank my family and friends for supports and encouragements.

References

[1] A.K. Dunker, Z. Obradovic, P. Romero, E.C. Garner, C.J. Brown, Intrinsic protein disorder in complete genomes, *Genome Inform Ser Workshop Genome Inform.* **11**, 161-171. (2000)

[2] M. Bustin, R. Reeves, High-mobility-group chromosomal proteins: architectural components that facilitate chromatin function, *Prog. Nucleic Acid Res. Mol. Biol.* **54**, 35-100. (1996)

[3] M. Bustin, M.P. Crippa, J.M. Pash, Expression of HMG chromosomal proteins during cell cycle and differentiation, *Crit. Rev. Eukaryot Gene Expr.* **2**, 137-143. (1992)

[4] M. Bustin, D.A. Lehn, D. Landsman, Structural features of the HMG chromosomal proteins and their genes, *Biochim. Biophys. Acta* **1049**, 231-243. (1990)

[5] Y. Nakamura, M. Shimizu, M. Yoshida, Distorted DNA structures induced by HMGB2 possess a high affinity for HMGB2, *J Biochem.* **131**, 153-160. (2002)

[6] K.-i. Yoshioka, K. Saito, T. Tanabe, A. Yamamoto, Y. Ando, Y. Nakamura, H. Shirakawa, M. Yoshida, Differences in DNA recognition and conformational change activity between boxes A and B in HMG2 protein, *Biochemistry* **38**, 589-595. (1999)

[7] K. Stott, M. Watson, F.S. Howe, J.G. Grossmann, J.O. Thomas, Tail-mediated collapse of HMGB1 is dynamic and occurs via differential binding of the acidic tail to the A and B domains, *J Mol Biol.* **403**, 706-722. (2010)

[8] M. Watson, K. Stott, J.O. Thomas, Mapping intramolecular interactions between domains in HMGB1 using a tail-truncation approach, *J Mol Biol.* **374**, 1286-1297. (2007)

[9] L. Cato, K. Stott, M. Watson, J.O. Thomas, The interaction of HMGB1 and linker histones occurs through their acidic and basic tails, *J Mol Biol.* **384**, 1262-1272. (2008)

[10] K. Stott, G.S. Tang, K.B. Lee, J.O. Thomas, Structure of a complex of tandem HMG boxes and DNA, *J Mol Biol.* **360**, 90-104. (2006)

[11] Y. Nakamura, K. Yoshioka, H. Shirakawa, M. Yoshida, HMG Box A in HMG2 Protein Functions as a Mediator of DNA Structural Alteration Together with Box B, *J. Biochem.* **129**, 643-651. (2001)

[12] A.K. Dunker, C.J. Oldfield, J. Meng, P. Romero, J.Y. Yang, J.W. Chen, V. Vacic,

Z. Obradovic, V.N. Uversky, The unfoldomics decade: an update on intrinsically disordered proteins, *BMC Genomics* **9,** (Suppl. 2) S1. (2008)

[13] H. Tossavainen, O. Koskela, P. Jiang, J. Ylanne, I.D. Campbell, I. Kilpelainen, P. Permi, Model of a Six Immunoglobulin-Like Domain Fragment of Filamin A (16–21) Built Using Residual Dipolar Couplings, *J. Am. Chem. Soc.* **134**, 6660-6672. (2012)

[14] M.W. Fischer, J.A. Losonczi, J.L. Weaver, J.H. Prestegard, Domain Orientation and Dynamics in Multidomain Proteins from Residual Dipolar Couplings, *Biochemistry* **38**, 9013-9022. (1999)

[15] S. Tate, A. Imada, N. Hiroguchi, Complementary Use of NMR to X-ray Crystallography for the Analysis of Protein Morphological Change in Solution, *InTech, Rijeka*, Croatia, (2011)

[16] S. Tate, Anisotropic nuclear spin interactions for the morphology analysis of proteins in solution by NMR spectroscopy. *Anal. Sci.* **24**, 39-50. (2008)

[17] N.K. Goto, N.R. Skrynnikov, F.W. Dahlquist, L.E. Kay, What is the Average Conformation of Bacteriophage T4 Lysozyme in Solution? A Domain Orientation Study Using Dipolar Couplings Measured by Solution NMR, J. *Mol. Biol.* **308**, 745-764. (2001)

[18] N.R. Skrynnikov, N.K. Goto, D. Yang, W.Y. Choy, J.R. Tolman, G.A. Mueller, L.E. Kay, Orienting Domains in Proteins Using Dipolar Couplings Measured by Liquid-state NMR: Differences in Solution and Crystal Forms of Maltodextrin Binding Protein Loaded with ß-Cyclodextrin *J. Mol. Biol.* **295**, 1265-1273. (2000)

[19] A. Bax, A. Grishaev, Weak alignment NMR: a hawk-eyed view of biomolecular structure, *Curr. Opin. Struct. Biol.* **15**, 563-570. (2005)

[20] S.E. Tsutakawa, G.L. Hura, K.A. Frankel, P.K. Cooper, J.A. Tainer, Structural analysis of flexible proteins in solution by small angle X-ray scattering combined with crystallography, *J. Struct. Biol.* **158**, 214-223. (2007)

[21] X. Wang, H.-W. Lee, Y. Liu, J.H. Prestegard, Structural NMR of Protein Oligomers using Hybrid Methods, *J. Struct. Biol.* **173**, 515-529. (2011)

[22] H.M. Weir, P.J. Kraulis, C.S. Hill, A.R. Raine, E.D. Laue, J.O. Thomas, Structure of the HMG box motif in the B-domain of HMG1, *EMBO J.* **12**, 1311-1319. (1993)

[23] C.H. Hardman, R.W. Broadhurst, A.R. Raine, K.D. Grasser, J.O. Thomas, E.D. Laue, Structure of the A-domain of HMG1 and its interaction with DNA as studied by heteronuclear three- and four-dimensional NMR spectroscopy,

Biochemistry **34** 16596-16607. (1995)

[24] A. Yamamoto, Y. Ando, K. Yoshioka, K. Saito, T. Tanabe, H. Shirakawa, M. Yoshida, Difference in Affinity for DNA between HMG Proteins 1 and 2 Determined by Surface Plasmon Resonance Measurements, *J. Biochem.* **122**, 586-594. (1997)

[25] M. Webb, J.O. Thomas, Structure-specific Binding of the Two Tandem HMG Boxes of HMG1 to Four-way Junction DNA is Mediated by the A Domain, *J. Mol. Biol.* **294**, 373-387. (1999)

[26] M. Brandl, M.S. Weiss, A. Jabs, J. Sühnel, R. Hilgenfeld, C-H···π-Interactions in Proteins, *J. Mol. Biol.* **307**, 357-377. (2001)

[27] J. Cavanagh, W.J. Fairbrother, A.G. Palmer III, N.J. Skelton, Heteronuclear NMR Experiments, *Academic Press, Inc.*, New York, (1996).

[28] D. Rovnyak, D.P. Frueh, M. Sastry, Z.-Y.J. Sun, A.S. Stern, J.C. Hoch, G. Wagner, Accelerated acquisition of high resolution triple-resonance spectra using non-uniform sampling and maximum entropy reconstruction, *J. Magn. Reson.* **170**, 15-21. (2004)

[29] J.C. Hoch, A.S. Stern, NMR Data Processing, *John Wiley & Sons, Inc.*, New York, (1996).

[30] F. Delaglio, S. Grzesiek, G.W. Vuister, G. Zhu, J. Pfeifer, A. Bax, NMRPipe: a multidimensional spectral processing system based on UNIX pipes *J. Biomol. NMR* **6**, 277-293. (1995)

[31] B.A. Johnson, R.A. Blevins, NMRView: A computer program for the visualization and analysis of NMR data, *J. Biomol. NMR* **4**, 603-614. (1994)

[32] N. Kobayashi, J. Iwahara, S. Koshiba, T. Tomizawa, N. Tochio, P. Güntert, T. Kigawa, S. Yokoyama, KUJIRA, a package of integrated modules for systematic and interactive analysis of NMR data directed to high-throughput NMR structure studies, *J. Biomol. NMR* **39**, 31-52. (2007)

[33] T. Ueki, Y. Hiragi, M. Kataoka, Y. Inoko, Y. Amemiya, Y. Izumi, H. Tagawa, Y. Muroga, AGGREGATION OF BOVINE SERUM ALBUMIN UPON CLEAVAGE OF ITS DISULFIDE BONDS, STUDIED BY THE TIME-RESOLVED SMALL-ANGLE X-RAY SCATTERING TECHNIQUE WITH SYNCHROTRON RADIATION, *Biophys. Chem.* **23**, 115-124. (1985)

[34] S. Tate, H. Shimahara, N. Utsunomiya-Tate, Molecular-orientation analysis based on alignment-induced TROSY chemical shift changes, *J. Magn. Reson.* **171**, 284-292. (2004)

[35] M. Ottiger, F. Delaglio, A. Bax, Measurement of J and Dipolar Couplings from

Simplified Two-Dimensional NMR Spectra, *J. Magn. Reson.* **131**, 373-378. (1998)

[36] Meier S, Häussinger D, Grzesiek S., Charged acrylamide copolymer gels as media for weak alignment, *J. Biomol. NMR* **24**, 351-356. (2002)

[37] J.J. Chou, S. Gaemers, B. Howder, J.M. Louis, A. Bax, *J. Biomol. NMR* **21**, 377-382. (2001)

[38] F. Mosteller, J. Tukey, Data Analysis and Regression: A Second Course in Statistics, *Addison-Wesley Publishing Co.*, Don Mills, Ontario, (1977)

[39] M. Matsumoto, T. Nishimura, Mersenne Twister: A 623-Dimensionally Equidistributed Uniform Pseudo-Random Number Generator, *ACM Trans. Model. Comput. Simul.* **8**, 3-30. (1998)

[40] C.D. Schwieters, J.J. Kuszewski, N. Tjandra, G.M. Clore, The Xplor-NIH NMR molecular structure determination package, *J. Magn. Reson.* **160**, 65-73. (2003)

[41] A. Grishaev, J. Ying, A. Bax, Pseudo-CSA Restraints for NMR Refinement of Nucleic Acid Structure, *J. Am. Chem. Soc.* **128**, 10010-10011. (2006)

[42] A. Grishaev, J. Wu, J. Trewhella, A. Bax, Refinement of Multidomain Protein Structures by Combination of Solution Small-Angle X-ray Scattering and NMR Data, *J. Am. Chem. Soc.* **127**, 16621-16628. (2005)

[43] R. Sanchez, A. Sali, Comparative Protein Structure Modeling: Introduction and Practical Examples with Modeller, *Methods Mol. Biol.* **143**, 97-129. (2000)

[44] S.H. Teo, K.D. Grasser, C.H. Hardman, R.W. Broadhurst, E.D. Laue, J.O. Thomas, Two mutations in the HMG-box with very different structural consequences provide insights into the nature of binding to four-way junction DNA, *EMBO J.* **14**, 3844-3853. (1995)

[45] T. Tanaka, Y. Kuroda, S. Yokoyama, Comparative Protein Structure Modeling: Introduction and Practical Examples with Modeller, *J. Struct. Funct. Genomics* **4**, 79-85. (2003)

[46] S. Ohnishi, H. Kamikubo, M. Onitsuka, M. Kataoka, D. Shortle, Conformational Preference of Polyglycine in Solution to Elongated Structure, *J. Am. Chem. Soc.* **128**, 16338-16344. (2006)

[47] J.R. Tolman, J.M. Flanagan, M.A. Kennedy, J.H. Prestegard, NMR evidence for slow collective motions in cyanometmyoglobin, *Nat. Struct. Biol.* **4**, 292-297. (1997)

[48] M.A. Larkin, G. Blackshields, N.P. Brown, R. Chenna, P.A. McGettigan, H. McWilliam, F. Valentin, I.M. Wallace, A. Wilm, R. Lopez, J.D. Thompson, T.J. Gibson, D.G. Higgins, Clustal W and Clustal X version 2.0, *Bioinformatics* **23**,

2947-2948. (2007)

[49] M. Ottiger, A. Bax, Bicelle-based liquid crystals for NMR-measurement of dipolar couplings at acidic and basic pH values, *J. Biomol. NMR* **13**, 187-191. (1999)

[50] M. Grasser, A. Lentz , J. Lichota, T. Merkle, K.D. Grasser, The Arabidopsis genome encodes structurally and functionally diverse HMGB-type proteins, *J.Mol.Biol.* **358**, 654-664. (2006)

[51] A. Yamamoto, Y. Ando, K. Yoshioka, K. Saito, T. Tanabe, H. Shirakawa, M. Yoshida, Difference in affinity for DNA between HMG proteins 1 and 2 determined by surface plasmon resonance measurements, *J Biochem* **122**, 586-594. (1997)

[52] H. Hamada, M. Bustin, Hierarchy of binding sites for chromosomal proteins HMG 1 and 2 in supercoiled deoxyribonucleic acid, *Biochemistry* **24**, 1428-1433. (1985)

[53] M.E. Bianchi, M. Beltrame, G. Paonessa, Specific recognition of cruciform DNA by nuclear protein HMG1, *Science* **243**, 1056-1059. (1989)

[54] S. Waga, S. Mizuno, M. Yoshida, Chromosomal protein HMG1 removes the transcriptional block caused by the cruciform in supercoiled DNA, *J Biol Chem* **265**, 19424-19428. (1990)

[55] S. Waga, S. Mizuno, M. Yoshida, Nonhistone protein HMG1 removes the transcriptional block caused by left-handed Z-form segment in a supercoiled DNA, *Biochem Biophys Res Commun* **153**, 334-339. (1988)

[56] J.O. Thomas, A.A. Travers, HMG1 and 2, and related 'architectural' DNA-binding proteins, *Trends Biochem.Sci.* **26**, 167-174. (2001)

[57] T.T. Paull, M.J. Haykinson, R.C. Johnson, The nonspecific DNA-binding and -bending proteins HMG1 and HMG2 promote the assembly of complex nucleoprotein structures, *Genes Dev* **7**, 1521-1534. (1993)

[58] K.B. Lee, J.O. Thomas, The effect of the acidic tail on the DNA-binding properties of the HMG1,2 class of proteins: insights from tail switching and tail removal, *J Mol Biol* **304**, 135-149. (2000)

公表論文

Preferential domain orientation of HMGB2 determined by the weak intramolecular interactions mediated by the interdomain linker

J. Uewaki, H. Kamikubo, J. Kurita, N. Hiroguchi, H. Moriuchi, M. Yoshida, M. Kataoka, N. Utsunomiya-Tate, S. Tate,

Chemical Physics. **419**, 212-223. (2013)

Provided for non-commercial research and education use.
Not for reproduction, distribution or commercial use.

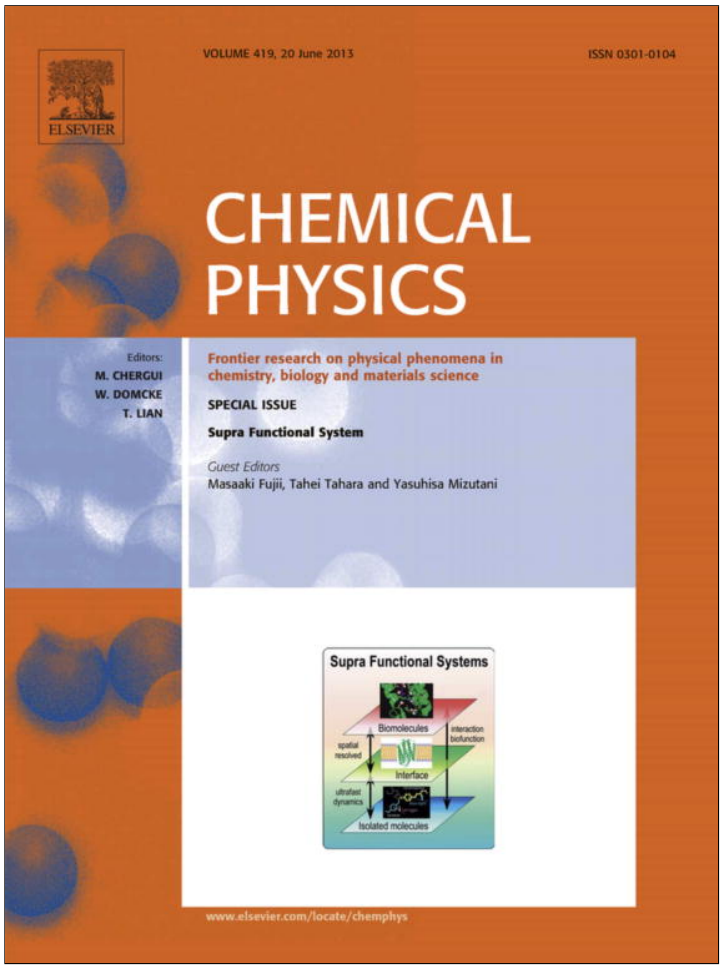

This article appeared in a journal published by Elsevier. The attached copy is furnished to the author for internal non-commercial research and education use, including for instruction at the authors institution and sharing with colleagues.

Other uses, including reproduction and distribution, or selling or licensing copies, or posting to personal, institutional or third party websites are prohibited.

In most cases authors are permitted to post their version of the article (e.g. in Word or Tex form) to their personal website or institutional repository. Authors requiring further information regarding Elsevier's archiving and manuscript policies are encouraged to visit:

http://www.elsevier.com/authorsrights

Author's personal copy

Chemical Physics 419 (2013) 212–223

Contents lists available at SciVerse ScienceDirect

Chemical Physics

journal homepage: www.elsevier.com/locate/chemphys

Preferential domain orientation of HMGB2 determined by the weak intramolecular interactions mediated by the interdomain linker

Jun-ichi Uewaki [a], Hironari Kamikubo [b], Jun-ichi Kurita [c], Noriteru Hiroguchi [a], Hiroshi Moriuchi [d], Michiteru Yoshida [e], Mikio Kataoka [b], Naoko Utsunomiya-Tate [d], Shin-ichi Tate [a,*]

[a] Department of Mathematical and Life Sciences, School of Science, Hiroshima University, 1-3-1 Kagamiyama, Higashi-Hiroshima 739-8526, Japan
[b] Nara Institute of Science and Technology, 8916-5 Takayama, Ikoma, Nara 630-0101, Japan
[c] Agilent Technologies Japan, Ltd., 4-16-36 Shibaura, Minato-ku, Tokyo 108-0023, Japan
[d] Research Institute of Pharmaceutical Sciences, Musashino University, 1-1-20 Shinmachi Nishitokyo, Tokyo 202-8585, Japan
[e] Department of Biological Science and Technology, Science University of Tokyo, 2641 Yamazaki, Noda, Chiba 278-8510, Japan

ARTICLE INFO

Article history:
Available online 13 February 2013

Keywords:
High-mobility group protein
Weak alignment
DIORITE
NMR spectroscopy
CH-π interaction
HMGB2
Domain orientation
Flexible linker
TROSY
SAXS

ABSTRACT

High mobility group box protein 2 (HMGB2) contains homologous tandem HMG box DNA-binding domains, boxes A and B. These two boxes are linked by a short basic linker having a sequence characteristic of an intrinsically disordered element. The combined use of NMR and small angle X-ray scattering (SAXS) showed that the two boxes assume a preferred orientation to make their DNA binding surface in opposite directions, although the linker does not keep any specific conformation. A series of site directed mutations to the residues in the linker showed that a network of CH-π interactions connects the N-terminal part of the linker to box A. The mutants having impaired intramolecular CH-π interactions changed the interdomain dynamics and their dynamic averaged orientation relative to the wild-type. This work demonstrates that the apparently unstructured linker plays a role in defining the preferential domain orientation through the intramolecular CH-π interactions, even though the interactions are weak and transient.

© 2013 Elsevier B.V. All rights reserved.

1. Introduction

Accurate view on the conformational state of the modular protein having the folding units joined by apparently unstructured short linkers should be essential for understanding its function. The type of proteins including intrinsically unstructured parts plays pivotal roles in biological processes through its structural flexibility that allows adopting various forms in binding to partner molecules [1]. In elucidating how the proteins work by using its structural plasticity, we have to see how the modular proteins exist in solution. The high resolution techniques do not give the right insights in the particular regards. X-ray crystallography may determine the conformation of the modular protein whose domain arraignment is artificially defined by crystal packing, in addition to the lack of the electron density for the flexible linker parts. NMR can give solution structures of such protein, but NOE-based distance restrains are often scarce in the dynamic interdomain linker, thus the obtained domain arrangements do not represent the realistic conformational state.

Alternative approaches are available for the structural elucidation of the modular proteins. Another type of NMR experiment using residual dipolar couplings (RDCs) provides long-range structural information that defines the relative domain orientation and interdomain dynamics [2–8]. Small angle X-ray scattering (SAXS) is also used for the same purpose by its ability to give molecular shape information [9]. Independent use of each approach, however, cannot accurately determine the structure of modular protein. The RDCs define the domain orientation but cannot give the inter-domain distance. SAXS gives rather limited structural details due to its intrinsically low resolution, in particular for the cases of medium sized proteins, although it can accurately determine the molecular radii [9]. NMR with the RDCs and SAXS are, therefore, the complementary methods in determining the modular protein structure determination [2,3,10].

High mobility group box 2 (HMGB2) protein consists of two DNA-binding domains, HMG boxes A and B and a short inter-domain linker ('l-region'), which connects the HMG boxes (Fig. 1a).

Abbreviations: HSQC, heteronuclear single quantum coherence; TROSY, transverse relaxation optimized spectroscopy; NOE, nuclear Overhauser effect; IPAP-HSQC, in-phase and anti-phase HSQC; RDC, residual dipolar coupling; SAXS, small-angle X-ray scattering; DIORITE, determination of the induced orientation by trosy experiments.

* Corresponding author. Tel./fax: +81 82 424 7387.
E-mail address: tate@hiroshima-u.ac.jp (S.-i. Tate).

0301-0104/$ - see front matter © 2013 Elsevier B.V. All rights reserved.
http://dx.doi.org/10.1016/j.chemphys.2013.02.004

Author's personal copy

HMGB2 and its homologous protein HMGB1 are non-histone chromosomal proteins abundant in eukaryotic cells [11–13]. HMGB1 and 2 share high sequence homology with their orthologues (Fig. 1a). The preceding works have solved the structures for the two HMG boxes in HMGB1, both of which showed characteristic 'L-shaped' structures [14,15]. The roles for each HMG boxes were characterized; box A has preferential affinity to the deformed DNA structure, while the box B shows strong DNA binding and bending ability [16,17]. The tandem aligned HMG boxes with different DNA binding ability have cooperative functions in DNA binding and inducing DNA bending [18–20]. The accumulated insights into the functional cooperation of the boxes in HMGB1 and 2 suggest that the spatial arrangement of the boxes has some functional meanings, which prompted us to see how the boxes in HMGB2 stay in solution with the combined use of NMR and SAXS.

In this work, we found the interdomain linker defines the relative domain orientation of the HMG boxes. A series of site-directed mutagenesis to the linker showed that a part of the linker has specific contact with box A; which is mediated by a network of CH-π interactions [21] as elucidated by the box A structure in HMGB1 in comparison with the counterpart in HMGB2 determined in this work [15]. HMG boxes in the wild-type HMGB2 showed preferential orientation to locate their DNA binding surfaces in the opposite side of the molecule. The interdomain linker mutants having impaired CH-π interactions changed the relative domain orientation with increased interdomain dynamics. This finding adds another functional role associated with the interdomain linker of HMGB2.

2. Materials and methods

2.1. Plasmids

The cDNA encoding porcine HMGB2 was provided by Prof. Yoshida. The fragments of HMGB2 used in this work are schematically described in Fig. 1b; HMGB2-A (residues 1–77), HMGB2-B (88–165), HMGB2-Al (1–87) and HMGB2-AlB (1–165). The box A used in this work has C23S mutation to improve the sample stability according to the previous work [15]. The gene encoding each fragment was cloned into pET28a (Merck Chemicals, Germany) using *Nde*I and *Eco*RI sites. Site-directed mutagenesis of HMGB2 was performed using QuickChange (Stratagene) and KOD-plus mutagenesis (Toyobo), to make the following mutants (P80G/P81G, K82G, D84G, K85G, K86G and Y78G).

2.2. Expression and purification of HMGB2 fragments

Each HMGB2 fragment was purified from *E. coli* grown in M9 minimal medium. For backbone assignment, medium also contained $^{15}NH_4Cl$ and ^{13}C glucose. The purification procedure is briefly described below. Cells were grown at 37 °C to OD_{600} = 0.6 and IPTG (isopropyl β-D-thiogalactopyranoside) was then added to the medium to induce protein expression (final conc. 0.5 mM). After induction, cell growth was continued for 5 h. Cells were collected by centrifugation and resuspended in buffer solution (50 mM Tris–HCl, pH 8.0; solution A), and then subjected to sonication. Cell debris was removed by centrifugation (15,000 rpm for 30 min) and supernatant was applied to a HisTrap affinity column (GE Healthcare). The column was washed with solution A containing 20 mM imidazole followed by the elution of the His-tagged HMGB2 fragment by solution A containing 500 mM imidazole. The His-tag was cleaved by thrombin for 12 h at 4 °C in a dialysis bag in solution A. The resultant protein was applied to Hi-Trap SP cation-exchanger equilibrated by solution A. The desired protein was purified using a linear NaCl concentration gradient from 0 mM to 800 mM in solution A. The purified protein was dialyzed against buffer solution (50 mM sodium phosphate, pH 6.4) prior to use in NMR experiments. All HMGB2 fragments used in this work were obtained using the above protocol. A three-residue attachment from the construct, having the sequence, GSH, is attached to the N-terminal part of the proteins used.

2.3. NMR experiments

NMR experiments were performed using solutions typically containing 1 mM protein; the buffer solution used was 50 mM sodium phosphate, pH 6.4, containing 1 mM PefaBloc (Sinus Biochemistry and Electrophoresis GmbH). All experiments were performed at 293 K or 298 K on a Bruker DMX600 or DRX700 spectrometer. The backbone resonance assignments were determined for the fragments HMGB2-A, HMGB2-B, HMGB2-Al, and HMGB2-AlB using a standard set of triple resonance spectra [22] collected in a non-uniform sampling manner [23] on a DMX600 spectrometer. 3D ^{15}N-edited NOESY (mixing time 100 ms) and ^{15}N-edited TOCSY (mixing time 40 ms) were also used for confirming the backbone resonance assignments [22]. The triple-resonance data were processed with the Roland NMR toolkit [24]. The ^{15}N-edited NOESY and TOCSY data were processed using the program, NMRPipe [25]. The backbone resonance assignments were determined on the NMRview software platform [26] using the KUJIRA suites [27].

Structures of the boxes A and B of HMGB2 were determined in a conventional manner using CYANA [28] and XPLOR-NIH [29]. The structure statistics are shown in Tables S1 and S2: the overlaid 30 structures and their energy minimized averaged structure are displayed in Fig. S1. The chemical shift assignments for the atoms in the boxes A and B of HMGB2 were deposited to the Biological Magnetic Resonance Bank (BMRB): codes for box A and B are 11429 and 11430, respectively. The structures were registered in the Protein Data Bank (PDB): the accession codes are 1J3X (box A) and 1J3D (box B).

2.4. SAXS experiments

SAXS measurements were carried out at BL-10C, Photon Factory, Tsukuba, Japan [30]. The wavelength of the X-ray was adjusted to 1.488 Å using a Si monochromater. All samples were prepared in 50 mM sodium phosphate, pH 6.4, containing 5 mM DTT. The scattering profiles were collected at 20 °C using an online imaging plate detector (R-Axis VII, Rigaku). The exposure time was 10 min. The obtained two-dimensional data were circularly averaged, and then the final one-dimensional data was obtained by subtracting the profile of the sample buffer solution. To eliminate inter-particle interference from the observed profiles, a series of the profiles at five different concentrations, ranging from 17.5 to 3.5 mg/ml, were extrapolated to obtain that at a concentration of zero.

2.5. Determining the alignment tensors for the HMG domains in HMGB2

The relative orientation of the HMG domains in the HMGB2-AlB fragment was estimated based on the alignment tensors obtained for each domain. The alignment induced TROSY shift changes were used to determine the alignment tensor for each HMG domain, which is referred to as DIORITE [5,31]. Because of the 'L-shape' of each HMG domain and the entirely extended structure of the HMGB2-AlB fragment, which has two HMG domains, the signals showed severe broadening under weak-alignment conditions; most of the anti-TROSY components on the IPAP-HSQC [32] spectra for the HMGB2-AlB fragment showed poor signals or disappeared.

Author's personal copy

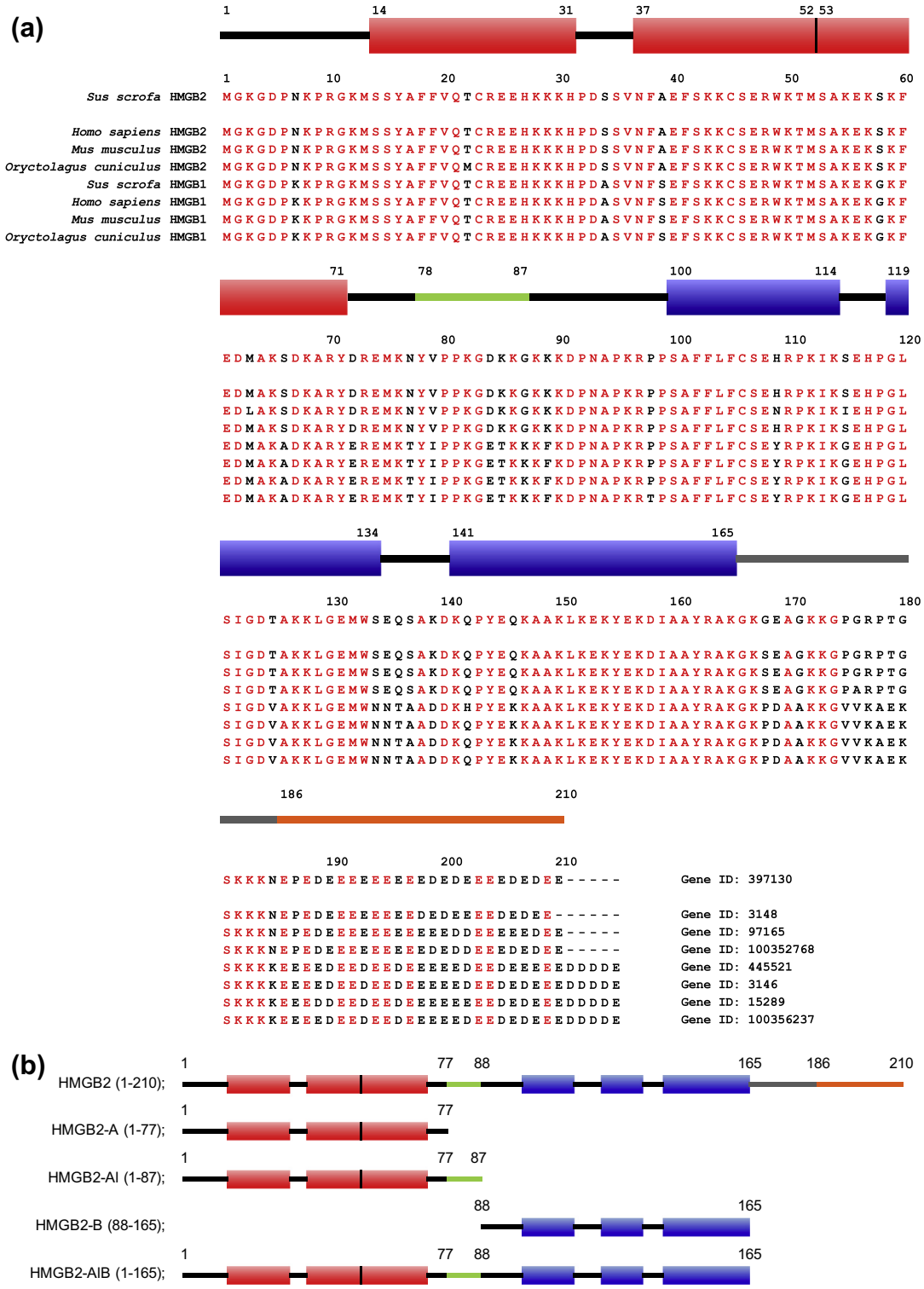

Fig. 1. Multiple alignment of HMGB2 and HMGB1 ortholog sequences from four representative species, which was prepared by ClustalW [45] (a). Gene ID and the species are indicated for each sequence. The HMGB2 sequence from *Sus scrofa* is shown on the top line, with the secondary structures defined in the NMR structures of boxes A and B (PDB: 1J3X and 1J3D). The domains in HMGB2 are defined as: box A (residues 1–77), linker (residues 78–87), box B (residues 88–165), joiner (residues 166–185) and the acidic tail (186–210). Identical amino acids are shown in red. The residue C23 in the present HMGB2 was changed to serine to increase the sample stability [15]; the residue is marked with asterisk. Schematic drawings of the HMGB2 fragments used in this work with full-length HMGB2 indicated at the top (b). The 'l' denotes the linker region (residues 78–87); Al and AlB stand for the fragments of box A with the linker and boxes A and B linked by the linker, respectively.

The alignment tensor determination was done according to the procedure described in our previous paper using optimized ^{15}N CSA tensor parameters [31]. The ^{15}N CSA tensor used for the residues in α-helix was $\Delta\sigma = -173.0$ ppm, $\eta = 0.23$, and $\beta = 19.8°$. In the present analysis, the ^{15}N CSA tensor value that is specific for α-helix was used.

Author's personal copy

The weak-alignment of proteins was achieved using stretched acrylamide gels [33]. Acrylamide and *N,N′*-methylenebisacrylamide (bis-acrylamide) copolymer was prepared at a monomer concentration of 5% with a 75:1 molar ratio of acrylamide to bis-acrylamide. Polymerization was achieved using 0.05% (w/v) ammonium persulfate (APS) and 0.2% (v/v) *N,N,N′,N′*-tetramethylethane-1,2-diamine (TEMED). One gel was cast in a Teflon block to make a rod of 4 mm diameter, which was used as the 'reference gel'. The other gel was a rod with an ellipsoidal cross-section having 7 mm and 5 mm diameters, which was used as the 'aligning gel'. The gels were extensively dialyzed against buffer (50 mM sodium phosphate, pH 6.4), for over three days to completely remove residual reagents from polymerization. Gels were then soaked in 250 μl protein solution containing 1 mM protein. The solutions were incubated at 4 °C for three days to allow complete uptake of protein into the gel rod. Each gel was inserted into an NMR tube with open ends (New Era) using a Teflon device having a tapered head [34]. The NMR tube was sealed at one end with an Ultem plug (New Era). At the other end, 50 μl sample solution was poured onto the gel and sealed with an inner glass rod from a Shigemi micro NMR tube (Shigemi). The NMR tube was then incubated for five days at 4 °C to allow it to achieve a steady-state gel length. After adjusting the inner rod position to exclude the solution squeezed from the gel, the sample was subjected to NMR measurement.

Before TROSY measurements, the ^{2}H split was measured to correct the chemical shift drift caused by residual quadrupole splitting of the ^{2}H signal used for the frequency lock. In the HMGB2-AlB fragment experiments, the residual quadrupole ^{2}H split was kept around 2 Hz for the weakly aligned samples. The reference chemical shifts were measured for the sample in the reference gel, where protein is not aligned but is dissolved in the same acrylamide non-stretched gel. It was confirmed that no ^{2}H split was observed for the sample solution in the reference gel.

The NMR refined structure coordinate HMGB2-A and -B domains were used for the alignment tensor calculation; PDB codes for boxes A and B are 1J3X and 1J3D, respectively.

The error estimation for the obtained tensor parameters was done by the jack-knife method [35]; 128 times with 10% of the experimental data reduction at random in each calculation. In random number generation, 'Mersenne twister' algorism [36] was used to improve the sampling.

2.6. Rigid-body minimization

The overall structure of the wild-type and Y78G mutant HMGB2-AlB were determined using the Δδ TROSY and SAXS data using XPLOR-NIH 2.31 software platform [37]: Δδ TROSY values

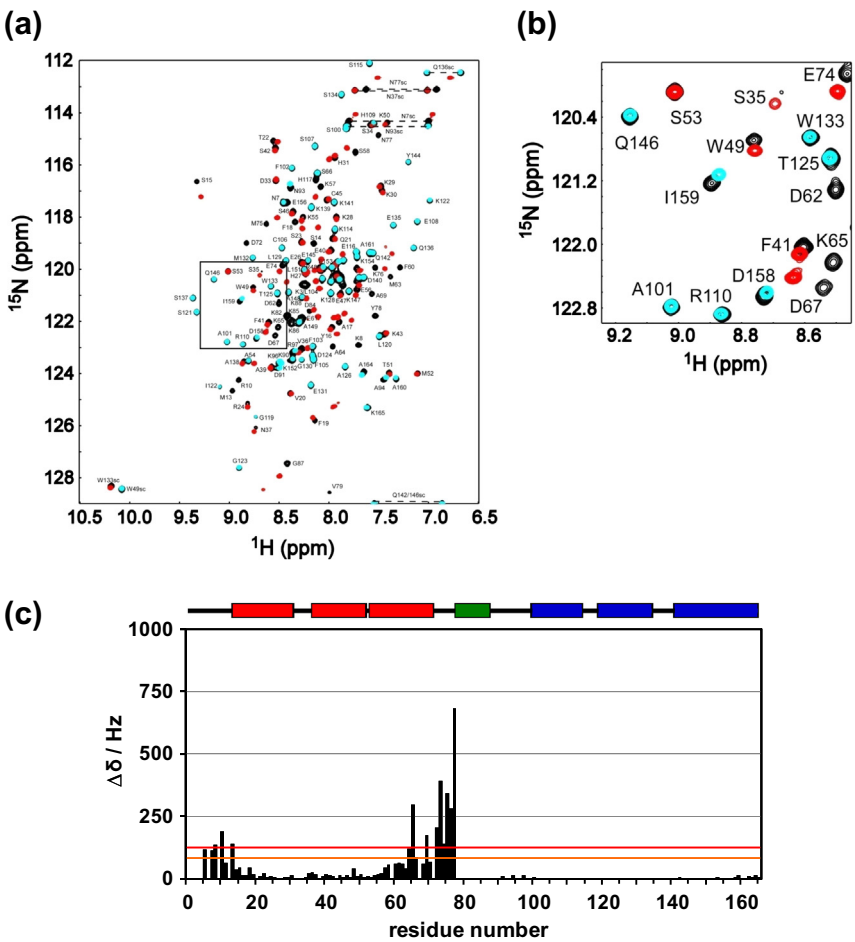

Fig. 2. ^{1}H-^{15}N HSQC spectra for HMGB2-A (red) and HMGB2-B (cyan) overlaid onto that for HMGB2-AlB with the resonance assignments (black) (a). Expanded part (boxed in a) of the overlaid ^{1}H-^{15}N HSQC spectra (b). The chemical shift differences observed between the spectra for HMGB2-AlB and those for HMGB2-A and HMGB2-B are plot against the residue number (c). Changes in backbone ^{1}H-^{15}N shifts (Δδ) are shown in Hz units. The lines represent the values of the average change plus one (red) and half (orange) standard deviations, respectively. The colored boxes on the top of the graph represent the positions for the helices in the HMGB2-AlB, which were determined by the NMR analyses in this work.

Author's personal copy

were incorporated into the calculation as pseudo CSA (PCSA) restraints for amide nitrogen atoms [38], which assumes the ^{15}N CSA to the above values for the α-helix part. The used python routine was generated with modifications from the one for CSA restraints in XPLOR-NIH. In the calculation, the structures for boxes A and B were treated as 'rigid bodies' by keeping the coordinates fixed, while the residues in the N-terminal and interdomain linkers were allowed to have free dihedral angle rotations during the calculation [6,7]. In the calculation, a low-temperature torsion angle dynamics simulated annealing, followed by a standard conjugate gradient minimization [6,7]. The calculation procedure used for determining the overall structure of HMGB2-AlB with the residual PCSA (RPCSA) and SAXS scattering data as structural constraints followed the preceding work [39].

The initial structures for the wild-type and Y78G mutant, which were subjected to the rigid-body refinement, were generated in the following way. The box A in the wild-type HMGB2-AlB was generated from the box A in HMGB1 (PDB: 1AAB) [15] by the homology modeling with the program MODELLER 9v8 [40]; the generated box A structure has altered orientation in the third helix and attached C-terminal segment comprising residues 78–84. In the case of the Y78G mutant, the box A NMR structure (residues 1–77) was used without any modifications. The box B structure (residues 88–165) was the NMR structure determined in this work. The HMGB2-AlB structure coordinate was generated by combining the boxes A and B with the computer generated interdomain linker (residues 85–87 for the wild-type, and residues 78–87 for the Y78G mutant) followed by energy minimization by XPLOR-NIH.

2.7. Linker peptide titration experiments

Synthetic peptide having the same sequence as the linker, Ac-YVPPKGDKKG-NH_2, was purchased in an HPLC purified grade (GL Biochem, Shanghai, China). The peptide was dissolved in

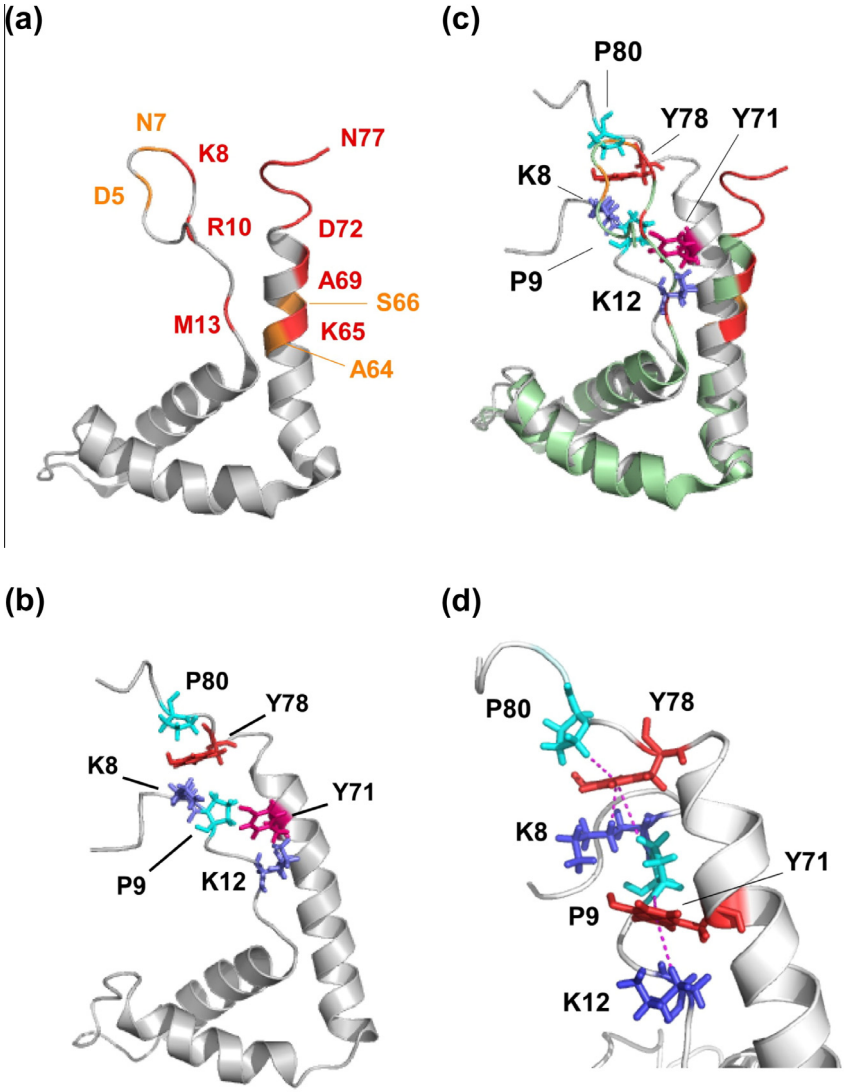

Fig. 3. HMGB2-A residues that showed significant chemical shift differences in the spectral comparison with HMGB2-AlB (Fig. 2c) are colored on the NMR structure (PDB: 1J3X) (a); the residues in red and orange showed chemical shift changes over the lines in red and orange in Fig. 2c, respectively. The residues in possible CH-π interactions are drawn in ball-and-stick format on the NMR structure of HMGB1 box A (PDB: 1AAB) (b): two tyrosine residues Y71 and Y78 are colored in red and orange, respectively, while prolines and lysines are colored in cyan and dark blue, respectively. Overlay of the structures of box A in HMGB1 (gray) and of box A in HMGB2 (green) (c). The potentially interacting residues in box A of HMGB1 are shown in the ball-and-stick representation and the residues showing significant chemical shift differences in box A in HMGB2 are colored as in Fig. 3a. The structure overlay was calculated to maximally fit the backbone atoms (N, Cα, C') in the helical parts; H1 (residues 15–29), H2 (39–51) and H3 (54–71). The calculation was performed using the program PyMol (Schrödinger, LLC) and the rmsd for the atomic displacement was 1.1 Å. A close-up view of the potentially interacting residues in box A in the HMGB1 structure (d). The pseudo atom position was assumed to be the center of the aromatic ring in the distance calculations for the parts defined by the dotted lines.

Author's personal copy

NMR buffer (50 mM sodium phosphate, pH 6.4), and its pH was adjusted to pH 6.4 using 0.1 M NaOH solution. The peptide was titrated against ^{15}N-labeled HMGB2-A or HMGB2-AlB fragment solutions at 0.7 mM protein. A series of HSQC spectra were collected for the samples with different molar ratios of the peptide (0.2, 0.5, 1.0, 1.5, 2.0 and 4.0) against the HMGB2 fragments.

3. Results and discussion

3.1. Specific interaction of the interdomain linker with box A revealed by chemical shift changes

The primary sequence of boxes A and B in HMGB2 are shown with those of the homologous HMGB1 proteins and the orthologues (Fig. 1a): the boxes A and B domains consist of the residues 1–77 and 88–165, respectively (Fig. 1b) [16]. It is noted that the residue number adopted here is for the immature HMGB proteins having initial methionine.

The sequence position of the box A in this work is different from that defined in the homologous HMGB1 box A (residues 1–84) [15]; the present box A position was defined according to the original report on HMGB2 by Yoshida and co-workers [16,17]. The box A in HMGB2 (residues 1–77) was determined based on the HMGB1 box A structure [14,41]: the HMGB1 box A has the structured part ended at T77 and the following segment, residues from Y78 to E84, is rich in amino acids of Pro, Gly, and Lys, which segment can be recognized as an unstructured linker due to its characteristic amino acid compositions (Fig. 1a) [42]. In also considering the box B structure [14], the part of the residues 78–87 in HMGB2 was defined as the interdomain linker in this work (Fig. 1a, shown in green). The box B position in HMGB2 was defined as for the case of HMGB1 [14]. The fragments used in this work are schematically summarized with domain structures of the entire protein (Fig. 1b); the interdomain linker is denoted as 'l', and the 'Al' stands for the fragment having the domain A with the interdomain linker, for example.

The ^{1}H-^{15}N heteronuclear single quantum coherence (HSQC) spectra for the fragments HMGB2-A, B and AlB are overlaid for comparison (Fig. 2a): each spectrum with resonance assignments is available as Supplementary material (Fig. S2). The spectral comparison showed the significant differences between the signals for HMGB2-A and the box A in HMGB2-AlB, while the signals for HMGB2-B mostly overlapped to those of the box B in HMGB2-AlB (Fig. 2a and b). The observed chemical shift differences are plotted against the residue number of HMGB2-AlB (Fig. 2c). The chemical shift changes were observed in the limited parts of box A, which may demonstrate that the inter-domain linker, Y^{78}VPPKGDKKG^{87}, specifically interacts with the N- and C- termini of the box A. The residues showing the changes over the average plus one standard deviation (σ), and those in the rage from an average +0.5σ to +1.0σ are marked in red and orange on the HMGB2-A structure, respectively (Fig. 3a): the HMGB2-A structure was determined in this work (Fig. S1a).

3.2. Estimation of the affinity of the interdomain linker to the box A using a synthetic peptide

We elucidated the affinity of the inter-domain linker to the box A by the NMR titration experiments using a synthetic peptide of the sequence, Ac-YVPPKGDKKG-NH_2. The four equimolar amount of the peptide input to ^{15}N-labeled HMGB2-A caused no apparent spectral change (data Fig. S3). The linker has, thus, only limited affinity to the box A; the K_D should be greater than 2×10^{-4} M, in assuming that a 1% population of the bound form gives observable spectral changes.

The same peptide was titrated to the ^{15}N labeled HMGB2-AlB fragment, which also caused no apparent spectral changes (data not shown).

The results showed that the interdomain linker has limited affinity to the box A in HMGB2; its tethering to the box A is essential to cause the specific contact of the linlker with the parts in the box A, which showed the significant spectral changes.

3.3. The interdomain linker contact to box A is primarily mediated by Y78

The spectral comparison between the HMGB2-AlB and Al fragments has shown that the signals for HMGB2-Al mostly overlapped onto the corresponding part of the signals for HMGB2-AlB (data Fig. S4a and b). Plot for the chemical shift changes along the residue number demonstrated no apparent spectral differences for the box A part between HMGB2-Al and HMGB2-AlB fragments (data Fig. S4c). In focusing on the residues in the interdomain linker, two amide-containing residues ($Y^{78}V^{79}$) in the N-terminal four-residue segment, Y^{78}VPP^{81}, showed the signals resonating very close to those of the corresponding part in the AlB fragment (Fig. S4c). The two residues are in remarkable contrast to the following interdomain linker residues, 82–87, showing apparent spectral changes; the changes should be ascribed to the end-effect by the truncation of the following part originally existing in the AlB (Fig. S4c). Although the four-residue segment, residues 78–81, is apparently unstructured in the HMGB1 box-A structure (Fig. 3b) [15], the spectral comparison between the Al and AlB fragments

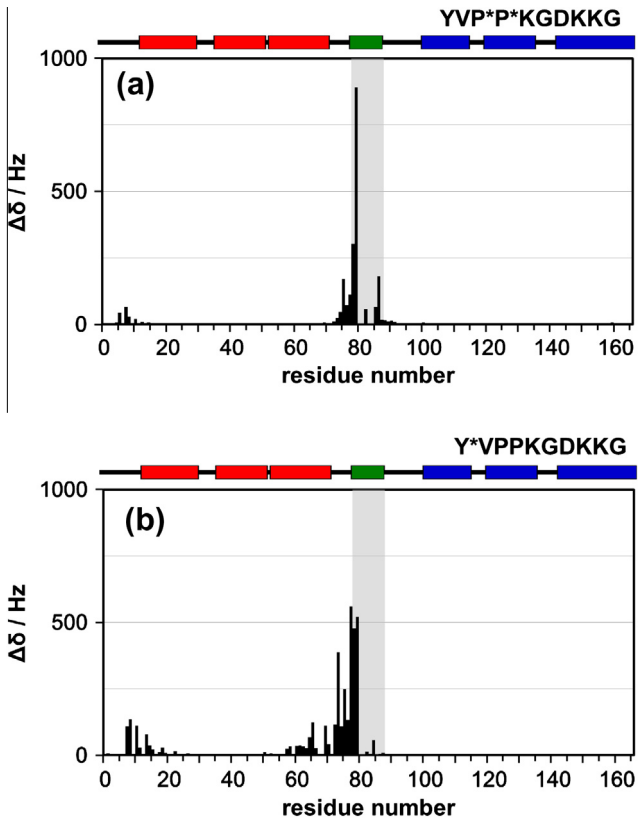

Fig. 4. Chemical shift changes caused by the mutations to the interdomain linker. Chemical shift differences observed on the ^{1}H-^{15}N HSQC spectra between the wild-type HMGB2-AlB and P80G/P81G mutant (a), and Y78G mutant (b). The colored boxes on each graph show the positions of the helices.

Author's personal copy

shows the N-terminal two residues, at least, in the interdomain linker should specifically contact to the box A, irrespective of the existence of the following part (Fig. S4c).

A series of the site-directed mutation to the residues in the interdomain linker was done to identify the residues primarily engaged in the contact to box A (Fig. S5). The results demonstrated that the Y78G mutation mostly reproduced the spectral changes observed for the spectral comparison between the HMGB2-AlB and HMGB2-A fragments (Figs. 4b and 2c); P80G/P81G mutation, also caused spectral changes, but the changes were rather limited to the C-terminal part of the box A (Fig. 4a). Y78 was, thus, identified as the primarily responsible residue for the interdomain linker contact to the box A.

3.4. Structural insight into the interdomain linker contact to box A

The structural details were explored in respect to the interaction between the interdomain linker and the box A (Fig. 3b). HMGB2-A lacks the segment ($Y^{78}VPPK^{82}$) that follows the structured part, while the box A in HMGB1 has the C-terminal extension as a part of the interdomain linker ($Y^{78}IPPKGE^{84}$) (PDB accession code: 1AAB) (Fig. 3c) [15]. HMGB1 and 2 have high sequence identity (Fig. 1a); the HMGB1 box A, residues 1–84, has only 11 different residues against the box A in HMGB2 (87% sequence identity) (Fig. 1a). The high sequence identity allows for exploring the binding mode of the interdomain segment, $Y^{78}VPPK^{82}$, to the box A through the structural comparison of the boxes A in HMGB1 and 2 (Fig. 3a and b).

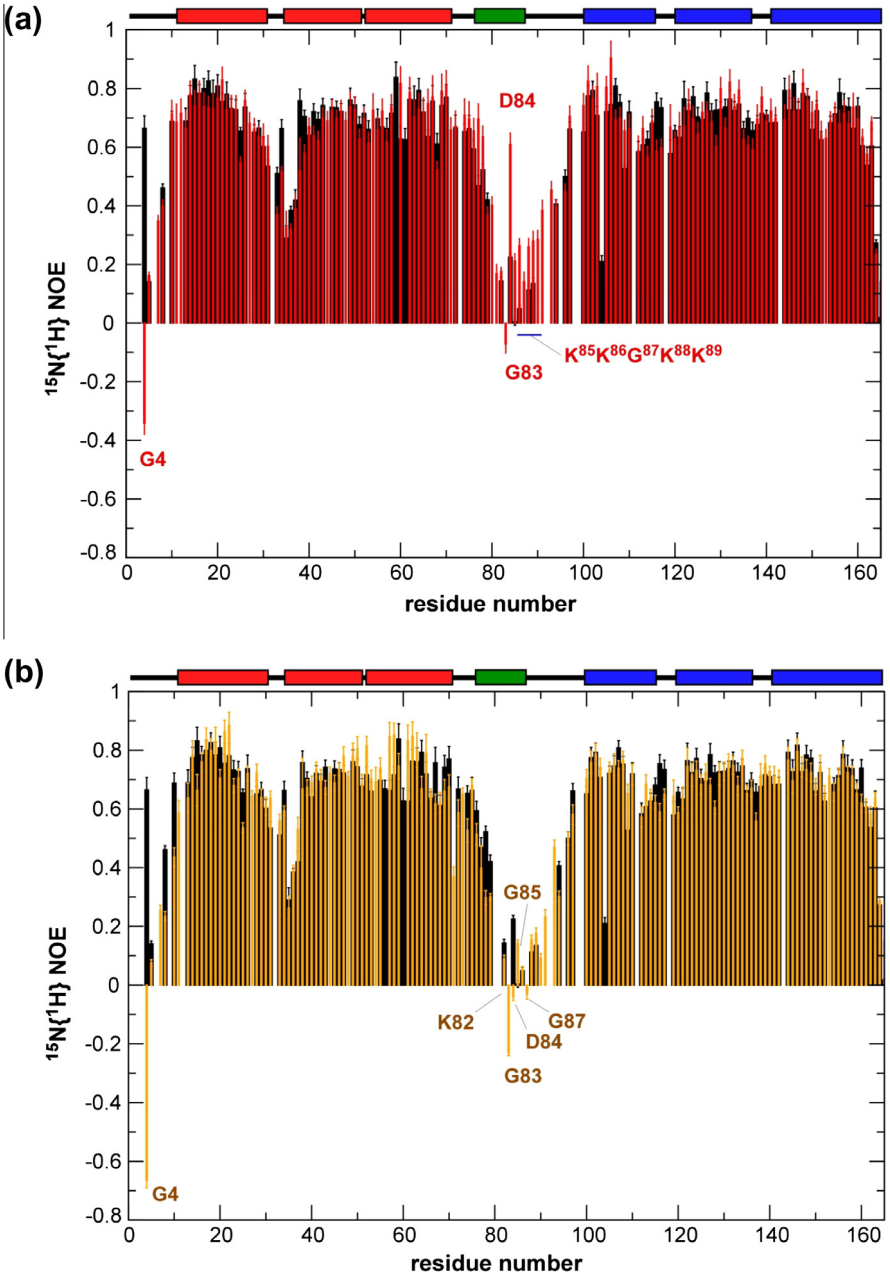

Fig. 5. Comparison of the $^{15}N\{^1H\}$ heteronuclear NOE profiles between the wild type and each mutant. The wild type (black bars) *versus* the P80G/P81G mutant (red bars) (a). The wild type (black bars) and the Y78G mutant (yellow bars) (b). The rectangular boxes above the graphs represent the positions of α-helices (red and blue boxes for boxes A and B, respectively) and the linker part (residues 78–87; green box).

Author's personal copy

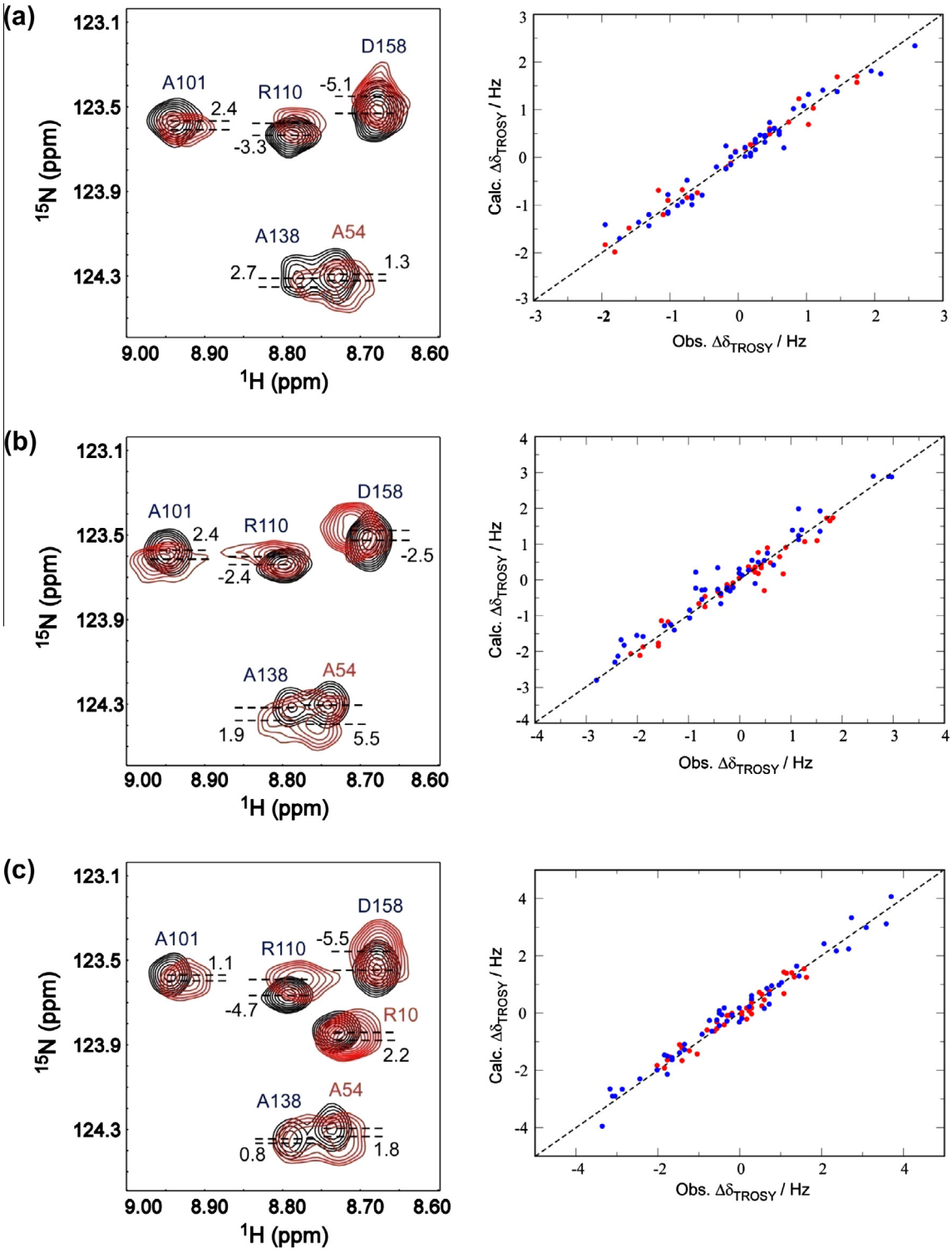

Fig. 6. Alignment tensor determination based on the ^{15}N TROSY shift changes induced by weak alignment. The expanded part of the overlaid ^{1}H-^{15}N TROSY spectra collected for the protein in isotropic (black) and aligned (red) states; wild type (a), P80G/P81G mutant (b) and Y78G mutant (c). The chemical shift differences observed for the signals collected in the isotropic and aligned states are drawn on the spectra in Hz; the chemical shift correction for the aligned spectrum is not applied to those spectra displayed, which is required due to the residual quadrupole splitting of the deuterium lock signal. In the alignment tensor calculation, the correction to each shift difference was applied based on the directly observed deuterium signal in the aligned state. The correlation between the observed $\Delta\delta$TROSY and the back calculated $\Delta\delta$TROSY from the determined alignment tensor is plotted on the right side of each observed spectrum. In each correlation plot, blue and red dots represent data from the residues in box A and box B, respectively. In the calculations, only residues in the secondary structure parts were considered in calculation.

The five-residue segment, Y^{78}VPPK^{82}, in the HMGB1 box A contacts the N-terminal part through Y78 (Fig. 3b). The side chain contacts in the NMR structure suggest that they are mediated through CH-π interactions; Y78 ring moiety may play as an acceptor π-system for the CH donors in P80, K8 and P9 (Fig. 3d). Similarly, Y71 may also be in the CH-π interactions with P9 and K12 (Fig. 3d);

Author's personal copy

the Y71 mediating interactions were noted as hydrophobic contacts in the original report on the structure of box A in HMGB1 (Fig. 3b) [15]. Because Y78 is in the floppy part in the overlaid structure presentation, the intramolecular interactions mediated by Y78 were not focused in that original report [15].

The CH-π interaction is a type of non-bonded interaction giving a stabilization energy of about 0.5–1.0 kcal/mol per interaction, being comparable to single hydrogen bond; CH-π interaction is formed between aliphatic CH donors and aromatic π-acceptors as in tyrosine-rings [21]. The structural details in the atomic interactions associated with Y71 and Y78 are summarized in Table S3, which demonstrate that they are recognized as CH-π interactions according to the criteria defined in previous report [21].

The role of Y78 found in the HMGB1 box A structure, which mediates the interactions between the interdomain linker and box A, consistently explains the chemical shift changes by Y78G in HMGB2-Al fragment (Fig. 4b): the spectral changes caused by the lack of the C-terminal part, after Y78, to the residues in the box A in HMGB2 were mostly reproduced by the Y78G mutation to the HMGB2-Al (Figs. 2c and 4b). The residues showing the significant spectral changes by Y78G are consistent with the residues in the CH-π interaction network (Fig. 3a and b).

Y78 in the unstructured interdomain linker, therefore, may direct the linker and the C-terminal half of the third helix of the box A in HMGB2, as expected by the structure comparison (Fig. 3c). It should be noted that the interdomain segment of the residues 78–84 in HMGB1 box A is not fixed in that conformation, but it may be in a dynamic equilibrium between the bound and unbound states (Fig. 3c): the distance restraints from NOEs bias the contact form of the segment. The structure fluctuation is evident for the interdomain segment by the low $^{15}N\{^1H\}$ NOE values, less than 0.5 (Fig. 4). The Y78 mediated interactions to direct the interdomain segment, therefore, should be weak and transient.

The role of Y78 in connecting the interdomain segment to box A was confirmed by the ^{15}N edited NOESY spectra (Fig. S6): the NOE signal between K8 amide proton and Y78 ring proton (Hε) was observed in the HMGB2-Al and the wild-type HMGB2-AlB (Fig. S6a and b), whilst the corresponding NOE signal was absent in the HMGB2-AlB (Y78G) mutant (Fig. S6c). It is noted that the NOE intensity observed between the residues K8 and Y78 in the wild-type HMGB2-AlB was extremely small relative to the sequential NOE between amide protons of K7 and K8, which may also suggest that the Y78 mediated interdomain segment contact to box A is transient (Fig. S6b).

3.5. The change in the dynamics of the interdomain linker by the mutation to Y78

The engagement of Y78 in the transient interactions of the interdomain linker to box A was found as described above. The changes in the dynamics, in psec–nsec time range, of the interdomain linker by Y78G and P80G/P81G mutation were elucidated by $^{15}N\{^1H\}$ NOEs (Fig. 5).

The P80G/P81G mutation slightly increased the order of the interdomain linker and also that of the C-terminal segment downstream of the third helix (residues 72–77) but significantly reduced the order of G4 (Fig. 5a). The unexpected increase in the order of the interdomain linker may be related to the intrinsically elongated shape of the polyglycine sequence as revealed by SAXS analysis [43]. The Y78G mutant reduced the order of the linker and the part of the residues 69–77 following the third helix (Fig. 5b).

The change in the $^{15}N\{^1H\}$ NOE profile for the Y78G mutant demonstrated that the impaired CH-π network mediated by Y78 increased the flexibility of the linker segment (Fig. 5b). The loss of the Y78 mediated interactions should have made the closed contact forms between the linker and the box A less populated. Although the Y78 mediated CH-π interactions have limited stabilization energies, the lack of them significantly increased the flexibility of the linker.

3.6. The altered reorientation dynamics of the tandem HMG boxes caused by linker mutation

The changes in the fluctuation of the interdomain linker by mutations, P80G/P81G and Y78G, should alter the interdomain dynamics in HMGB2-AlB. The interdomain dynamics was elucidated through the alignment tensors determined by the residual pseudo-^{15}N CSA (RPCSA), which are measured as the TROSY chemical shift differences between the isotropic and aligned states [4,5,31,38].

The observed TROSY shift changes, ΔδTROSY, induced by weak-alignment are shown on the overlaid spectra for the wild-type, P80G/P81G and Y78G mutants (Fig. 6a–c, left). The correlations between the observed and back calculated ΔδTROSY values using the

Table 1
Summary of the alignment tensors[a] determined from ΔδTROSY.

Sample	Box[b]	D_a/Hz	D_r/Hz	Euler angles /deg.			Q-factor[c] [rmsd Hz]
				α	β	γ	
HMGB2-AlB wild-type[d]	A	−3.3 (0.4)	−1.4 (0.7)	100 (7)	100 (4)	113 (9)	0.17 [0.17]
	B	−3.9 (0.5)	−1.6 (0.5)	111 (7)	66 (2)	104 (4)	0.20 [0.19]
HMGB2-AlB P80G/P81G[d]	A	−3.8 (0.5)	−1.5 (0.4)	120 (16)	104 (5)	124 (5)	0.24 [0.23]
	B	−5.3 (0.8)	−3.2 (1.2)	100 (7)	68 (4)	110 (7)	0.35 [0.24]
HMGB2-AlB Y78G[d]	A	−3.5 (0.6)	−2.0 (0.6)	139 (8)	105 (8)	122 (5)	0.21 [021]
	B	−7.2 (0.8)	−3.6 (1.0)	95 (5)	63 (2)	109 (4)	0.17 [0.31]

[a] Values in parentheses are the standard errors estimated by the jack-knife method [35]; 128 times with 10% of the experimental ΔδTROSY data reduction at random in each calculation. The calculation was done by home-written program using 'Mersenne twister' algorithm for random number generation [36].

[b] The lowest energy structure among the NMR refined coordinates was used for each analysis. In each structural refinement, the RDC derived constraints were also used (Kurita et al. in preparation). The PDB codes for boxes A and B were 1J3X and 1J3D, respectively.

[c] The quality factor Q is defined as $Q = \sqrt{\sum_{i=1,N} \frac{(\Delta\delta^{obs.}_{TROSY} - \Delta\delta^{calc.}_{TROSY})^2}{\sum_{i=1,N}(\Delta\delta^{obs.}_{TROSY})^2}}$, which is in accordance with the Q-factor defined for the RDC analysis[46].

[d] In the tensor determination, the residues were selected according to the following criteria; the residues (1) being in the secondary structure, (2) showing $^{15}N\{^1H\}$ NOE value greater than 0.6, 3) giving small chemical shift changes (less than 10 Hz) on the ^1H-^{15}N HSQC spectra between the mutant, P80G/P81G or Y78G, and the wild-type HMGB2-AlB. As exceptions, the residues S15 and F18, which showed 23 Hz and 29 Hz shift changes caused by Y78G mutation, respectively, were incorporated in the tensor calculation for the wild-type, with intention to increase the number of input data: the addition of these two data did not significantly change the resultant tensor value. The residues used in the calculation were the followings: the wild-type (box A), residues 15–30 and 38–55, the P80G/P81G mutant (box A), residues 15–30 and 38–64, and the Y78G mutant (box A), residues 15–30 and 38–71. For the box B, the residues 102–116 and 120–161 were used in all the fragments, the wild-type, P80G/P81G and Y78G mutants. Some residues showing severe signal overlaps and low signal intensities were omitted in the calculation.

Author's personal copy

alignment tensors for the boxes A and B are also shown (Fig. 6a–c, right). In considering the possible structural difference between the isolated box A lacking the C-terminal segment $Y^{78}VPPK^{82}$ and the box A in the HMGB2-AlB (Fig. 3c), we limited the residues used in the alignment tensor calculation for the box A; the residues having shown the chemical shift changes by mutations were omitted (see Section 2 and the legend to Table 1). The determined alignment tensors and the root mean square deviation (rmsd) values, with corresponding Q-factors, between the observed and back calculated $\Delta\delta$TROSY are listed in Table 1. The good correlations between the observed and back calculated values, as evidenced by the small values for the rmsds and Q-factors, credit the tensors are well determined.

The alignment tensor magnitude, D_a, shows the extent of the domain reorientation dynamics. The larger difference in D_a values between boxes A and B demonstrates the increased independency for their reorientation motions [3]. Significant difference in D_a values was observed between boxes A and B in both P80G/P81G and Y78G mutants, while the D_a values were coincident within the errors for the wild-type (Table 1). The greater alignment magnitude, as indicated by large D_a value, for box B than for box A show that box B has preferential contact with the aligning medium [3]. The changes in the aligning magnitudes for the proteins (Table 1) show the two boxes in the wild-type HMGB2-AlB reorient within the restricted space, whilst the boxes in the Y78G mutant reorient rather independently. The boxes in P80G/P81G mutant, showing the moderate differences in D_a values imply the less significant interdomain dynamics relative to Y78G mutant.

The $^{15}N\{^1H\}$ NOE profiles for the P80G/P81G and Y78G mutants shared the cooperative reduction in the values for G4 and G83 relative to the wild-type (Fig. 5). The increased flexibility to the parts including G4 and G83 residues, thus, may be responsible for enhancing the interdomain dynamics, irrespective of the flexure of the following segment to the residues; G83, in contact to G4, might play as a joint to link the reorienting domains (Fig. 5).

The wild-type HMGB2-AlB showed close alignment tensor magnitudes, D_a and D_r, between boxes A and B, which allows for determining the relative domain orientation by the alignment tensors of the individual domains. P80G/P81G and Y78G mutants, instead, showed significantly different alignment tensor magnitudes, therefore their domain orientations are not readily determined [2,3,44]. In the mutants, two domains are simply described as in a pronounced motion in a cone with approximate half angles of the bounding cone for P80G/P81G and Y78G, 47° and 53°, respectively [44].

3.7. Relative domain orientation of the boxes A and B in HMGB2-AlB

The pair-distance distribution functions $P(r)$ from SAXS measurements for the wild-type and the Y78G mutant HMGB2-AlB fragments were compared (Fig. 7). The profiles were significantly different; the wild-type has greater values over the mutant in the longer pair-distance (r) region over 30 Å (Fig. 7). This observation may imply that the boxes in the wild-type HMGB2-AlB are populated to form more extended forms relative to the Y78G mutant (Fig. 6). The Kratky plots for the wild-type and Y78G mutant showed the increased unfolded structural parts in the mutant, as demonstrated by the greater values for the mutant in the q-range greater than 0.3 $Å^{-1}$ (Fig. S7).

The RPCSA values for boxes A and B and the scattering data from SAXS measurements for the wild-type HMGB2-AlB were directly used as structural restraints to determine the entire structure: it is noted that the RPCSA-based structure calculation was possible due to the close aligning magnitudes for the boxes A and B in the wild-type HMGB2-AlB (Table 1). The structures fulfilling the experimental restraints from RPCSA and SAXS were obtained by

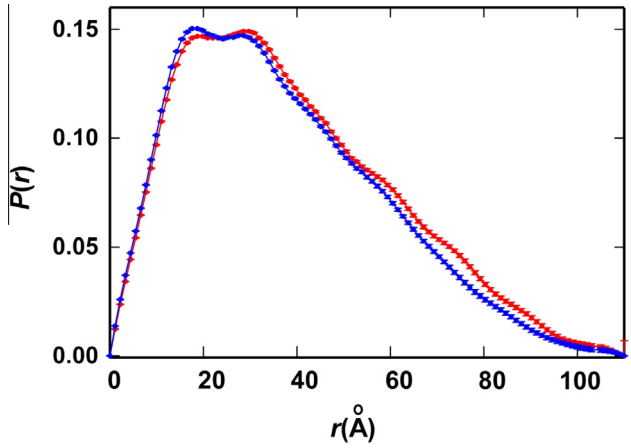

Fig. 7. Atom-pair distributions for HMGB2-AlB fragments. The $P(r)$-vs-r profiles for the wild-type and Y78G mutant are plot in red and blue, respectively.

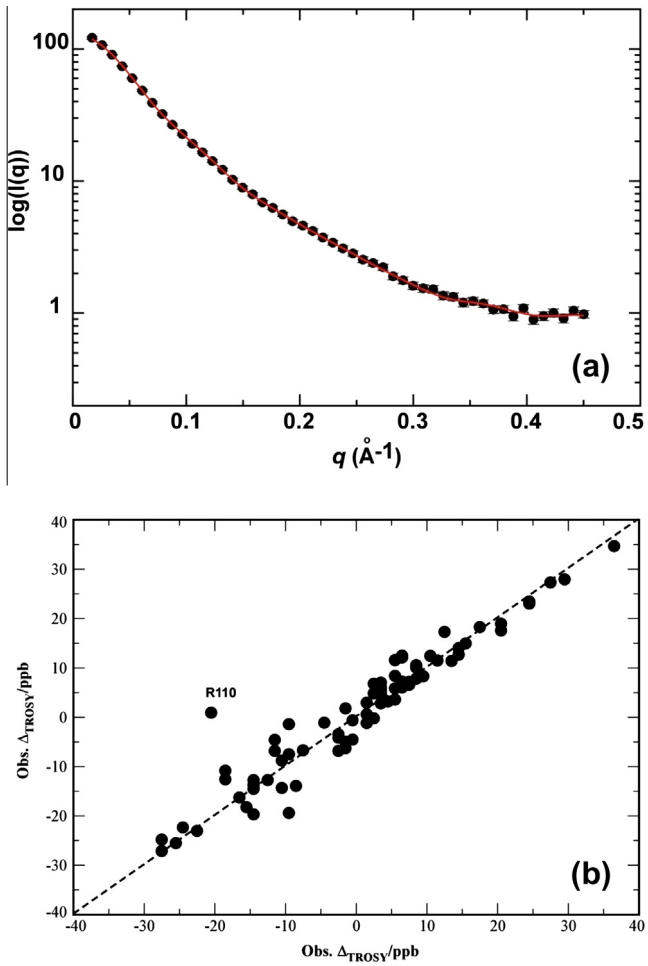

Fig. 8. Quality of the wild-type HMGB2-AlB domain arrangement determined using the RPCSA ($\Delta\delta$TROSY) and SAXS derived restraints. Experimental scattering profile for the wild-type HMGB2-AlB (●) and the calculated scattering curve in red (a). The correlation between the experimental RPCSA ($\Delta\delta$TROSY) values for the wild-type HMGB2-AlB and those calculated from the refined structure by XPLOR-NIH calculation (Fig. 9a) (b). Q-factor, and rmsd for the fitting quality against the experimental RPCSAs were 0.30, and 4.1 ppb (0.29 Hz), respectively. (For interpretation of the references to color in this figure legend, the reader is referred to the web version of this article.)

Author's personal copy

the rigid-body minimization using XPLOR-NIH (Fig. 8). The SAXS scattering profile was reproduced within experimental errors by the resultant structure (Fig. 8a), while the correlation between the observed and back calculated $\Delta\delta$TROSY values became worse relative to those for the isolated domains (Figs. 8b and 6a): the reduced correlation would come from the neglecting interdomain dynamics assumed in the present calculation, which is significant in reality. In spite of the reduced fitting quality, the correlation for the RPCSA was still good, which implies the interdomain dynamics in the wild-type HMGB2-AlB should be rather limited. The lowest energy structure, the best consistent structure with the experimental data, is depicted in the ribbon representation (Fig. 9a), which demonstrates the dynamically averaged structure for the HMGB2-AlB in solution. It is noted that the sole SAXS data without RPCSA merely ambiguously defines the domain orientation, although the ensemble structures reproducing the SAXS scattering profile share the extended arrangement of the boxes (Fig. S8).

Because of the larger domain dynamics for the Y78G mutant, as evident by the mismatch in the alignment tensor magnitudes for the boxes, the RPCSA based orientation restraints cannot be used to determine the structure. The entire structure of the Y78G mutant was calculated by only SAXS data; the structure giving the closest scattering profile to the observed data is depicted (Fig. 9b). The structure comparison demonstrates that the wild-type has more elongated structure than that of the Y78G mutant (Fig. 9), which is consistent with the $P(r)$ profiles (Fig. 7). The relative domain angle differences between the wild-type and Y78G seems close to the estimated half angle of the bounding cone, 52°, which was calculated from the difference in the alignment magnitudes between the boxes A and B in Y78G mutant (Table 1) [44].

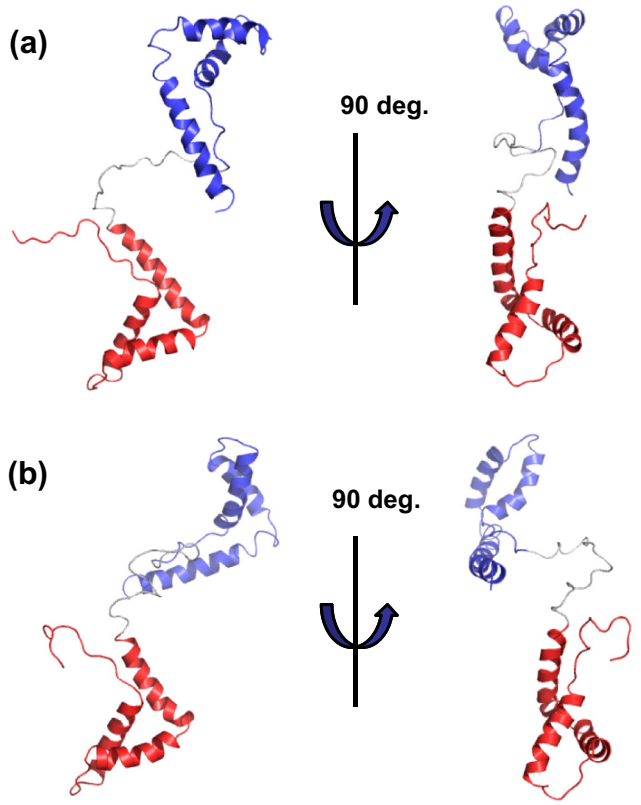

Fig. 9. Structures for the wild-type and Y78G mutant HMGB2-AlB. The lowest energy structure of the wild-type HMGB2-AlB refined by the constraints from RPCSA and SAXS (a). The lowest energy structure of the Y78G mutant HMGB2-AlB determined by only the constraints from the SAXS scattering data (b).

4. Conclusions

The present work has shown that the interdomain linker (residues 78–87) has a role to define the overall structure having preferential domain orientation. The N-terminal part of the interdomain linker, $Y^{78}VPP^{81}$, is particularly connected to the N-terminus of box A through a CH-π interaction network primarily mediated by the conserved Y78 (Fig. 3d). The weak and transient intramolecular interactions make the DNA binding surfaces of the boxes A and B preferentially stay in the opposite direction (Fig. 9a). The Y78G mutant having impaired intramolecular interactions altered preferential domain orientation and the interdomain dynamics, as revealed by the alignment tensors determined by RPCSA (Table 1), which suggests Y78 mediating weak and transient interactions are structurally significant. The usefulness of the hybrid use of SAXS and NMR with RPCSA was also emphasized to the structure analysis of the modular protein like HMGB2.

Acknowledgments

This work was supported by a Grant-in-Aid for Scientific Research for Priority Areas: "Molecular Science for Supra Functional Systems – Development of Advanced Methods for Exploring Elementary Process" from the Japan Society for the Promotion of Science (JSPS). Part of the work was also supported by a Grant-in-Aid for Scientific Research on Innovative Areas: "Molecular Science on Fluctuation toward Biological Functions" from JSPS. The technical part of the work was supported by the JST-SENTAN project. S.T. acknowledges JST-PRESTO for financial support. S.T. also acknowledges financial support from a Grant-in-Aid of the Creative Scientific Research Program (18GS0316). N.U.-T. acknowledges the financial support of a Grant-in-Aid for Scientific Research (C) from JSPS. The authors thank the RIKEN NMR facility (Yokohama, Japan) for providing instrument time to enable the collection of part of the NMR data used in this research. The authors appreciate Prof. Kohda in the Medical Institute of Bioregulation at Kyushu University for the access to 700 MHz NMR instrument. The experiments at Photon Factory BL-10C were performed under the approval of the Photon Factory Advisory Committee (Proposal No. 2010G091 and 2012G043). We thank Dr. Shogo Nakano for his help in generating a homology modeled structure used in this work.

Appendix A. Supplementary data

Supplementary data associated with this article can be found, in the online version, at http://dx.doi.org/10.1016/j.chemphys.2013.02.004.

References

[1] A.K. Dunker, C.J. Oldfield, J. Meng, P. Romero, J.Y. Yang, J.W. Chen, V. Vacic, Z. Obradovic, V.N. Uversky, BMC Genomics 9 (Suppl. 2) (2008) S1.
[2] H. Tossavainen, O. Koskela, P. Jiang, J. Ylanne, I.D. Campbell, I. Kilpelainen, P. Permi, J. Am. Chem. Soc. 134 (2012) 6660.
[3] M.W. Fischer, J.A. Losonczi, J.L. Weaver, J.H. Prestegard, Biochemistry 38 (1999) 9013.
[4] S. Tate, A. Imada, N. Hiroguchi, Complementary Use of NMR to X-ray Crystallography for the Analysis of Protein Morphological Change in Solution, InTech, Rijeka, Croatia, 2011.
[5] S. Tate, Anal. Sci. 24 (2008) 39.
[6] N.K. Goto, N.R. Skrynnikov, F.W. Dahlquist, L.E. Kay, J. Mol. Biol. 308 (2001) 745.
[7] N.R. Skrynnikov, N.K. Goto, D. Yang, W.Y. Choy, J.R. Tolman, G.A. Mueller, L.E. Kay, J. Mol. Biol. 295 (2000) 1265.
[8] A. Bax, A. Grishaev, Curr. Opin. Struct. Biol. 15 (2005) 563.
[9] S.E. Tsutakawa, G.L. Hura, K.A. Frankel, P.K. Cooper, J.A. Tainer, J. Struct. Biol. 158 (2007) 214.
[10] X. Wang, H.-W. Lee, Y. Liu, J.H. Prestegard, J. Struct. Biol. 173 (2011) 515.
[11] M. Bustin, R. Reeves, Prog. Nucleic Acid Res. Mol. Biol. 54 (1996) 35.
[12] M. Bustin, M.P. Crippa, J.M. Pash, Crit. Rev. Eukaryot Gene Expr. 2 (1992) 137.

Author's personal copy

[13] M. Bustin, D.A. Lehn, D. Landsman, Biochim. Biophys. Acta 1049 (1990) 231.
[14] H.M. Weir, P.J. Kraulis, C.S. Hill, A.R. Raine, E.D. Laue, J.O. Thomas, EMBO J. 12 (1993) 1311.
[15] C.H. Hardman, R.W. Broadhurst, A.R. Raine, K.D. Grasser, J.O. Thomas, E.D. Laue, Biochemistry 34 (1995) 16596.
[16] A. Yamamoto, Y. Ando, K. Yoshioka, K. Saito, T. Tanabe, H. Shirakawa, M. Yoshida, J. Biochem. 122 (1997) 586.
[17] Y. Nakamura, K. Yoshioka, H. Shirakawa, M. Yoshida, J. Biochem. 129 (2001) 643.
[18] K. Yoshioka, K. Saito, T. Tanabe, A. Yamamoto, Y. Ando, Y. Nakamura, H. Shirakawa, M. Yoshida, Biochemistry 38 (1999) 589.
[19] M. Webb, J.O. Thomas, J. Mol. Biol. 294 (1999) 373.
[20] Y. Nakamura, M. Shimizu, M. Yoshida, J. Biochem. 131 (2002) 153.
[21] M. Brandl, M.S. Weiss, A. Jabs, J. Sühnel, R. Hilgenfeld, J. Mol. Biol. 307 (2001) 357.
[22] J. Cavanagh, W.J. Fairbrother, A.G. Palmer III, N.J. Skelton, Heteronuclear NMR Experiments, Academic Press, Inc., New York, 1996.
[23] D. Rovnyak, D.P. Frueh, M. Sastry, Z.-Y.J. Sun, A.S. Stern, J.C. Hoch, G. Wagner, J. Magn. Reson. 170 (2004) 15.
[24] J.C. Hoch, A.S. Stern, NMR Data Processing, John Wiley & Sons, Inc., New York, 1996.
[25] F. Delaglio, S. Grzesiek, G.W. Vuister, G. Zhu, J. Pfeifer, A. Bax, J. Biomol. NMR 6 (1995) 277.
[26] B.A. Johnson, R.A. Blevins, J. Biomol. NMR 4 (1994) 603.
[27] N. Kobayashi, J. Iwahara, S. Koshiba, T. Tomizawa, N. Tochio, P. Güntert, T. Kigawa, S. Yokoyama, J. Biomol. NMR 39 (2007) 31.
[28] P. Güntert, Eur. Biophys. J. 38 (2009) 129.
[29] C.D. Schwieters, J.J. Kuszewski, N. Tjandra, G. Marius Clore, J. Magn. Reson. 160 (2003) 65.
[30] T. Ueki, Y. Hiragi, M. Kataoka, Y. Inoko, Y. Amemiya, Y. Izumi, H. Tagawa, Y. Muroga, Biophys. Chem. 23 (1985) 115.
[31] S. Tate, H. Shimahara, N. Utsunomiya-Tate, J. Magn. Reson. 171 (2004) 284.
[32] M. Ottiger, F. Delaglio, A. Bax, J. Magn. Reson. 131 (1998) 373.
[33] S. Meier, D. Haussinger, S. Grzesiek, J. Biomol. NMR 24 (2002) 351.
[34] J.J. Chou, S. Gaemers, B. Howder, J.M. Louis, A. Bax, J. Biomol. NMR 21 (2001) 377.
[35] F. Mosteller, J. Tukey, Data Analysis and Regression: A Second Course in Statistics, Addison-Wesley Publishing Co., Don Mills, Ontario, 1977.
[36] M. Matsumoto, T. Nishimura, ACM Trans. Model. Comput. Simul. 8 (1998) 3.
[37] C.D. Schwieters, J.J. Kuszewski, N. Tjandra, G.M. Clore, J. Magn. Reson. 160 (2003) 65.
[38] A. Grishaev, J. Ying, A. Bax, J. Am. Chem. Soc. 128 (2006) 10010.
[39] A. Grishaev, J. Wu, J. Trewhella, A. Bax, J. Am. Chem. Soc. 127 (2005) 16621.
[40] R. Sanchez, A. Sali, Methods Mol. Biol. 143 (2000) 97.
[41] S.H. Teo, K.D. Grasser, C.H. Hardman, R.W. Broadhurst, E.D. Laue, J.O. Thomas, EMBO J. 14 (1995) 3844.
[42] T. Tanaka, Y. Kuroda, S. Yokoyama, J. Struct. Funct. Genomics 4 (2003) 79.
[43] S. Ohnishi, H. Kamikubo, M. Onitsuka, M. Kataoka, D. Shortle, J. Am. Chem. Soc. 128 (2006) 16338.
[44] J.R. Tolman, J.M. Flanagan, M.A. Kennedy, J.H. Prestegard, Nat. Struct. Biol. 4 (1997) 292.
[45] M.A. Larkin, G. Blackshields, N.P. Brown, R. Chenna, P.A. McGettigan, H. McWilliam, F. Valentin, I.M. Wallace, A. Wilm, R. Lopez, J.D. Thompson, T.J. Gibson, D.G. Higgins, Bioinformatics 23 (2007) 2947.
[46] M. Ottiger, A. Bax, J. Biomol. NMR 13 (1999) 187.